UNIVERSITAT POLITÈCNICA DE CATALUNYA
BARCELONATECH

Optimization of a CSI Inverter and DC/DC Elevator with Silicon Carbide Devices, for Application in Electric Traction Systems

By

Efrén Esteban Fernández Palomeque

Thesis submitted in partial fulfillment of the requirements of the degree of Doctor of Philosophy in Electronics Engineering

Supervisors:
Dr. José Luis Romeral
Dr. Vicent Sala

"Odié cada minuto de mi entrenamiento, pero dije "No renuncies. Sufre ahora y vive el resto de tu vida como un campeón"

Muhammad Ali

Abstract

The applications of electric traction systems currently focus on developing technologies with greater energy efficiency and lower environmental impact. Manufacturers of hybrid and electric vehicles are looking for ways to improve and optimize the efficiency of their models.

Manufacturers are looking for more efficient and more compact converter topologies. The use of new band gap materials in the construction of these topologies has generated many debates and new lines of research especially in the optimization of these topologies. The silicon carbide (SiC) based switching devices provide significant performance improvements in many aspects, including lower power dissipation, higher operating temperatures, and faster switching, compared with conventional Si devices, all these features make that these devices generate interest in applications for electric traction systems.

This work presents a method for improving total harmonic distortion (THD) in the currents of output and efficiency in SiC current source inverter for future application in an electric traction system. The method proposed consists in improving the coupling of a bidirectional converter topology V-I and CSI. The V-I converter serves as a current regulator for the CSI and allows the recovery of energy. The method involves an effective selection of the switching frequencies and phase angles for the carriers signals present in each converter topology. With this method, it is expected to have a reduction of the total harmonic distortion THD in the output currents. In addition, an analysis of the losses in the motor and topologies of power converters is developed considering the optimization method previously analyzed. The weighted average efficiency of the whole system (power converters + motor) in differents conditions of operations is presented.

Keywords

Silicon Carbide *Power Losses* *Current Source Inverter*

High Frequency *Total Harmonic Distortion*

Power Converter *V-I Converter*

Acknowledgement.

Primero quiero dedicar este trabajo a mi Esposa y mi pequeño hijo Matías sin su apoyo, amor y comprensión este logro no se pudo haber hecho realidad gracias por estar siempre a mi lado y haber soportado lo bueno y malo durante nuestra estancia por cuatro años. Además, quiero agradecer a mis padres y hermano que durante todo este tiempo estuvieron siempre pendientes de nosotros y este logro es también parte de ellos. A mi familia en especial a mi Tío Santiago por su ejemplo de lucha y fortaleza.

También el agradecimiento a mis directores de tesis, Luis Romeral y Vicent Sala, por su guía y ayuda en el desarrollo de la tesis. A Luis por su apoyo y confianza para poder llegar al grupo de investigación, porque que sin conocerme me dio la oportunidad. A Vite, por su guía, charlas y llamados de atención que me sirvieron mucho para mejorar cada día y llegar a cumplir este objetivo.

Como no agradecer a todo el grupo MCIA por su amistad y compañía. En especial a mis entrañables amigos Carles, Alejandro y Carlitos, gracias por toda su ayuda durante estos cuatro años, en realidad me hicieron sentir como en casa, a Carles por sus charlas productivas y polémicas que siempre las recordaré, Carlitos por su inocencia y alegría que transmitía en el despacho (quiero esa camiseta del Barça) y Alejandro por su amistad y seguridad, me ayudaste mucho de eso he aprendido y nunca olvidare todo lo que hiciste por mí. Todos formamos el mítico y recordado despacho 160.

Mi agradecimiento a mi amigo y profesor Antoni García, por estar siempre pendiente de familia y mi persona, gracias por todos los consejos que me enseñaron a seguir luchando por esta meta, nunca olvidare las charlas y tequis que me enseñaron a seguir adelante.

A mis amigos del Fútbol Thierry, Danny, Carlos, Memo, Santiago, Ivo, Jimmy, Xavi, Canario, Liam, Pablito, Kenny, Juan y cuantos más pasaron por la pista de la UPC en donde se consolidó una fuerte amistad y hermandad que fue un apoyo constante para seguir adelante con nuestras labores y estudio gracias mis queridos amigos.

Quiero también agradecer a la Senescyt Ecuador por la Beca brindada para poder solventar los gastos de estudio y de manutención gracias por la confianza depositada en mi persona y a la Universidad del Azuay por todo el apoyo brindado durante mis estudios.

Contents of the document

Index of figures

Index of tables

1.

Introduction

This chapter presents the main lines of research, general structure and delimitation of this research thesis. It describes a brief introduction of the field of research, hypothesis, specific objectives and chapter description that are presented within the document.

CONTENTS:

1. Introduction

1.1 Research Topics

Electric and hybrid vehicles present a major challenge for car designers, especially in terms of size, weight, choice of electronic systems efficiency and controls. For the HEV and EV industry to continue to grow, these challenges must be overcome with efficient and cost-effective solutions. Current hybrid and electric vehicle platforms, which use silicon-based power electronics, are subject to the challenges named above: size, weight and efficiency. One option to overcome the problems is the deployment of silicon carbide (SiC) [1]-[2]-[3]. This technology provides means to improve the efficiency of the electric vehicle system, reduces the need to develop robust thermal management systems that add size, weight and cost to vehicles in addition allows to work at a higher frequency of operation, which will reduce the size of the passive elements [4]-[5].

The voltage source inverter (VSI) topology controls the operation of electric motor in electric traction systems, it usually uses isolated gate bipolar transistors (IGBTs) as a switching element with return silicon diodes. Furthermore, if a DC-DC voltage booster is used it is coupled into a single module that is placed inside the compartment to the electric motor to minimize the parasitic inductance and reduce the weight of the wiring [6]-[7]. However, the operating limitations in silicon technology, means that the electronic components of silicon cannot meet the demands of new HEV platforms and then it appears an area to think about upgrading the electric car solutions. At this point it is possible to consider silicon carbide devices. The SiC devices can operate at higher temperatures, higher power density and higher switching frequencies. The combination of these features would allow to obtain more efficient electric traction systems and to increase power density of the whole powertrain.

The SiC has a series of properties [8] that make it interesting to operate with high performance behavior. In particular, these properties can be summarized in the following points:

- Power of the big band.
- High thermal conductivity
- High breaking electric field
- High saturation speed
- High thermal stability.
- Good chemical behavior.

Several studies have developed different approaches to optimize topologies of converters with SiC devices for differents applications [9]-[10]-[11]-[12]. The results show the improvement in efficiency and reduction of power losses and the advantages of using these devices and their potential use to optimize the different topologies of inverters.

SiC converters present challenges that must be overcome before they can reach the energy levels demanded by electric vehicles and become economically feasible, so the present thesis topic is considered as a contribution to the scientific community that will allow to consolidate this type of technology within the electric traction systems.

1.2 Research Problem

- The trend of manufacturers is focused on using a topology of voltage source inverter (VSI) with semiconductor of silicon and control techniques for electric motors. This topology involves a series of problems that reduce the efficiency and performance of the inverter [13]-[14], this leads to search and investigate new alternatives of topologies that allow improving the operating characteristics of the inverter.
- VSI is a buck topology, the output AC voltage cannot exceed the input DC, so this is the reason to place a DC / DC converter at the input of the converter. This involves large passive elements such as capacitors on the DC bus that are used as filters, these get to occupy 30% of the size of the inverter. [15]
- The IGBTs of each branch of the inverter cannot be activated at the same time, this would cause a short circuit that would damage the converter, therefore the need to use a dead time between the activation of each element, which produces distortion in the output AC current of the converter, which increases the ripple of the motor torque [15]-[16].
- The size, power losses, weight and efficiency reduction are the most common problems in power converters designed for electric traction systems [17]. To this should be added the problems that can be generated when using a VSI topology with Silicon devices that have to work a temperature range less of 120 ^{0}C and at switching frequency below 10 kHz, thus adapting a very robust cooling system that adds more weight to the system [18]-[19].

As a conclusion, a research on topologies of alternative converters such as current source inverter and quasi Z source inverter with SiC devices switching at high frequency in electrical

traction systems applications is necessary to improve efficiency and power density, while maintaining control performances and voltage and current waves quality.

1.3 Hypothesis

The hypothesis that supports this thesis is summarized as follows:

The analysis and investigation of an inverter with CSI topology based on a bidirectional DC / DC elevator, working with Silicon SiC carbide power elements, with high frequency operating ranges, allows reducing the converter volume, power losses and improving efficiency.

In this way, this thesis will contribute to the development of this technology in the application of traction systems for electric vehicles and improve the efficiency of these systems.

Therefore the hypothesis to be demonstrated is the design and optimization of an inverter system with SiC power elements, for an electric car powertrain system. This analysis should include:

- Implementation of a PWM control technique, for the high frequency activation of the SiC power elements.
- Implementation of a control technique to synchronize the Dc-Dc converter with regulated current for the CSI topology at different switching frequencies This implies the design of a method for reducing the harmonic distortion (THD) and improves the efficiency in the power converters topologies
- Evaluate the power losses and efficiency of the proposed topology and carry out a comparative study with topologies implemented with conventional silicon devices.

These exposed assumptions represent the basis of the resulting thesis research. The hypothesis is investigated by means of the research work reflected in this thesis document.

1.4 Objectives and contributions.

In this section we present the objectives within the proposed research thesis.

a) The first objective proposes a model and control of CSI converter topology with a bidirectional Dc-Dc elevator with SiC devices at high frequency operating ranges. In addition, a study of CSI topology with different topologies of impedance networks bidirectional to analyze advantages and disadvantages in comparison with the topology proposed. This objective will be faced in chapter 3 of the dissertation.

b) The second objective proposes the development of a control algorithm to couple the Dc-Dc power converter and the CSI inverter to obtain constant current source. This includes

the search of a method for search the best frequency of switching and phase angle of carrier signals in each converter for obtained the best efficiency and reduction of total harmonic distortion (THD). The entire study is implemented with SiC technology.

c) The third objective of this study provides an evaluation on the efficiency of power converter in differents conditions of load and frequency of switching. This evaluation includes power losses by conduction, switching, and comparison with conventional Silicon devices. This section is present in the chapter 5 of the dissertation.

1.5 Chapter description.

Based on the flow of the possible contributions and objectives, this thesis is divided into six chapters.

Chapter 1 present the differents research topics, problems detected as well as the hypothesis and objectives behind this research.

Chapter 2 provides a general review of power inverters topologies in applications of electric traction systems. In addition, it includes a brief analysis on the current state of silicon carbide devices and their application in topologies of power converters.

The **chapter 3** presents the operations of CSI inverter topology with a bidirectional Dc-Dc for electric traction system. Finally, different topologies of CSI inverters with power converter for the DC link current control are discussed, the advantages and disadvantages between the topologies analyzed are presented.

The focus of **chapter 4** is propose a control algorithm to couple the Dc-Dc power converter and the CSI inverter with SiC devices. Two points of proposed controlling method are evaluated, including the coupling to DC-DC converter to CSI inverter for obtained the current of input constant and a method for reduce the THD in the currents output in the power converter through the synchronization of the carrier signals. Proposed controlling method is evaluated by computer simulations are performed to validate the theoretical assessment.

In **chapter 5**, the author evaluates the efficiency of prototype SiC power converter in different conditions of operation of frequency and loads. The different losses of power by conduction and switching are analyzed these experimental evaluations are conducted to evaluate the efficiency of the SiC topology of power converter, which verifies the theoretical developments, previously analyzed.

In the **chapter 6** the general conclusions are presented and the future works are discussed. Finally in the **chapter 7** the dissemination of result of this research are presented.

1.6 References.

[1] A. Stefanskyi, L. Starzak and A. Napieralski, "Silicon carbide power electronics for electric vehicles," *2015 Tenth International Conference on Ecological Vehicles and Renewable Energies (EVER)*, Monte Carlo, 2015, pp. 1-9.

[2] S. Coffa, M. Saggio and A. Patti, "SiC- and GaN-based power devices: Technologies, products and applications," *2015 IEEE International Electron Devices Meeting (IEDM)*, Washington, DC, 2015, pp. 16.8.1-16.8.5.

[3] A. Bindra, "Wide-Bandgap-Based Power Devices: Reshaping the power electronics landscape," in *IEEE Power Electronics Magazine*, vol. 2, no. 1, pp. 42-47, March 2015.

[4] B. Ozpineci, L. M. Tolbert, S. K. Islam and M. Hasanuzzaman, "Effects of silicon carbide (SiC) power devices on HEV PWM inverter losses," *Industrial Electronics Society, 2001. IECON '01. The 27th Annual Conference of the IEEE*, Denver, CO, 2001, pp. 1061-1066 vol.2.

[5] S. Yin *et al*., "Evaluation of power loss and efficiency for 50 kW SiC high power density converter," *2016 Asian Conference on Energy, Power and Transportation Electrification (ACEPT)*, Singapore, 2016, pp. 1-6.

[6] M. A. Samonig, G. Stojcic, S. Hecht, P. Nussbaumer and T. M. Wolbank, "Interactive simulation for teaching the influence of power management on hybrid electric cars overall energy consumption," *2013 7th IEEE International Conference on e-Learning in Industrial Electronics (ICELIE)*, Vienna, 2013, pp. 120-125.

[7] I. Sefik and T. Hiyama, "Performance evaluation of hybrid powertrain system simulation model for Toyota Prius car," *International Aegean Conference on Electrical Machines and Power Electronics and Electromotion, Joint Conference*, Istanbul, 2011, pp. 404-407.

[8] R. Vrtovec and J. Trontelj, "SiC MOSFETs in automotive motor drive applications and integrated driver circuit," Microelectronics Proceedings - MIEL 2014, 2014 29th International Conference on, Belgrade, 2014.

[9] E. J. Dede, J. Jordán and V. Esteve, "The practical use of SiC devices in high power, high frequency inverters for industrial induction heating applications," *2016 IEEE 2nd Annual Southern Power Electronics Conference (SPEC)*, Auckland, 2016, pp. 1-5.

[10] Z. Zhang, F. Wang, L. M. Tolbert, B. J. Blalock and D. J. Costinett, "Evaluation of Switching Performance of SiC Devices in PWM Inverter-Fed Induction Motor Drives," in *IEEE Transactions on Power Electronics*, vol. 30, no. 10, pp. 5701-5711, Oct. 2015.

[11] C. Schöner, A. Hensel and J. C. Z. Cambero, "Investigation of 3-level-topology MNPC for aerospace applications with SiC-MOSFET-based power modules," *8th IET International Conference on Power Electronics, Machines and Drives (PEMD 2016)*, Glasgow, 2016, pp. 1-6.

[12] Wei Fu, Qianqian Jiao, R. Hosseini, R. Cuzner and A. Lemmon, "Methodology for the volume minimization in non-isolated SiC based PV inverters," *2015 International Conference on Renewable Energy Research and Applications (ICRERA)*, Palermo, 2015, pp. 1236-1242.

[13] D. N. Zmood and D. G. Holmes, "Improved voltage regulation for current-source inverters," in *IEEE Transactions on Industry Applications*, vol. 37, no. 4, pp. 1028-1036, Jul/Aug 2001.

[14] Dong Shen and P. W. Lehn, "Modeling, analysis, and control of a current source inverter-based STATCOM," in *IEEE Transactions on Power Delivery*, vol. 17, no. 1, pp. 248-253, Jan 2002.

[15] *Haizhong Ye, Y. Yang and A. Emadi, "Traction inverters in hybrid electric vehicles,"* 2012 IEEE Transportation Electrification Conference and Expo (ITEC)*, Dearborn, MI, 2012, pp. 1-6.*

[16] K. P. M. Shafi, J. Peter and R. Ramchand, "Space vector based hybrid PWM for VSI fed variable speed induction motor drives," *2016 IEEE Annual India Conference (INDICON)*, Bangalore, 2016, pp. 1-6.
[17] A. Di Gioia and I. P. Brown, "Silicon and hybrid Si-SiC tandem inverter analytical loss characterization and comparison to PWM-modulated voltage source inverter," *2015 IEEE Energy Conversion Congress and Exposition (ECCE)*, Montreal, QC, 2015, pp. 4664-4670.

[18] D. Kaczorowski, B. Michalak and A. Mertens, "A novel thermal management algorithm for improved lifetime and overload capabilities of traction converters," 2015 17th European Conference on Power Electronics and Applications (EPE'15 ECCE-Europe), Geneva, 2015, pp. 1-10.

[19] Kim, S.C. Thermal Performance of Motor and Inverter in an Integrated Starter Generator System for a Hybrid Electric Vehicle. *Energies* 2013, *6*, 6102-6119.

2.

Review of Power Converter Topologies and Silicon Carbide Technology for Electric Traction Systems EV/HEV

The Electric Traction Systems have different elements between which emphasizes the power converters. The power converter internally is composed for various semiconductors devices (power transistors and diodes), and passive devices (resistors, capacitors and inductors), which are controlled by algorithms and modulation techniques to improve its operation and optimize its energy. Several manufacturers have concentrated their studies and research in the development of power converters with greater energy efficiency, dissipation power, size reduction and manufacturing costs.

This chapter presents an analisys of the state of the topologies of power converters used in electric traction systems, focusing in the power supply and applications of devices semiconductors to improve the operation of the power converter. Besides, it presents a brief analysis on the state of silicon carbide devices and the use in the topologies of converters in electric traction systems.

CONTENTS:

2.1 Introduction

The definition of power converter implies the transformation of one mode of energy to another. Usually there are converters that provide electrical energy from mechanics, or mechanics from energy released from chemical reactions or thermal energy [1].

The difference between the converters could be according to whether they are static or non-static. The denomination of static is related to the characteristic of not having moving parts. In contrast, an example of a converter with moving parts is the association of successive electric machines and electric motors [2]. The topologies of Dc-Dc converters and inverters are considered very important for the implementation of electric traction systems. As a result, several manufacturers and research groups focus their studies on the design of this type of topology to improve their efficiency and obtain optimal electric traction systems.

The study of these types of power converters involves the adequate knowledge of the power electronics, which is considered as an efficient alternative in applications of power converters. Most of the energy innovations use power electronics as a fundamental part for the conversion of electricity for the control of electric motors, process control of industrial equipment, transport and distribution. The power electronics is an interdisciplinary branch that includes different topics, a new stage of research in materials and manufacturing processes that contribute with new studies and optimization of converters topologies to improve the efficiency and operating features.

Due to the needs and demands of energy efficiency but with less pollutant emissions, the power electronics contribute with two fundamental roles. The first where the generation of alternative renewable energies is insufficient to meet current needs, so storage capacity is a priority and similarly coupling renewable energy systems with existing systems is very complex in this situation where the input power electronics allowing coupling the two structures [3].

The second role of power electronics is the development of systems with semiconductor elements that allow the activation of electric motors, which are implemented in traction systems in electric and hybrid vehicles [3]. The trend towards these systems has grown and the future needs for integration require great challenges. With current technology it is complicated (bulky and expensive) to reach large power densities in small spaces, the current trend is to work at higher frequencies by reducing the size of components that are normally bulky, inductors and capacitors for example. The current and voltage can be presented continuously or alternately. The power converters are responsible for transforming energy into both formats. Depending on the form of input or output of a power converter have different topologies (Fig.1).

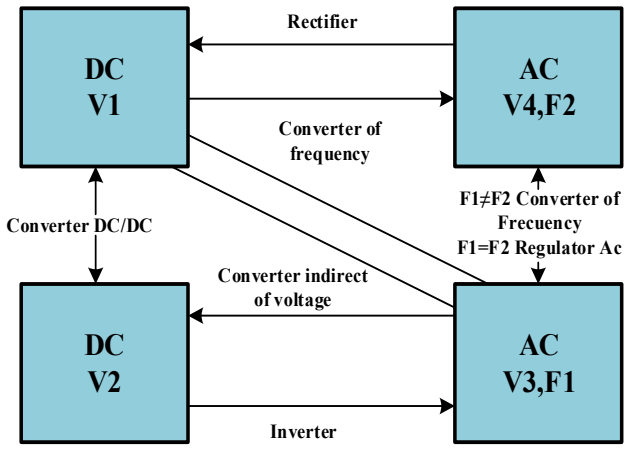

Fig.1. Topologies of power Converters in function of input and output.

The rectifier allows transforming to the voltage AC to constant or variable DC voltage, there are controlled rectifiers and uncontrolled rectifiers and uncontrolled rectifiers are those that use diodes as rectifying elements, whereas the controlled use thyristors or transistors.

Phase control regulator allows to transform the AC current from constant voltage to AC of variable voltage, allows to regulate the voltage that receives a load supply with AC. Do not allow to vary the frequency.

Inverter; allows transforming the DC voltage and current to AC voltage and current with variable frequency. These topologies are more use in electric traction systems.

The frequency converter transforms the AC voltage to AC allowing varying the frequency always being the output frequency lower than the input frequency.

The power converter DC/DC transforms the DC voltage to DC voltage or current fixed or variable.

Rectifiers, DC-DC converters and power inverters can be found in electric powertrains for the electrical vehicles.

2.2 Review of power converters

A converter is a system that has the objective of converting electric energy into two different formats, DC voltage or current in AC voltage or current. In addition, important aspects such as efficiency, bidirectional, volume, reliability and technology should be considered in the system of power converter [4]. The Fig. 2 shows a basic converter structure.

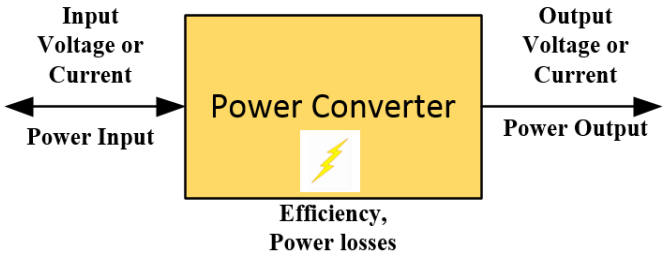

Fig.2. Structure basic of power converter.

The power converter for application in electric traction system can be classified in function of four parameters, for power supply, the switching activation, for topology and control technique (Fig.3).

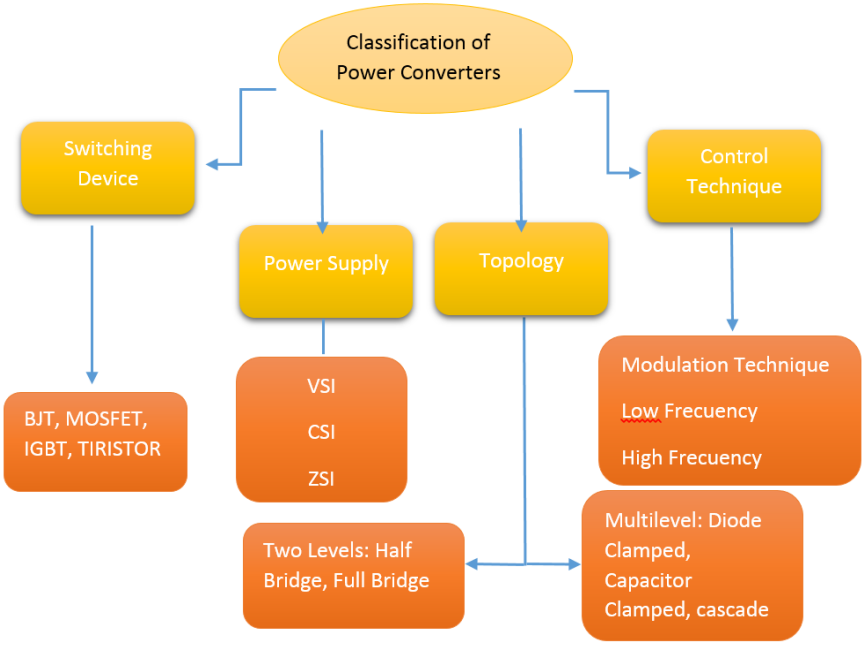

Figure 3. Classification of power converters.

For the switching device the power converters can be designed with Mosfet, TBJ, IGBTs and thyristors [5]-[6], the number of devices depends on the selected topology if it is single-phase, three-phase, etc. Also, consider whether they are two-level or multi-level stages where devices increase (Fig.4).

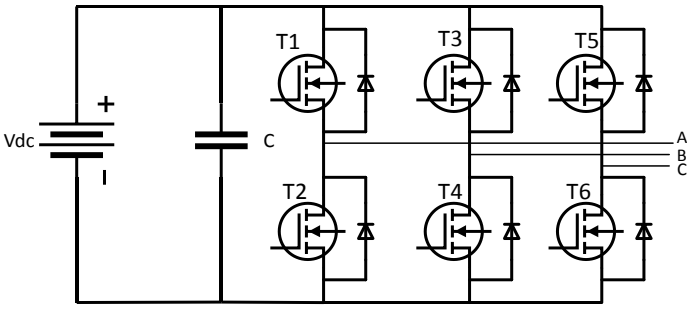

a) Two level topology

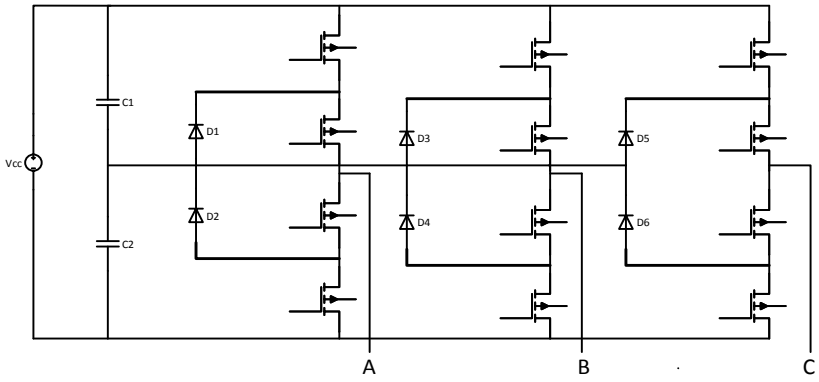

b) Three level Topology by fixed diode.

Fig.4. Topologies with various devices of switching.

Considering the power supply the power converters can be voltage source inverter VSI and current source inverter CSI [7]-[8], these two types of converters have the structure shown in Fig. 5.

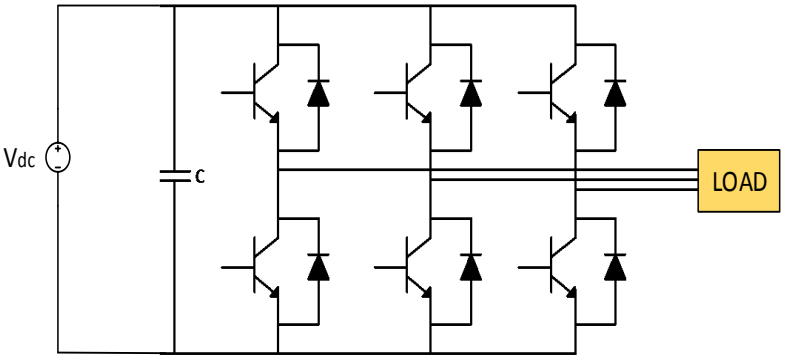

a) VSI Topology

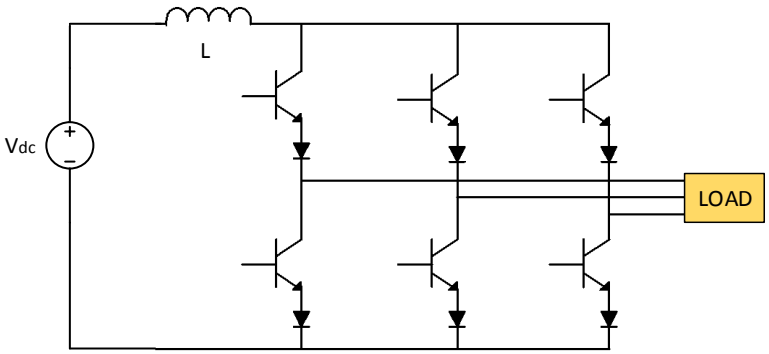

b) b) CSI Topology

Fig.5 Types of Power converters for power supply.

The VSI topology is the more used in electric traction systems for electric and hybrid vehicles, this is because the energy storage devices for electric and hybrid vehicles are battery voltage [9], it has three legs, and capacitor of high power, in each leg there are two activation

elements can be power transistors FETs, MOSFETs and IGBTs. For this topology in applications for electric traction systems is need the use of a DC / DC bidirectional power converter for the purpose of increasing the input voltage in the case of commercial vehicles such as Toyota manufacturer, coupled in a single module assembly power converter for controlling two bidirectional motors (Fig.6), in conjunction with the DC / DC [10].

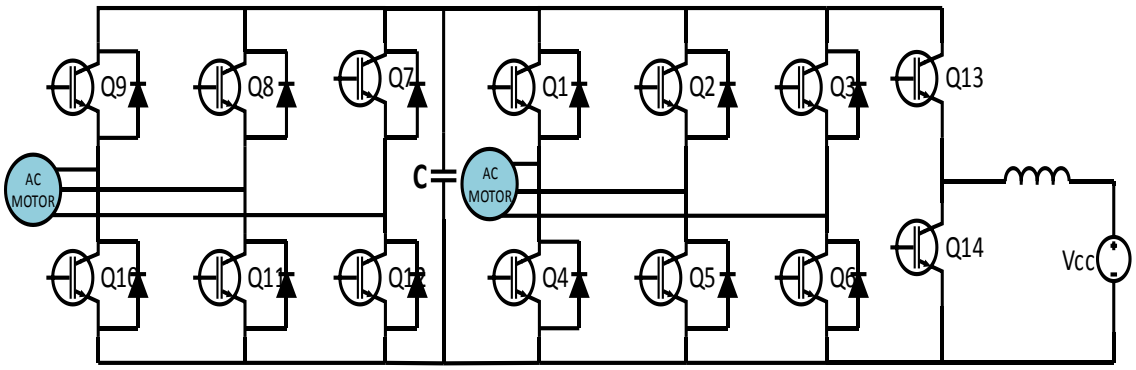

Fig. 6. VSI topology with DC-DC power converter.

This topology uses a large capacitor in the DC bus to filter the input pulse stream and maintain a constant voltage level. In HEV/EV applications, the cost and volume of capacitors could be more than 30% of the inverter [9]. The switching of the transistors must be at intervals and it cannot be active at the same time two of the same branch because that would cause a short circuit. Therefore, it implies the need for a time-out which will bring some distortion of the output current AC, which increases ripple torque [11]. This is particularly evident when the engine speed is low.

The current source inverter (CSI) is a different topology that has a coil that replaces the capacitor and is used as the energy storage component (Fig.7). This topology have several advantages, such as high voltage capability, short-circuit protection and sinusoidal output voltage by the effect of the output filter capacitors AC, which are much smaller than the capacitor in the voltage source inverter [12].

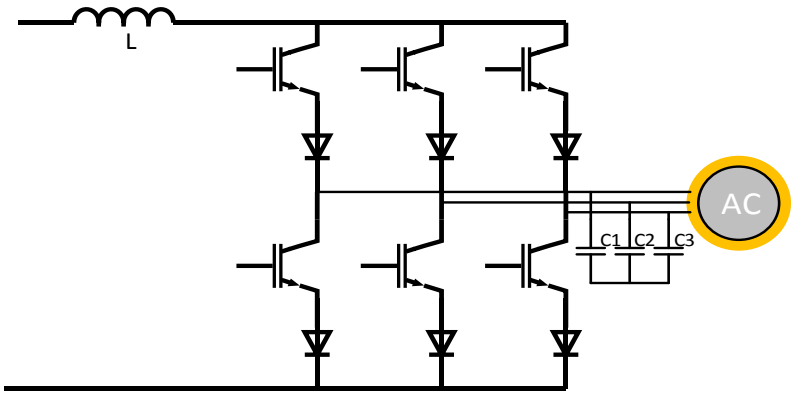

Fig. 7. Current source Inverter Topology.

In electric traction systems, this topology has increased its research, in several works; analyze its reliability, performance within these systems [13] - [14]. The CSI topology offers important advantages for electric traction system: no need antiparallel diode, provides natural action natural protection circuit, provides sinusoidal voltages to the motor due to the effect of AC output filters capacitors, and can increase the output voltage at a higher level than the source voltage to activate the motor to operate at higher speeds. These advantages may translate into substantial cost reduction of the inverter in the volume, higher reliability and improved engine efficiency and lifetime. All these features make CSI topology generate interest for applications in EV / HEV [14]. However, the CSI converter need a current source as input satge.

The impedance network source power converter (ZSI) topology can be used for this function. This topology has an impedance network Z that is coupled to the input of the inverter; the voltage can be increased by controlling the shots through the interval times of the inverter, therefore it does not need a DC / DC converter, and it obtains a buck-boost topology [15].

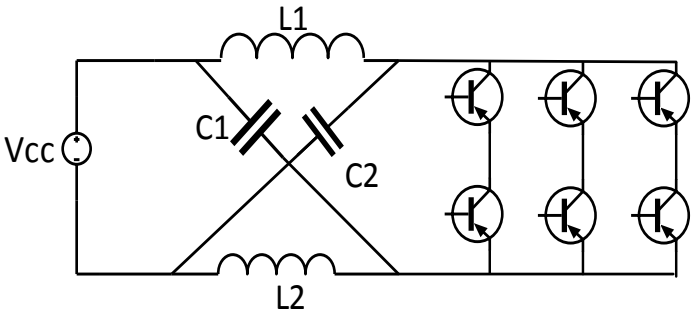

Fig. 8. Impedance Z Network Inverter Topology.

This type of converter presents problems such as the discontinuous input current in the pulse mode when the converter is powered by voltage and high current of stress in the case of powered by current, although there are some proposals that allow to solve these disadvantages [16] - [17].

In addition, for the operation of power converter is necessary the use of modulation techniques, the techniques more used are the sinusoidal pulse width modulation (SPWM) and space vector modulation. The main objective of a modulation technique is to obtain low THD waveforms of current or voltage while maintaining minimal losses, and also to allow reduction of the common voltage [18]. Various authors present in [19]-[20]-[21]-[22] novel methods of techniques of modulations for differents topologies of power converters, they focus on finding better operating conditions, efficiency and loss reduction.

2.3 Silicon carbide devices

Silicon carbide devices (SiC) are growing in importance in recent years due to its more mature manufacturing technology and increased market sales. Among the construction characteristics of these elements are its electric breakdown field eight times higher and three times more thermal conductivity this makes them much higher than Si devices, [23]-[24]. Recent research have shown that the SiC is a very promising electronic material especially for use in semiconductor devices with high ranks of work at higher temperatures, high power and higher frequencies, by these characteristics generate expectations in its application in electrical systems traction [25]-[26].

The use of these devices at high frequencies activation reduces the size of the converters; the high frequency minimizes the size of the passive elements in converter topologies [5]. In addition, SiC has a significantly lower intrinsic carrier concentration, resulting in a much higher temperature capability [6], this allows to use cooling systems more compact and small.

The SiC material has significant advantages over silicon (Fig.9), but has a disadvantage that is in the manufacturing process that is more complicated than conventional silicon; however, manufacturers such as CREE, Fuji Electric, Infineon, and ST devices have manufactured and developed with this technology at reasonable prices and quality some new methods that apply for construction.

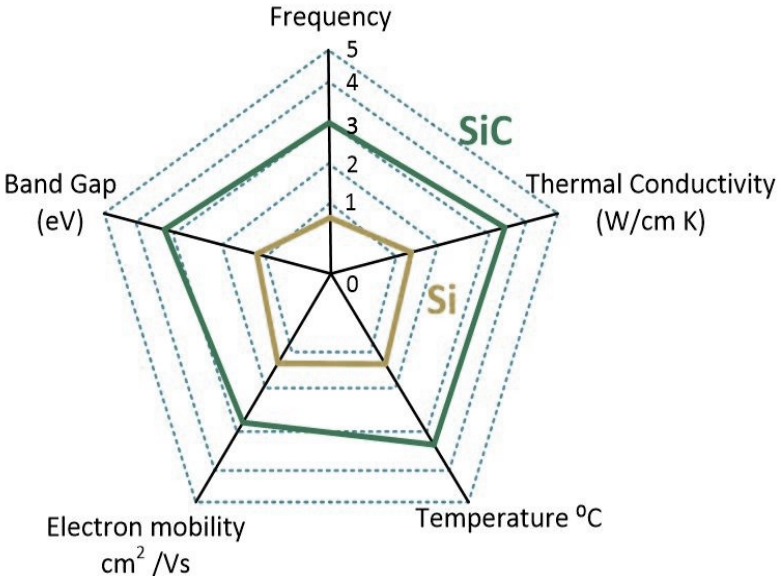

Fig. 9. SiC advantages on Si devices.

The SiC devices are considered as a suitable replacement for silicon devices, comparing the key features 4H-SiC and conventional silicon are presented in Table 1 [27].

Table1
Features of materials SiC vs Si

Features	4H SiC	Silicon
Ec Critical electric field [V/cm]	0.3	3
Eg Energy Bandgap [eV]	3.26	1.12
λ Thermal Conductivity [W/(cm K)]	4.9	1.5
μ Electron mobility [cm 2 /(Vs)]	900	1400

The SiC devices more used for converters are Diodes and Mosfet, but manufacturers have worked on developing various devices that are used in different power systems; in the Fig.10 a classification of SiC devices found on the market is presented.

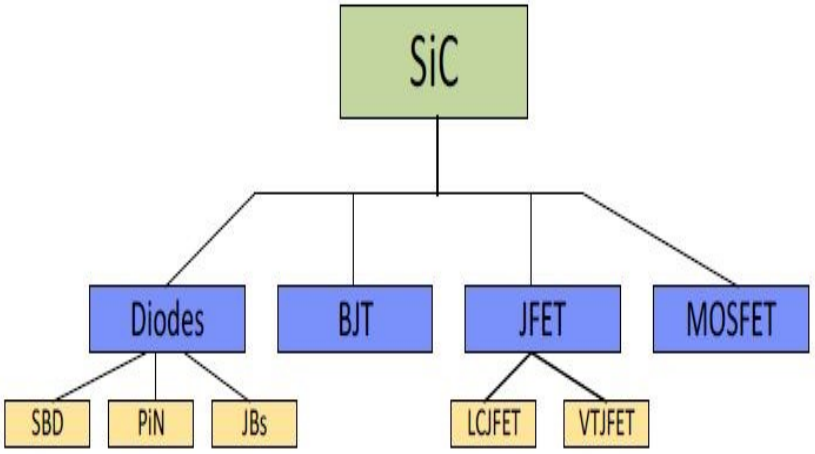

Fig. 10. Classification of SiC devices.

The SiC diodes have different features compared with ultra-fast silicon diode. The most important differences are the missing reverse recovery charge and the positive temperature coefficient of the forward voltage of the SiC diode [28]. The main advantages of these diodes are the recovery reverse and switching losses. These devices usually have a Q_{RR} low compared with the values of silicon diodes, and positive temperature coefficient that reduce EMI [29].At present there are three types of SiC diodes Sckotty barrier diodes (SBD), PiN y junction barrier Sckotty (JSB) presented in [23]-[30]. The manufacturers provide different types of diodes with ranges of very extensive work; usually can be found devices that are between ranges of 500V-1200V and 5A-100A, the Fig. 11 shows a state of properties of SiC diodes and operating ranges maximum.

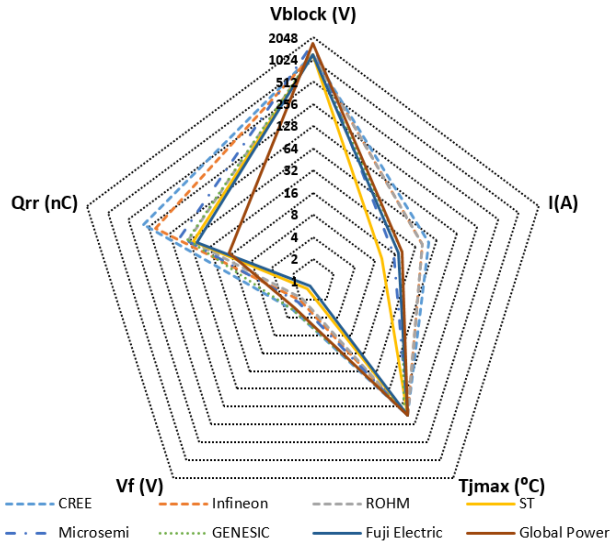

Fig.11. Properties of SiC diodes and operating ranges maximum.

The BJT SiC is a bipolar device that is off by default, the features more important of these devices are low voltage drops and low voltage driving base-emitter cancellation of base-collector and fast switching behavior of voltage [31]. The problem with these devices are controlled by current and the control driver are more difficult to implement. These devices improve compared with conventional silicon between these include the good performance of voltage and temperature preventing the oxide structure to deteriorate.

The operating ranges of these devices are in the range of 3-160 amperes and an HFE of 104. Fig. 12 shows the properties and operating ranges of the SiC BJTs and the manufacturers that produce them.

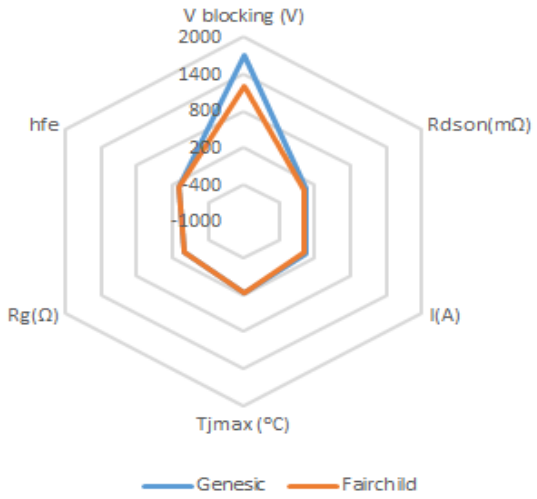

Fig. 12. Properties of SiC BJTs and operating ranges.

The JFET device substrate SiC was improved, among the most important characteristics of these devices are the threshold voltage for the power off or not depends on the temperature, p-n junctions exist that enable high temperature operation without stability problems, and can be adjusted conduction resistance with temperature [32]. These SiC elements can be found two types:

LCJFET "Lateral-Channel JFET" is a normally ON SiC JFET, where the load current can flow in both directions through the channel depending on the circuit condition [33].

The second commercially available SiC JFET is the Vertical Trench JFET (VTJFET). The type of the device, the cross-section is identical, except from the thickness of the vertical channel and the doping levels of the structure [34].The DMVTJFET does not take into structure an antiparallel diode, for that reason, it is of great interest for many applications.

The SiC MOSFET combines the normally OFF behavior on the one hand, with the voltage-controlled gate-source junction on the other hand [34]. Thus, it is a favorable power device to the designers of power electronics converters compared to the normally ON SiC JFET and the SiC BJT, which both have drawbacks from the systems perspective and employs simple driver circuits. These devices have a load similar to silicon gate IGBTs and, for these reasons, may be used with the same control circuits. The problem of these elements is the lack of robustness because the gate oxide can lose stability and reliability, but manufacturers are currently working to solve this problem [35]. The operating ranges of these devices are very broad the Fig. 13 present an analysis of the properties and work ranges between manufacturers of these devices.

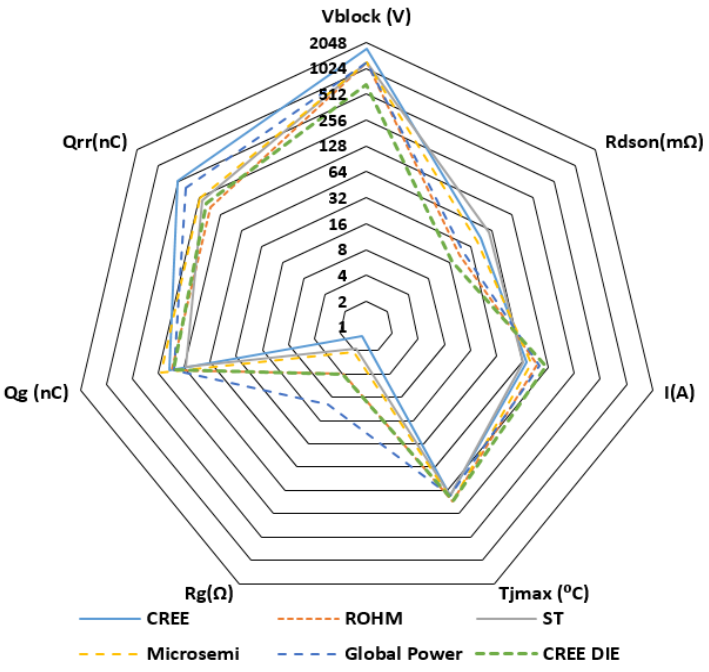

Fig.13. Properties of SiC Mosfet and operating ranges maximum.

2.4 VSI Topology in Electric Traction Systems

DC-DC boost converter followed by VSI is a common solution for the electric powertrain in EV. Manufacturers have selected this type of topology (Fig.14) based on their costs production and for being a technology already tested in vehicles present in the market. However, this topology present a series of problems that reduce the efficiency of the converter, these factors open new lines of research in alternative topologies that allow to improve efficiency and operation of the inverter. Recent research [36] has been found that the dv / dt in a converter VSI resultant modulation PWM, has a negative impact on the engine causing isolation of high frequency greater than 1 MHz with high fluctuations in the current, and electromagnetic noise on the drive system, this will involve the design of expensive filters to the output. Another disadvantage of this VSI high power density is the high temperature working systems in hybrid electric vehicle that deteriorates the capacitor bulky carrying that these systems adds [37]. High power density and high temperature deteriorate the bulky capacitor which carry these systems, increasing the risk of problems in the converter stage. So a large capacity cooling system is required [38]. Moreover, they are sensitive to EMI emissions that can generate loss of states of activation of the transistors [38].

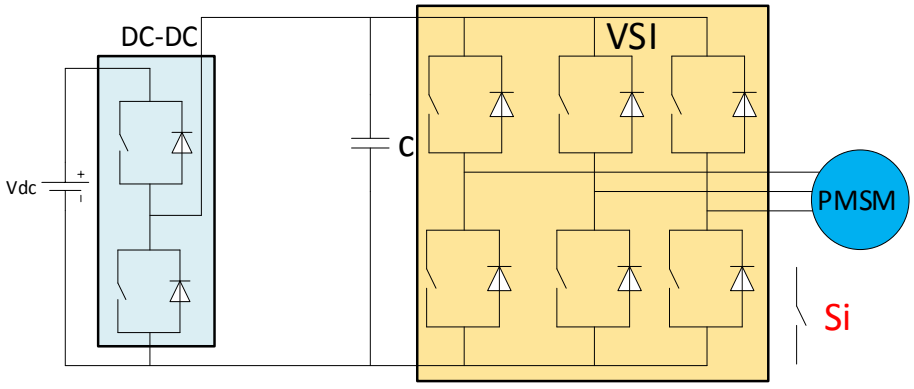

Fig.14 Voltage source inverter (VSI) topology for applications in Electric traction systems.

Regarding the applications of SiC devices in voltage source inverter (VSI) drives, several design methodologies are considered in [39]-[40]. In [41] the authors provide a methodology for overall system level design of a high-power density inverter; they use interleaved DC-DC boost topology and a three-phase voltage source inverter (VSI) with SiC modules, the aim is reduce the size, weight and loss of passive components.

In [42] the design of a high power module in combination with a low inductance DC-link and analyzed the switching behavior is considered and the significant improvements of SiC power devices offer in terms of efficiency over silicon IGBTs . The results show that the

proposed design is valid and minimizes losses, the frequency operating proposed in the design is of 40 kHz of switching.

The power loss models of a SiC VSI inverter based on the test results of latest JFET´s SiC devices and the performance of HEVs are analyzed in [43]. The conditions of switching frequency is 20 kHz, the proposal and results are validated with a study comparative between the SiC technology and IGBT´s and reduces the power losses in the motor drive and the system efficiency is improved, and the vehicles consume less energy.

In [28] authors evaluated the impact of efficiency, power density in industrial inverter drives and of dc–dc converter with new SiC devices based on analytical optimization procedures and prototype, in a section specify that the VSI topology is the most used in the electric traction systems and is considered within the category of low voltage with operating ranges between 400-600 volts of DC link and with operating frequency between 4 to 16 kHz. The results demonstrate that improve the efficiency and the use of SiC devices contribute to increase the power density.

The construction and implementation of system of air-cooling to 120 °C with the use of SiC power semiconductors (JFET´s) is presented in [44]. The topology proposed is the VSI SiC with a switching frequency of 50 kHz and the authors present a system more compact, flexible on position and low cost.

2.5 CSI Topology in Electric Traction Systems.

This topology has been gaining ground on the development of applications for electric vehicles traction systems (Fig.15) [13], with this topology is possible to get high power density and the use of this topology increases the option to implement to high frequencies, allowing the usage of SiC, and will reduce the size of the input inductor [37]. The CSI offers many significant advantages for electric vehicle applications: CSI do not need anti-parallel diodes in the switches, provides an action of short circuit protection and sinusoidal voltages to the motor due to the effect of AC output filter capacitors. Other feature is that it can increase the output voltage to a higher voltage source to activate the motor to operate at higher speeds level.

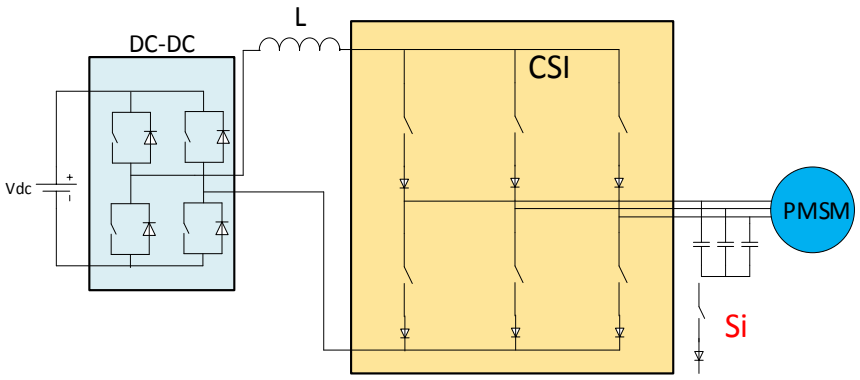

Fig.15 Current source inverter (CSI) topology for applications in Electric traction systems.

But various factors have contributed to this topology not being consolidated in the production commercial and are described in [45]. The difficulty of the battery recharge is limited in the CSI topology but can be solved with the use of bidirectional Dc-Dc power converter [46], V-I power converter [11]-[12] and impedance network source [47]-[48].

The recent achievements of CSI which are the use of new generation silicon carbide (SiC) devices (SiC JFETs and SiC Schottky diodes) and lineal control are presented in [49], the authors present the advantages and efficiency improvements. The results prove the reduction of DC-link inductor and passive output filters is possible with the use of high frequency of switching.

The research with frequency applications <20 kHz, with Si IGBTs elements are presented in [50]. Different CSI topologies are analyzed and compared to VSI topologies at the level of power losses and analyze the efficiency between the topologies presented. Recent investigations of high frequency activation> 100 kHz with JFETs and SiC diodes have created a huge influence on CSI-based applications and create possibilities for their implementation in EV / HEV traction systems [49].

The topology presented in [51]-[11], show the design of electric traction system of 55 kW of power based in CSI and V-I power converter. The V-I power converter is the solution for the problem of regeneration of the current to the battery [12]. The topology use RBIGBT modules to 15 kHz of switching frequency. The modeling and experimental results show the CSI can drive the motor to rated speed even at reduced dc source voltage levels.

2.6 Impedance Network Source Power Converter in Electric Traction Systems.

Research and development of this topologies of converters have been increasing since 2002; the use of news topologies of impedance network source have allowed increase the studies and analisys to the point of considering them as an emerging topology in electric traction systems due to their ability to work, and save component costs by using a single conversion stage [52]-[53]-[54]. The topologies of power converters with impedance network more used in electric traction systems is the Quasi Z for voltage-fed and current-fed (Fig.16). These topologies provide a buffer between the source and the inverter bridge and facilitates a short- and an open-circuit at any time depending on the mode of operation, that do not allow in the VSI and CSI conventional topologies in [55]-[56] detailing these advantages.

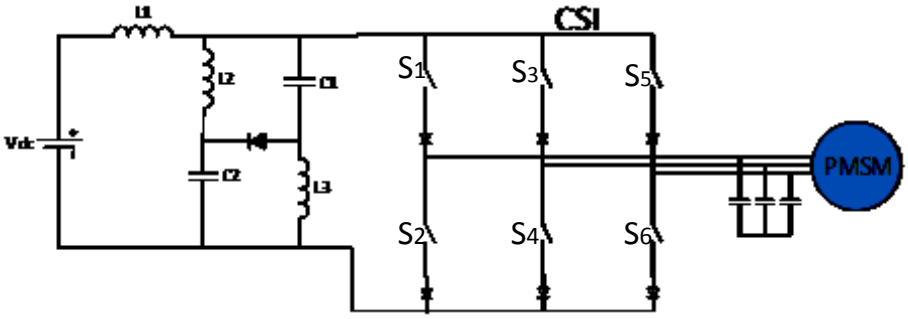

a) Quasi Z Current Source Inverter.

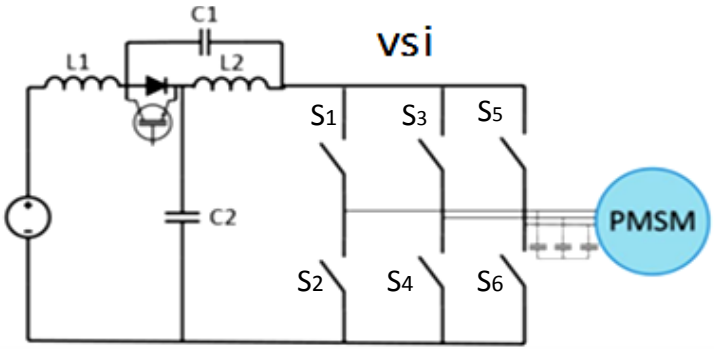

b) Quasi Z Voltaje Source Inverter.

Fig.16. Quasi Z impedance Source network converter topologies in electric traction systems.

A point to favor of this topology is the efficiency and low cost, compared with the conventional topologies, this requires smaller inductors and capacitors with high reliability with respect to the reduction of EMI emissions [57].

The authors present in [58], a control strategy for Z power converter VSI with conventional Si devices to 30 kHz of frequency of switching. The results show the reducing both the overestimation of the dc bus voltage and losses in the inverter. In [59] the authors present a improved control strategy for a quasi Z power inverter (QZSI) in electric traction system, the aim is to improve the efficiency of the powertrain, they use the sliding-mode control (SMC) method in the power converter whereas flatness-based control is proposed to drive the actuator for generate the peak dc bus voltage reference. The result shows improvements in the efficiency and reduction of the size of passive elements.

The research presented in [60] shows the comparison between differents topologies with alternative topologies such as Z-source inverter (ZSI) or quasi Z-source inverter (QZSI) and analyzed differents features such as stress in its elements passive elements weight, size, or cost. The currents rms values, the step-up voltage ratio and the power losses are also considered. For the analisys the IGBTs devices are used to 10 kHz of switching frequency. The results show that the QZSI present advantages in terms of passive elements size since the stored energy during one operating cycle is lower than that for the conventional topologies.

The use of silicon carbide devices in Quasi Z power converters are analyzed in [61], the features and comparison with the Si devices are discussed. The results obtained confirm the beneficial influence of SiC power devices on the performance of these topologies of power inverter. Besides, the power losses of quasi-Z source converter with SiC power devices was significantly reduced in comparison with Si-IGBT, this indicates that the use of devices is promising within these topologies.

The use of impedance source network in power converters in electric traction systems have added news lines of development in powertrain systems for electric vehicles; its use in applications and prototypes allows to overcome the barriers and limitations of the topologies VSI and CSI; improving the efficiency and relation of weight volume in the designs of electric traction systems.

But the non-consolidation of these topologies within electric traction systems is due to the fact that in their design, modifications must be made to obtain bidirectional topologies that allow the recovery of energy. Furthermore still making these modifications the energy recovery is not constant only takes place for short times.

2.7. References.

[1] A. Emadi, A. Khaligh, C. H. Rivetta and G. A. Williamson, "Constant power loads and negative impedance instability in automotive systems: definition, modeling, stability, and control of power electronic converters and motor drives," in IEEE Transactions on Vehicular Technology, vol. 55, no. 4, pp. 1112-1125, July 2006.

[2] V. Valdivia, A. Barrado, A. Lázaro, M. Sanz, D. López del Moral and C. Raga, "Black-Box Behavioral Modeling and Identification of DC–DC Converters With Input Current Control for Fuel Cell Power Conditioning," in IEEE Transactions on Industrial Electronics, vol. 61, no. 4, pp. 1891-1903, April 2014.

[3] M. Elbuluk and N. R. N. Idris, "The role power electronics in future energy systems and green industrialization," 2008 IEEE 2nd International Power and Energy Conference, Johor Bahru, 2008, pp. 1-6.

[4] R. Karimi, T. Koeneke, D. Kaczorowski, T. Werner and A. Mertens, "Low voltage and high power DC-AC inverter topologies for electric vehicles," 2013 IEEE Energy Conversion Congress and Exposition, Denver, CO, 2013, pp. 2805-2812.

[5] Mohan N, Undeland T, Robbins W (2003) Power electronics: converters, applications, and design. Wiley, New York

[6] Wu B (2006) High-power converters and AC drives. Wiley, New York.

[7] T. Nagai, G. Ando and K. Akatsu, "Consideration of CSI drive for SRM compared with VSI drive," Proceedings of the 7th International Power Electronics and Motion Control Conference, Harbin, 2012, pp. 1087-1094.

[8] S. von Malottki and K. Hameyer, "Extended base speed range by using a current-source-inverter-fed IPMSM for automotive application," 2014 16th European Conference on Power Electronics and Applications, Lappeenranta, 2014, pp. 1-8.

[9] Haizhong Ye, Y. Yang and A. Emadi, "Traction inverters in hybrid electric vehicles," 2012 IEEE Transportation Electrification Conference and Expo (ITEC), Dearborn, MI, 2012, pp. 1-6.

[10] Y. Yang and A. Emadi, "Integrated electro-mechanical transmission systems in hybrid electric vehicles," in Proc. IEEE Vehicle Power and Propulsion Conference, Chicago, IL, Sept. 2011.

[11] Su, G. and Tang, L., "A Current Source Inverter Based Motor Drive for EV/HEV Applications," SAE Technical Paper 2011-01-0346, 2011

[12] Zhiqiao Wu; Gui-Jia Su, "High-performance permanent magnet machine drive for electric vehicle applications using a current source inverter," Industrial Electronics, 2008. IECON 2008. 34th Annual Conference of IEEE, vol., no., pp.2812, 2817, 10-13 Nov.2008.

[13] Hak-Jun Lee; Sungho Jung; Seung-Ki Sul, "A Current Controller Design for Current Source Inverter-Fed AC Machine Drive System," Power Electronics, IEEE Transactions on , vol.28, no.3, pp.1366,1381, March 2013.

[14] Gui-Jia Su; Lixin Tang, "Current source inverter based traction drive for EV battery charging applications," Vehicle Power and Propulsion Conference (VPPC), 2011 IEEE, vol., no., pp.1, 6, 6-9 Sept. 2011.

[15] Fang Zheng Peng et al., "Z-source inverter for motor drives," in IEEE Transactions on Power Electronics, vol. 20, no. 4, pp. 857-863, July 2005.

[16] Y. Tang, S. Xie, and J. Ding, "Pulsewidth modulation of Z-source inverters with minimum inductor current ripple," IEEE Trans. Ind. Electron., vol. 61, no. 1, pp. 98–106, Jan. 2014.

[17] P. C. Loh, C. J. Gajanayake, D. M. Vilathgamuwa, and F. Blaabjerg,"Evaluation of resonant damping techniques for Z-source current-type inverter," IEEE Trans. Power Electron., vol. 23, no. 4, pp. 2035–2043,Jul. 2008.

[18] F. Z. Peng, "Z-source inverter," IEEE Trans. Ind. Appl., vol. 39, pp.504-510, Mar/Apr 2003.

[19] E. R. C. da Silva, E. C. dos Santos and B. Jacobina, "Pulsewidth Modulation Strategies," in IEEE Industrial Electronics Magazine, vol. 5, no. 2, pp. 37-45, June 2011.

[20] P. Qashqai, A. Sheikholeslami, H. Vahedi and K. Al-Haddad, "A Review on Multilevel Converter Topologies for Electric Transportation Applications," 2015 IEEE Vehicle Power and Propulsion Conference (VPPC), Montreal, QC, 2015, pp. 1-6.

[21] S. Huang, D. C. Pham, K. Huang and S. Cheng, "Space vector PWM techniques for current and voltage source converters: A short review," 2012 15th International Conference on Electrical Machines and Systems (ICEMS), Sapporo, 2012, pp. 1-6.

[22] Q. Lei, D. Cao and F. Z. Peng, "Novel SVPWM switching pattern for high efficiency 15KW current-fed quasi-Z-source inverter in HEV motor drive application," 2012 Twenty-Seventh Annual IEEE Applied Power Electronics Conference and Exposition (APEC), Orlando, FL, 2012, pp. 2407-2420.

[23]] J. Millán, P. Godignon, X. Perpiñà, A. Pérez-Tomás and J. Rebollo, "A Survey of Wide Bandgap Power Semiconductor Devices," in IEEE Transactions on Power Electronics, vol. 29, no. 5, pp. 2155-2163, May 2014.

[24] R. Singh and S. Sundaresan, "Fulfilling the Promise of High-Temperature Operation with Silicon Carbide Devices: Eliminating bulky thermal-management systems with SJTs," in IEEE Power Electronics Magazine, vol. 2, no. 1, pp. 27-35, March 2015.

[25] K. Kumar, M. Bertoluzzo and G. Buja, "Impact of SiC MOSFET traction inverters on compact-class electric car range," 2014 IEEE International Conference on Power Electronics, Drives and Energy Systems (PEDES), Mumbai, 2014, pp. 1-6.

[26] Jahdi, S.; Alatise, O.; Fisher, C.; Li Ran; Mawby, P., "An Evaluation of Silicon Carbide Unipolar Technologies for Electric Vehicle Drive- Trains," in Emerging and Selected Topics in Power Electronics, IEEE Journal of , vol.2, no.3, pp.517-528, Sept. 2014.

[27] R. Vrtovec and J. Trontelj, "SiC MOSFETs in automotive motor drive applications and integrated driver circuit," Microelectronics Proceedings - MIEL 2014, 2014 29th International Conference on, Belgrade, 2014.

[28] J. Biela, M. Schweizer, S. Waffler and J. W. Kolar, "SiC versus Si—Evaluation of Potentials for Performance Improvement of Inverter and DC–DC Converter Systems by SiC Power Semiconductors," in IEEE Transactions on Industrial Electronics, vol. 58, no. 7, pp. 2872-2882, July 2011.

[29] M.-S. Lee, J.-H. Lee, B.-S. Jin, J.-B. Lee, D.-W. Chung, and W. Frank, "New intelligent power module with silicon carbide diode," in International Conference on Power Electronics and ECCE Asia (ICPE ECCE), May 2011, pp. 1083–1086.

[30] J. Millán, "A review of WBG power semiconductor devices," CAS 2012 (International Semiconductor Conference), Sinaia, 2012, pp. 57-66.

[31] H. Yu, J. Lai, X. Li, Y. Luo, L. Fursin, J. Zhao, P. Alexandrov, B. Wright, and M. Weiner, "An IGBT and MOSFET gated SiC bipolar junction transistor," in Conference Record of the Industry Applications Conference, 2002, pp. 2609–2613.

[32] P. Friedrichs and R. Rupp, "Silicon carbide power devices - current developments and potential applications," 2005 European Conference on Power Electronics and Applications, Dresden, 2005, pp. 11 pp.-P.11.

[33] J. Rabkowski, D. Peftitsis, and H.-P. Nee, "Silicon carbide power transistors: A new era in power electronics is initiated," IEEE Industrial Electronics Magazine, vol. 6, no. 2, pp. 17 – 26, 2012.

[34] H. Mirzaee, A. De, A. Tripathi, and S. Bhattacharya, "Design Comparison of High-Power Medium-Voltage Converters Based on a 6.5- kV Si-IGBT/Si-PiN Diode, a 6.5-kV Si-IGBT/SiC-JBS Diode, and a 10-kV SiC-MOSFET/SiC-JBS Diode," IEEE Transactions on Industry Applications, vol. 50, no. 4, pp. 2728–2740, July 2014.

[35] M. Ostling, R. Ghandi, and C. M. Zetterling, "SiC power devices; Present status, applications and future perspective," in Symposium on Power Semiconductor Devices and ICs (ISPSD), May 2011, pp. 10–15.

[36] Y. Yang and A. Emadi, "Integrated electro-mechanical transmission systems in hybrid electric vehicles," in Proc. IEEE Vehicle Power and Propulsion Conference, Chicago, IL, Sept. 2011.

[37] Adamowicz, M.; Morawiec, M., "Advances in CSI-fed induction motor drives," Compatibility and Power Electronics (CPE), 2011 7th International Conference-Workshop , vol., no., pp.276,282, 1-3 June 2011.

[38] Haizhong Ye; Yinye Yang; Emadi, A., "Traction inverters in hybrid electric vehicles," Transportation Electrification Conference and Expo (ITEC), 2012 IEEE , vol., no., pp.1,6, 18-20 June 2012.

[39] S. K. Singh, N. K. Pilli, F. Guedon and R. McMahon, "PMSM drive using silicon carbide inverter: Design, development and testing at elevated temperature," 2015 IEEE International Conference on Industrial Technology (ICIT), Seville, 2015, pp. 2612-2618.

[40] H. Muhsen, S. Hiller and J. Lutz, "Three-phase voltage source inverter using SiC MOSFETs — Design and Optimization," 2015 17th European Conference on Power Electronics and Applications (EPE'15 ECCE-Europe), Geneva, 2015, pp. 1-9.

[41] D. Rahman et al., "Design methodology for a planarized high power density EV/HEV traction drive using SiC power modules," 2016 IEEE Energy Conversion Congress and Exposition (ECCE), Milwaukee, WI, 2016, pp. 1-7.

[42] A. Bucher et al., "Design of a full SiC voltage source inverter for electric vehicle applications," 2016 18th European Conference on Power Electronics and Applications (EPE'16 ECCE Europe), Karlsruhe, 2016, pp. 1-10.

[43] H. Zhang, L. M. Tolbert and B. Ozpineci, "Impact of SiC Devices on Hybrid Electric and Plug-In Hybrid Electric Vehicles," in IEEE Transactions on Industry Applications, vol. 47, no. 2, pp. 912-921, March-April 2011.

[44] B. Wrzecionko, D. Bortis and J. W. Kolar, "A 120 °C Ambient Temperature Forced Air-Cooled Normally-off SiC JFET Automotive Inverter System," in IEEE Transactions on Power Electronics, vol. 29, no. 5, pp. 2345-2358, May 2014.

[45] Gui-Jia Su; Lixin Tang, "Current source inverter based traction drive for EV battery charging applications," Vehicle Power and Propulsion Conference (VPPC), 2011 IEEE, vol., no., pp.1,6, 6-9 Sept. 2011.

[46] D. Lusignani, D. Barater, G. Franceschini, G. Buticchi, M. Galea and C. Gerada, "A high-speed electric drive for the more electric engine," 2015 IEEE Energy Conversion Congress and Exposition (ECCE), Montreal, QC, 2015, pp. 4004-4011.

[47] D. Cao, Q. Lei and F. Z. Peng, "Development of high efficiency current-fed quasi-Z-source inverter for HEV motor drive," 2013 Twenty-Eighth Annual IEEE Applied Power Electronics Conference and Exposition (APEC), Long Beach, CA, 2013, pp. 157-164.

[48] S. Yang, F. Z. Peng, Q. Lei, R. Inoshita and Z. Qian, "Current-fed quasi-Z-source inverter with voltage buck-boost and regeneration capability," 2009 IEEE Energy Conversion Congress and Exposition, San Jose, CA, 2009, pp. 3675-3682.

[49] T. Friedli, S. D. Round, D. Hassler and J. W. Kolar, "Design and Performance of a 200-kHz All-SiC JFET Current DC-Link Back-to-Back Converter," in IEEE Transactions on Industry Applications, vol. 45, no. 5, pp. 1868-1878, Sept.-oct. 2009.

[50] Wiechmann, E.P.; Aqueveque, P.; Burgos, R.; Rodriguez, J., "On the Efficiency of Voltage Source and Current Source Inverters for High-Power Drives," Industrial Electronics, IEEE Transactions on, vol.55, no.4, pp.1771, 1782, April 2008.

[51] L. Tang and G. J. Su, "Boost mode test of a current-source-inverter-fed permanent magnet synchronous motor drive for automotive applications," 2010 IEEE 12th Workshop on Control and Modeling for Power Electronics (COMPEL), Boulder, CO, 2010, pp. 1-8.

[52] Y. P. Siwakoti, F. Z. Peng, F. Blaabjerg, P. C. Loh and G. E. Town, "Impedance-Source Networks for Electric Power Conversion Part I: A Topological Review," in IEEE Transactions on Power Electronics, vol. 30, no. 2, pp. 699-716, Feb. 2015.

[53] Y. P. Siwakoti, F. Z. Peng, F. Blaabjerg, P. C. Loh, G. E. Town and S. Yang, "Impedance-Source Networks for Electric Power Conversion Part II: Review of Control and Modulation Techniques," in IEEE Transactions on Power Electronics, vol. 30, no. 4, pp. 1887-1906, April 2015.

[54] O. Ellabban, J. Van Mierlo, P. Lataire and P. Van den Bossche, "Z-source inverter for vehicular applications," 2011 IEEE Vehicle Power and Propulsion Conference, Chicago, IL, 2011, pp. 1-6.

[55] A. Battiston, J. P. Martin, E. H. Miliani, B. Nahid-Mobarakeh, S. Pierfederici and F. Meibody-Tabar, "Comparison Criteria for Electric Traction System Using Z-Source/Quasi Z-Source Inverter and Conventional Architectures," in IEEE Journal of Emerging and Selected Topics in Power Electronics, vol. 2, no. 3, pp. 467-476, Sept. 2014.

[56] Q. Lei, D. Cao and F. Z. Peng, "Novel Loss and Harmonic Minimized Vector Modulation for a Current-Fed Quasi-Z-Source Inverter in HEV Motor Drive Application," in IEEE Transactions on Power Electronics, vol. 29, no. 3, pp. 1344-1357, March 2014.

[57] Yonghuan Ding, Lei Li and Jiaojiao Liu, "High frequency transformer isolated cascaded Quasi-Z-source inverter," 2012 7th IEEE Conference on Industrial Electronics and Applications (ICIEA), Singapore, 2012, pp. 792-796.

[58] M. Yam anaka and H. Koizumi, "A bi-directional Z-source inverter for electric vehicles," 2009 International Conference on Power Electronics and Drive Systems (PEDS), Taipei, 2009, pp. 574-578.

[59] A. Battiston, E. H. Miliani, S. Pierfederici and F. Meibody-Tabar, "Efficiency Improvement of a Quasi-Z-Source Inverter-Fed Permanent-Magnet Synchronous Machine-Based Electric Vehicle," in IEEE Transactions on Transportation Electrification, vol. 2, no. 1, pp. 14-23, March 2016.

[60] A. Battiston, J. P. Martin, E. H. Miliani, B. Nahid-Mobarakeh, S. Pierfederici and F. Meibody-Tabar, "Comparison Criteria for Electric Traction System Using Z-Source/Quasi Z-Source Inverter and Conventional Architectures," in IEEE Journal of Emerging and Selected Topics in Power Electronics, vol. 2, no. 3, pp. 467-476, Sept. 2014.

[61] M. Li, H. Abu-Rub, Y. Liu, B. Ge and Z. Salam, "SiC power devices and applications in quasi-z-source converters/inverters," 2015 IEEE Conference on Energy Conversion (CENCON), Johor Bahru, 2015, pp. 331-336.

3.

Current Source Inverter Bidirectional Topologies and Operation.

The current source inverter (CSI) has been gaining ground in development of applications in electric traction system. This topology presents several advantages among which is the increase of the power density and the elimination of dc bus capacitors, tolerance of phase leg short-circuit conditions, better output voltage and current waveforms and the frequency of switching. For the correct operation of CSI in electric traction systems a V-I converter is required and it is responsible for the control of the regulation of input current to CSI and recovery energy in the battery system.

This chapter present an analisys of the operations of CSI topology for applications in electric traction systems. Besides, a brief analysis on differents CSI inverters topologies with power converters for the DC link current control (DC-DC; V-I and impedance network) are discussed.

CONTENTS:

3.1 Introduction

The topologies of converters with a current source are used more frequently in different industrial applications. Currently, the behavior of this topology within the electric traction systems is analyzed and studied, differents research show the several advantages and benefits of this topology.

The current source inverter (CSI) is a topology of power converter that deserves to be studied in applications for electric traction systems. The topology has an inductor instead of a capacitor and uses it as the energy storage component [1]. It has several advantages such as high voltage capacity, short circuit protections, higher power density, and a sinusoidal output voltage because of the alternating current filter capacitors that are smaller in comparison with the VSI topology [2].

This topology has gradually been gaining ground in electric vehicle traction systems considering the advantages previously described with the VSI, also can increase the output voltage to a higher level than the source voltage to activate the motor to operate at higher speeds [3]. This topology is considerate as an emerging topology within electric traction systems.

The use of this topology increases the option of working at high frequencies, which would allow of silicon carbide device (SiC) to be used, which in turn will reduce the size of the input inductor [4-5]. The comparison and features between VSI and CSI power converter are present in the Table 2.

Table 2
VSI and CSI Comparisson and Features.

VSI	CSI
VSI is fed from a DC voltage source having small impedance.	CSI is fed with adjustable current from a DC voltage source of high impedance.
Input voltage is maintained constant	The input current is constant but adjustable.
Output voltage does not dependent on the load	The amplitude of output current is independent of the load.
The waveform of the load current as well as its magnitude depends upon the nature of load impedance.	The magnitude of output voltage and its waveform depends upon the nature of the load impedance.
VSI requires feedback diodes.	The CSI does not require any feedback diodes.
The commutation circuit is complicated.	Commutation circuit is simple.

3.2 Current source inverter

The current source inverter is one of which the input of current is constant and adjustable, the output of current is independent of the load. The CSI consist in six semiconductors (Mosfet, IGBTs or SCRs) or switches with gate drive for turn On/Off control and six diodes in series. The six devices form three phase legs (A, B and C) within the inverter, the center point of each leg being a connection point for the load being driven (Fig 17). Each device conducts for an interval of 120 °; when a device is fired, it that instant activate the transistor in the same group T_1,T_2,T_3 from the top group and T_4,T_6 T_2 from the bottom group [6]. This topology presents two problems; is a topology unidirectional and has voltage boost operation making impossible to be used in electric traction systems.

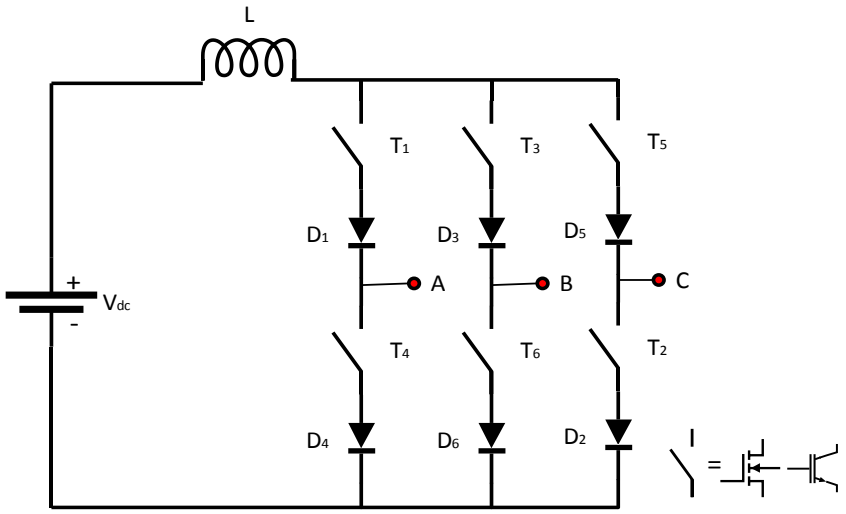

Fig.17. Current source inverter topology.

The activation signals for semiconductors T1 to T6 can be applied to the output frequency, for six-step operation, or using a high-frequency pulse width modulation scheme and space vector modulation. Six-step operation of a CSI is similar to a VSI system with each switch operating once during the output period, 2π (0.02 seconds), except with an 'on' duration of 2 π /3 radians. Each phase leg is offset by π /3 radians, creating six equal intervals (I to VI) during one output period [6]. The switching order is the number order of the switches and results in there always being one switch from top row and one switch from the bottom row conducting at all times. The Fig 18 shows the control signals for the switching devices for a constant voltage output.

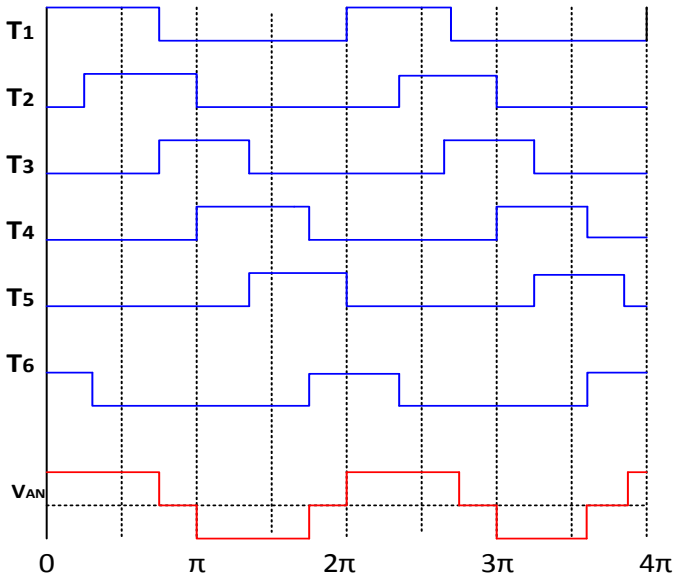

Fig.18. Gating signals for CSI six-step operation.

The CSI converter topology guarantees a good protection against faults, the same topology controls the output short circuit on simultaneous conduction in an inverter leg and therefore they are more resistant and very reliable apart from being a simple topology. This topology can be used in speed control applications of Ac motors, induction heating and permanent magnet motors.

3.3 Modulation Techniques in CSI

The pulsewidth modulation (PWM) technique have main objective obtaining waveforms of current or voltage where the losses are minimal, and this feature also allows reduction the common medium voltage and minimization of harmonics [7]. These techniques has been the subject of intensive research [8]-[9], different PWM techniques have been studied for CSI, [10-12]; but for the consulted literature it can be established that the most used methods of PWM for current source inverter are the carrier sinusoidal PWM (CSPWM) [13-15], trapezoidal modulation (TPWM) [16-18], space vector modulation (SVPWM) [19-20] and selective harmonic elimination method (SHE) [21-23].

3.3.1 Carrier Sinusoidal PWM (SPMW)

The carrier sinusoidal PWM, introduced by Schonung in 1964 [24] produce an output voltage or current waveform, this technique consists in the comparison between a sinusoidal control signal (modulating control signals) and a triangular signal (carrier signal) Fig.19. This generates gating signals for CSI using the mapping circuits, the CSPWM is generally employed with high switching frequency to obtain a near-sinusoidal output voltage and current [1].

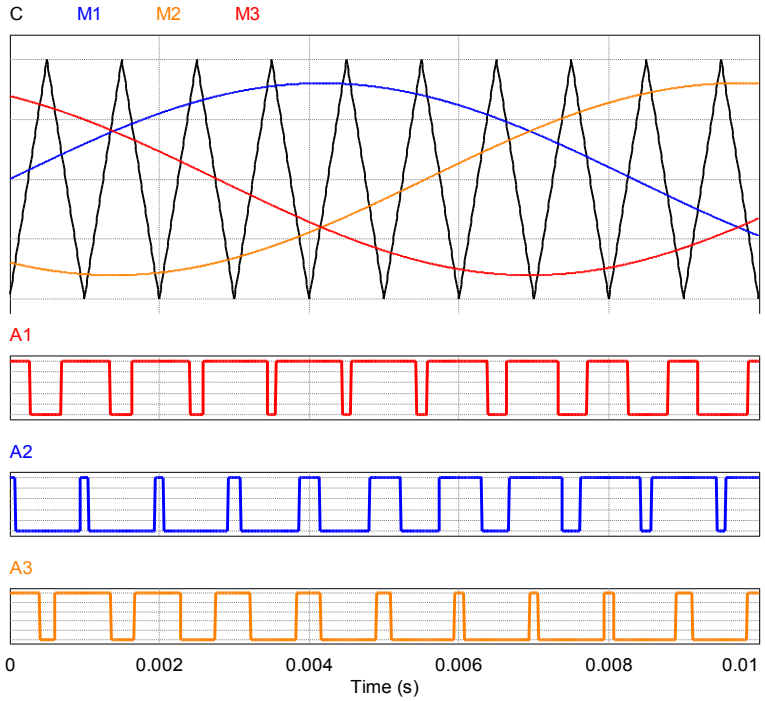

Fig.19. Sinusoidal PWM (SPWM).

In the CSPWM the modulation index m is defined as the relation between the peak amplitude A of the sinusoidal wave and the amplitude of the and the triangular signal amplitude A_m and can be represented by the expression (1) [11]:

$$m = \frac{A}{A_m} \tag{1}$$

The use of an SPWM technique allows the reduction of low frequency harmonics, for this modulates the first and the last of a half cycle (π/3 or 60°), with this condition the low frequency harmonics are reduced to a level that can be considered eliminated. For the operation of the CSI topology, it is necessary to generate typical patterns and add short-circuit pulses to obtain the activation signals (Fig.20). These pulses create a short bus through one leg of the inverter whenever either top or all bottom switches are open [25].

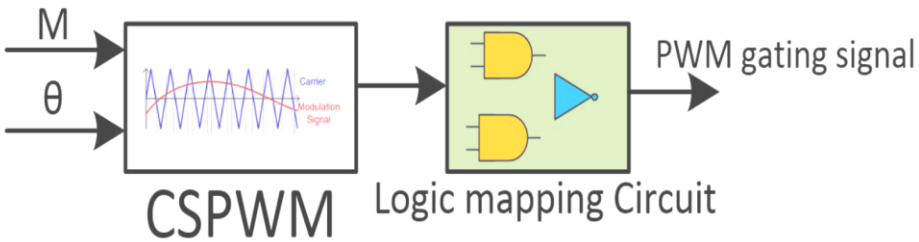

Fig.20. Carrier based sinusoidal PWM for CSI topology.

3.3.2 Space Vector Modulation SVPWM.

Space Vector modulation (SVM) technique was originally developed as a vector approach to pulse-width modulation (PWM) for three-phase inverters [26]. An SVPWM uses complex voltage or current vector for control is a technique that consists of generating sinusoidal signals to supply a high current to the load (electric motors) with less harmonic distortion. Generates spatial vectors that are placed according to the region or zone where the vector of the output voltage o current is located.

The first studies to use the complex voting vector in the PWM control were presented by Jardan [27] and the SVPWM technique was presented by Busse and Holtz [28]. It has been demonstrated that the SVPWM is an effective modulation technique for inverter topologies, because it reduces the switching time of the switches, reduces the harmonic distortion in the voltage and output current, also reduces the switching losses

The SVPWM for current source inverter there are six states actives ($\overrightarrow{I_1}$, to $\overrightarrow{I_6}$) and three states zero ($\overrightarrow{I_7}$, $\overrightarrow{I_8}, \overrightarrow{I_9}$,) Fig 21.The zero states represents the activation of two switches of the same leg which means a circulation of direct current through the coil of the converter. For an active state only one switch of the upper leg is turned on just like one of the lower leg at any time other three switches on either half leg turn on and off complementarily, this is to avoid short circuits since the output phases are connected to capacitors and if two legs are connected at the same time it can cause this problem; besides the input current must circulate through a direct circuit without causing deviations. [29]

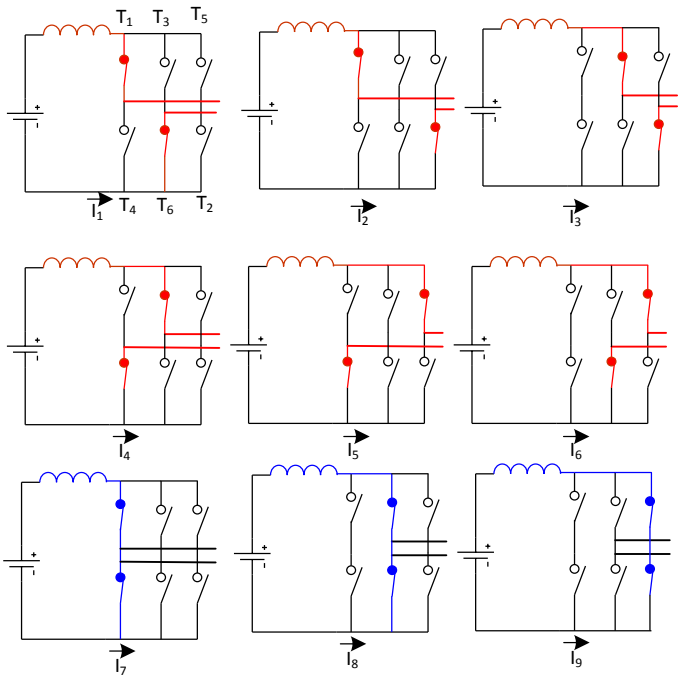

Fig.21. Space vector modulation for CSI (SVPWM-CSI).

The active states form a hexagon divided in six equal sectors and zero vectors are in the center of the hexagon Fig.22a [30]. The reference vector is given by a phase of the power converter and can be written by the expression (2) and (3):

$$I_{ref} = \frac{2}{3}\left(i_{wa} + i_{wb}e^{\frac{2\pi}{3}j} + i_{wc}e^{\frac{4\pi}{3}j}\right) \quad (2)$$

$$I_{ref} = I_{ref\alpha} + I_{ref\beta} = \left|I_{ref}\right|e^{j\theta} \quad (3)$$

Where $I_{ref\alpha}$ and $I_{ref\beta}$ is the length of the axes α and β of the complex plane Fig. 22b.

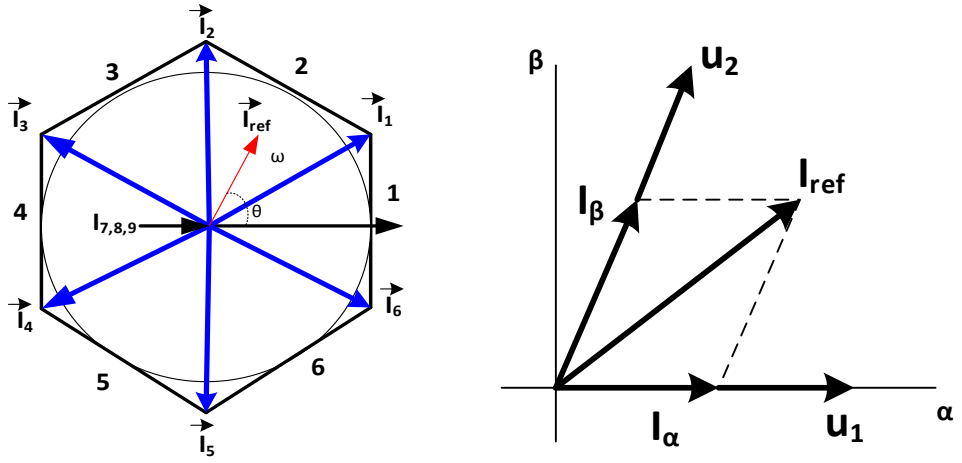

a) b)

Fig.22 Vectors of current of SVM for CSI, a) Hexagon and sector of vectors of currents, b) Irefα, and Irefβ

The technique of SVPWM approximated the reference vector I_{ref}, using the nine vectors shown in Table III, when the vector Iref is between two vectors I_K, I_{K+1}, and when these are combined with one $I_{7,8,9}$ vectors null form the vector I_{ref} [30].

$$I_K = \begin{cases} \frac{2}{\sqrt{3}} I_{DC} e^{j(k-1)\left(\frac{\pi}{3}-\frac{\pi}{6}\right)} & k = 1 \dots 6 \\ 0 & k = 1 \dots 6 \end{cases} \quad (3)$$

This implies that one, two or three zero vectors can be selected in each sector. In three-phase balanced system the current output equation is given by the expression (4)

$$I_{ref}T_s = I_i T_i + I_{i+1}T_{i+1} + I_0 T_0 \quad (4)$$

Where T_i, T_{i+1}, T_0 are the dwell times for the adjacent vectors I_i, I_{i+1},I_0 and can be calculated by the expression (5),(6),(7) respectively.

$$T_i = mT_s Sin\left(\frac{\pi}{6} - \theta + (n+1)\right)\frac{\pi}{6} \quad (5)$$

$$T_{i+1} = mT_s Sin\left(\frac{\pi}{6} - \theta - (n+1)\right)\frac{\pi}{6} \quad (6)$$

$$T_0 = T_s - T_i - T_{i+1} \tag{7}$$

Where m is the modulation index and n is the number of sector. The Table 3 shown the state active and zero of the space vector modulation for current source inverter.

Table 3
CSI space vectors.

State	On	Interrupt On	Space Vector
Zero States	[14]	1-2	$\overrightarrow{I_8}$
	[36]	3-6	$\overrightarrow{I_7}$
	[52]	5-2	$\overrightarrow{I_9}$
Activate States	[16]	1-6	$\overrightarrow{I_1}=\frac{2}{\sqrt{3}}I_{DC}e^{j\frac{\pi}{6}}$
	[12]	1-2	$\overrightarrow{I_2}=\frac{2}{\sqrt{3}}I_{DC}e^{j\frac{\pi}{2}}$
	[23]	2-3	$\overrightarrow{I_3}=\frac{2}{\sqrt{3}}I_{DC}e^{j\frac{5\pi}{6}}$
	[34]	3-4	$\overrightarrow{I_4}=\frac{2}{\sqrt{3}}I_{DC}e^{j\frac{7\pi}{6}}$
	[45]	4-5	$\overrightarrow{I_5}=\frac{2}{\sqrt{3}}I_{DC}e^{j\frac{3\pi}{6}}$
	[56]	5-6	$\overrightarrow{I_6}=\frac{2}{\sqrt{3}}I_{DC}e^{j\frac{11\pi}{6}}$

This technique is the most used within three-phase inverter systems because has a wide range of modulation associated with the injection of the third harmonic automatically, has a better efficiency in DC power supply, increases the output capacity of SPWM without distorting the waveform of the output voltage of the line and avoiding unnecessary switching, which results in less power loss. Differents problems and new optimization are analyzed in [31-33] and establish several recommendations for use in different applications.

3.3.3 Trapezoidal PWM Method.

For the switching of the CSI topology the trigger pattern must satisfy two conditions: first, the input current must be continuous and second, the PWM current of the inverter must be defined. These conditions imply a restriction in the switching which consists in any instant of time there are only two switches working one in the upper part and another in the lower part of the inverter. If two switches are activated at the same time the PWM current is not defined by a commutation pattern and with only one activated the continuity of the input current deteriorates.

To comply with this rule in addition to the techniques previously studied, the Trapezoidal PWM method can be used. This method consists in comparing a triangular carrier signal with a trapezoidal modulating signal and generating the sequence shown in Fig 23. [17]- [34]

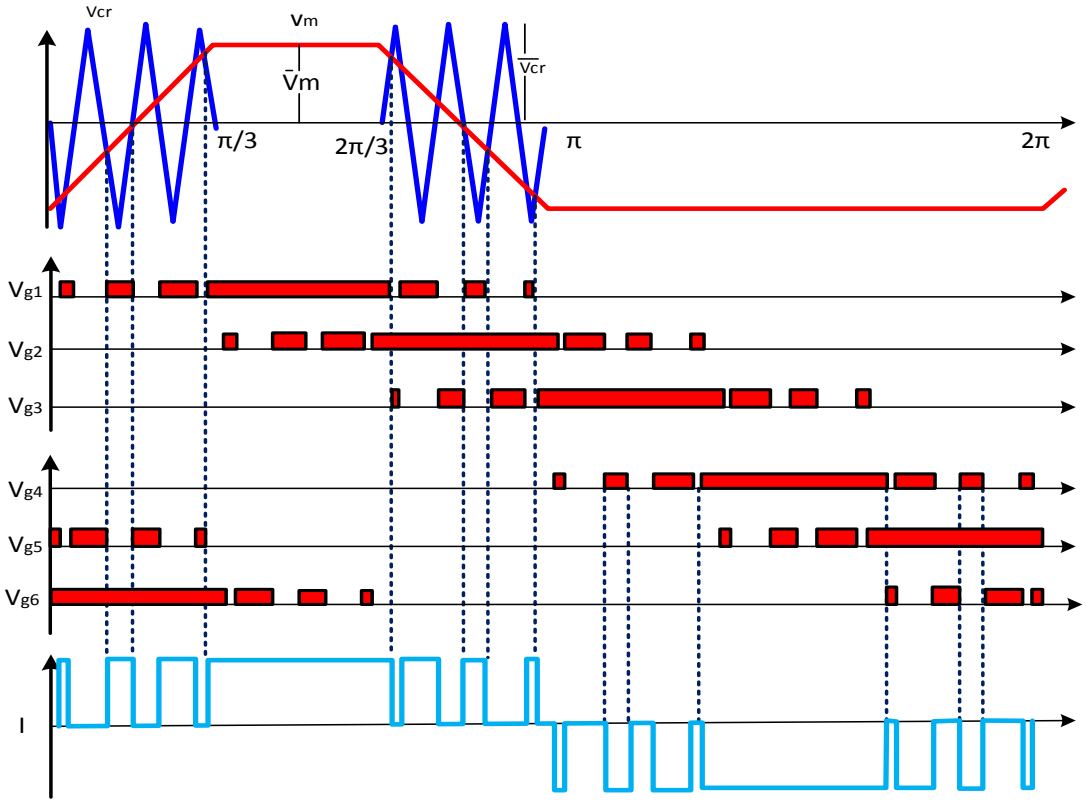

Fig.23 Trapezoidal PWM Method for CSI.

Where V_m is a trapezoidal modulating wave and V_{cr} is a triangular carrier wave. The amplitude modulation index is defined by (8):

$$m = \frac{\overline{V_m}}{\overline{V_{cr}}} \tag{8}$$

Where, $\overline{V_m}$ and $\overline{V_{cr}}$ are the values of amplitude of carrier signal and trapezoidal signal. The trapezoidal PWM method does not generate pulses in the segment of π/3 of the positive half-cycle or in the negative half-cycle of the inverter fundamental frequency. This is to comply with the switching restrictions in the CSI.

3.3.4 Selective Harmonic Elimination Method (SHE).

Selective Harmonic Elimination technique (SHE) is an alternative that has been researched along with the traditional PWM modulation technique. The objective of this technique is to generate a train of pulses such that the fundamental component of the resultant waveform has a specified frequency and amplitude [35].

His technique consists of simplifying a PWM waveform modifying his pulse pattern to eliminate the selected order of harmonics, this means that the technique uses the highest

frequency regions with the purpose of attenuating the harmonics that are in the low regions frequency

SHE is an offline strategy technique based on obtaining angles that enable the on-off switching of the static converter devices (Fig.24), both inverter topologies voltage source and current source, with the purpose of obtain a content lower current harmonic [36]. The advantages of this type of modulation are the obtaining of low switching losses is desired to remove even if a large number of harmonics and remove more harmonics than conventional PWM techniques [22]. One problem this technique is the amplitude modulation index m has no wide operating range, because does not have adequate control over the amplitude of the voltage or current [36].

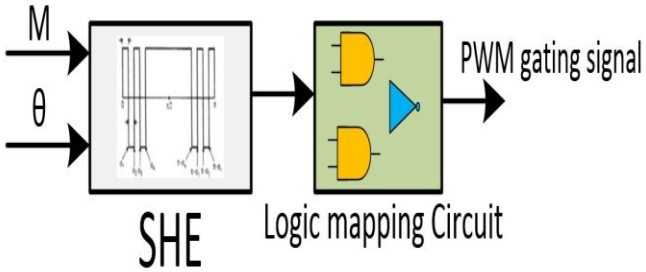

Fig.24 Selective Harmonic Elimination technique.

If a comparative study is made between these three analyzed techniques applied to the operation of the CSI, several advantages and disadvantages can be established in each technique, which are presented in Table 4.

Table 4
Analysis of modulation techniques for CSI

Technique	**Features**	**Modulation Index**	**Applications**
SPWM and TPWM	Smaller low order harmonics for $f_S > 2$ kHz Simple Modulation	$0 \leq m \leq 1$ It can be controlled	Power Inverters Medium power IGBT and Mosfet
SVPWM	Low harmonics For $f_S > 2$ kHz Complex modulation	$0 \leq m \leq 1$ It can be controlled	Power Inverter
SHE	Minimum harmonics of low order $f_S < 1$ kHz	controlled in discrete steps	Medium and high power converters

3.4 DC-DC Topologies for Current Source Inverter.

The CSI topology is considered as an alternative topology and it does not consolidate for its application in electric traction systems. The main reason for not being considered within these applications is the limitation in the regeneration of the current, this topology allows the flow of the current in only one direction. This factor has been very influential for the converter with current supply to be limited to electric vehicle traction systems.

To solve this problem several solutions are presented in [37-39] - [3], several authors propose different topologies of DC-DC and V-I converters and bidirectional impedance networks. Each topology has certain operating conditions that in some points favors and not others, so the selection of an efficient topology is essential for the use of a CSI converter in an electric traction system (Fig.25).

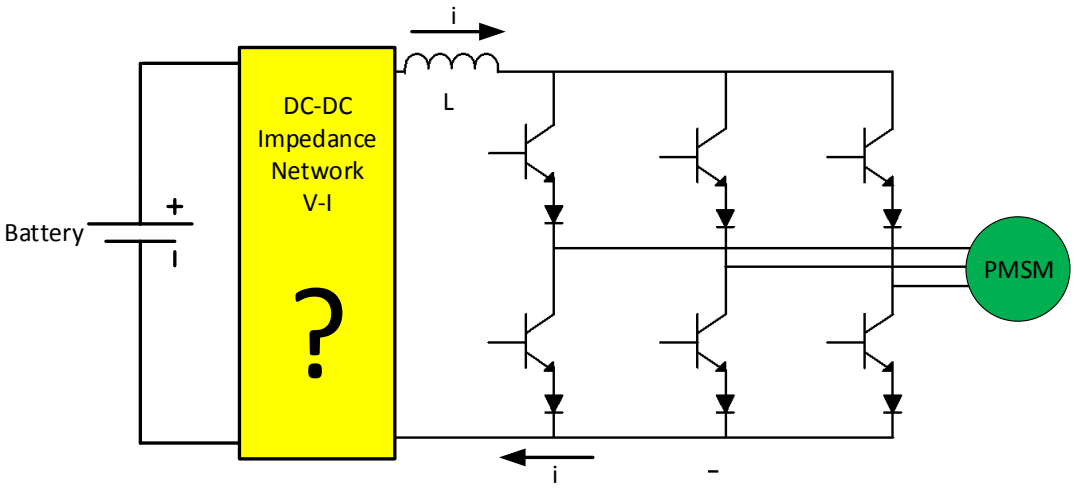

Fig.25 Current source inverter and proposed of topologies bidirectional.

In this section we study these proposed topologies to analyze their advantages and disadvantages in order to validate the most efficient for their application within the topology of CSI for electric traction system.

3.4.1 DC-DC power converter full bridge for CSI.

This topology is bidirectional (Fig.26), consists of four switches that are activated depending on the mode of operation. In general, this topology has two modes of operation, the first when it provides input current and the second when the current is regenerated to the battery [40].

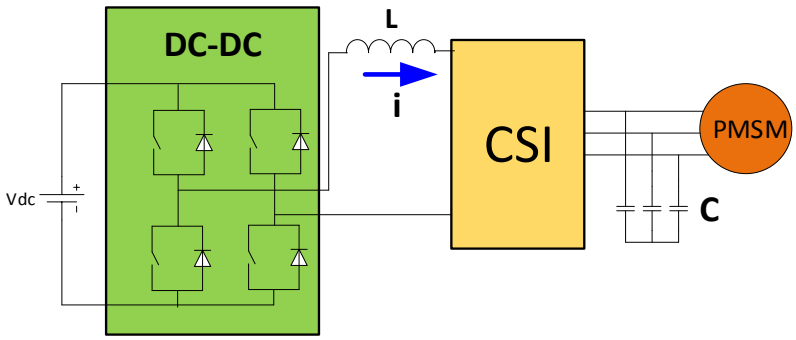

Fig.26. Current source inverter and proposed of topologies bidirectional.

The fist mode of operation consists of the activation of T_1 and T_4, the current flows from the DC / DC converter to the CSI and electric motor (Fig.27), the current has to be controlled so it is necessary to use some type of control for the switching of the transistors.

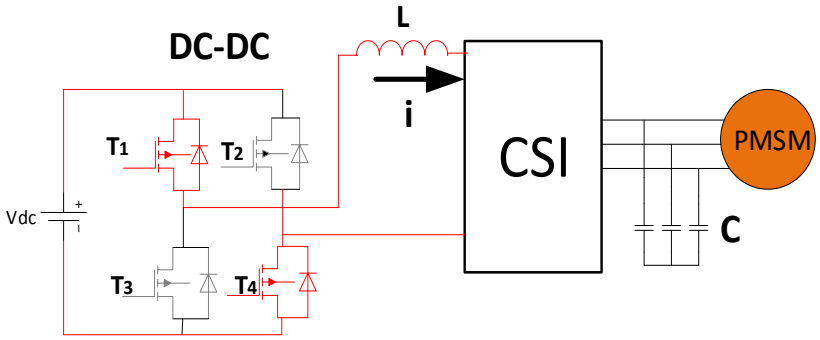

Fig.27. First mode of operation DC-DC power converter.

The second mode of operation consists of the activation of T_2 and T_3, the current flows from the electric motor through CSI to battery (Fig.28), this condition is known as regenerative braking.

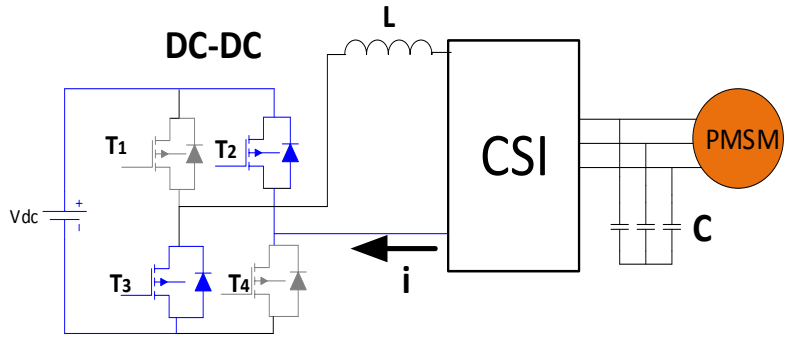

Fig.28. Second mode of operation DC-DC power converter.

Analyzing this topology in the first mode of operation in simulation with a control loop Pi for the current of output, we obtain the results shown in the Fig 29a. Without a control loop over the current, there is no stable current control output (Fig 29b), which hinders the correct functioning of the CSI converter topology.

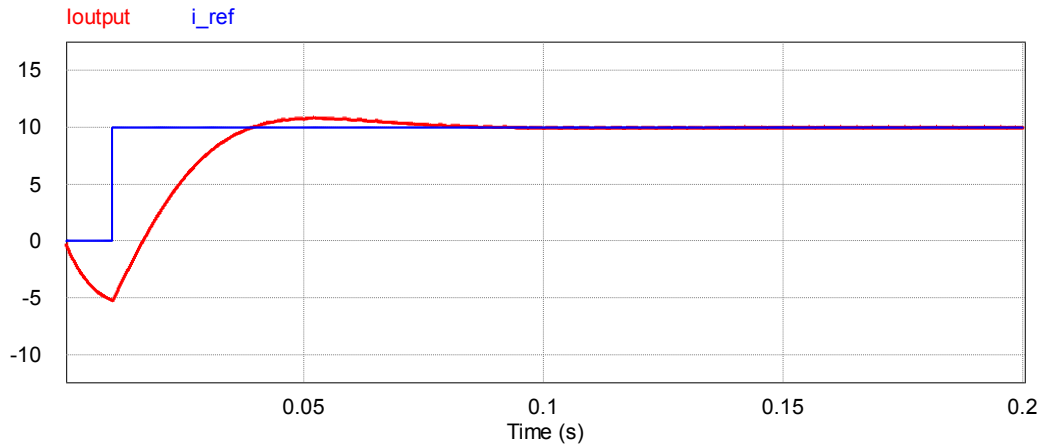

a)

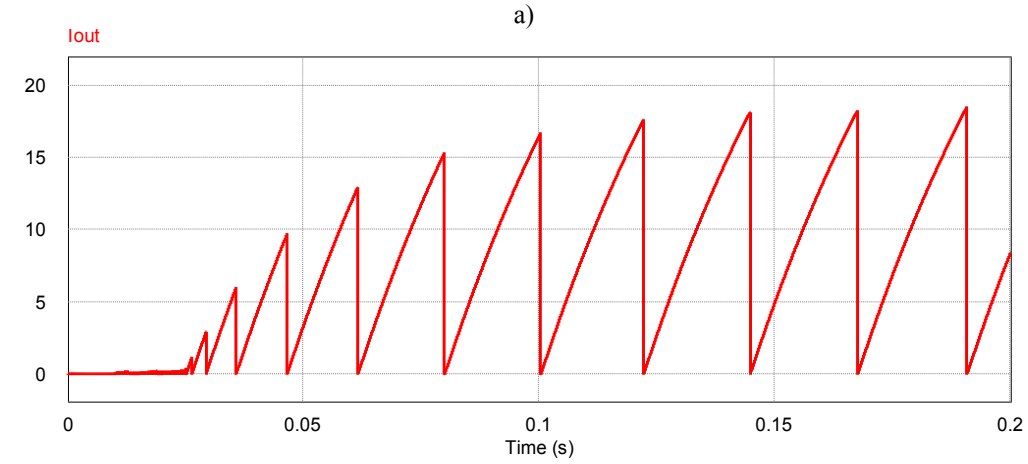

b)

Fig.29. First mode of operation in simulation, a) with control loop b) Without control loop.

The control strategy consists of defining the duty cycle to drive the switches using the sample of the circuit output current and PI control, so in this strategy we can remove the redundancy of the classic control where both current input and voltage are needed. Some of the advantages of this strategy comparing with the classic strategy is greater robustness and simplicity, less susceptibility to noise and a smoother turn-on characteristic [41]. The scheme of the control technique implemented is shown in Fig.30.

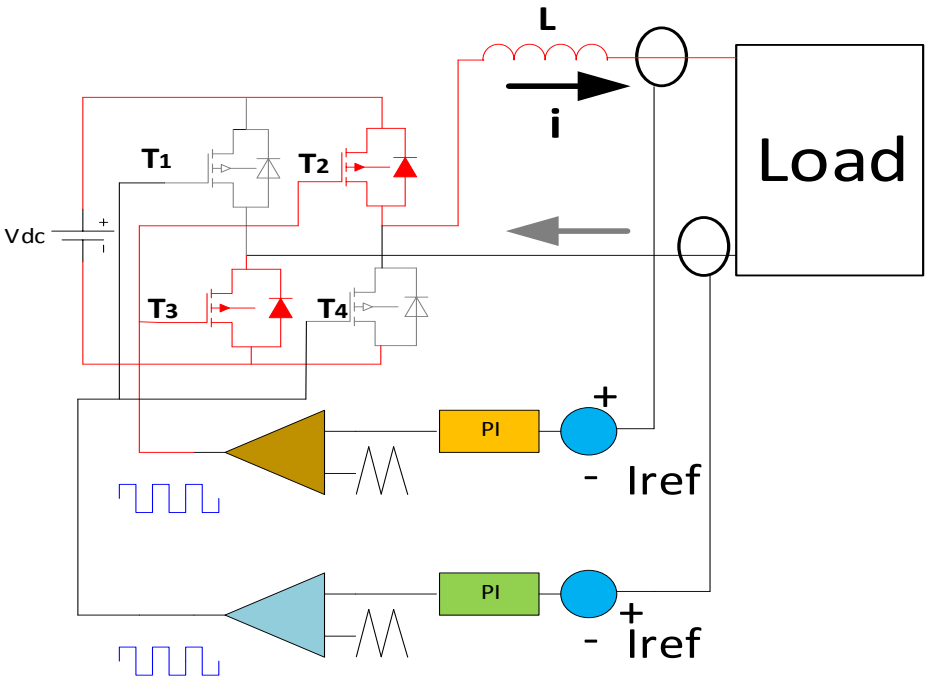

Fig.30. Control strategy for DC-DC power converter.

This topology can be a solution to the problem of energy recovery in the CSI inverter for electric traction systems, but it is not the most efficient, the use of several semiconductor devices in this Dc-Dc topology increases the losses of power by conduction and switching, which reduces efficiency in the system. In addition, the control of the activation of the transistors in the two operating modes requires the use of PI controllers.

3.4.2 Bidirectional Impedance Source Networks

The impedance networks topologies in power converters used for the development of drive systems for electric vehicles help to overcome the voltage and current limitations that frequently occur in the conventional topologies VSI and CSI [42]. In the development of power converters with an input source current and impedance network coupling, the voltage and current can be increased by controlling shooting time intervals through the converter so there is no need for a DC / DC converter [43]. The common schematic of a network with an impedance converter using power semiconductor devices used in drive systems is shown in Fig.31.

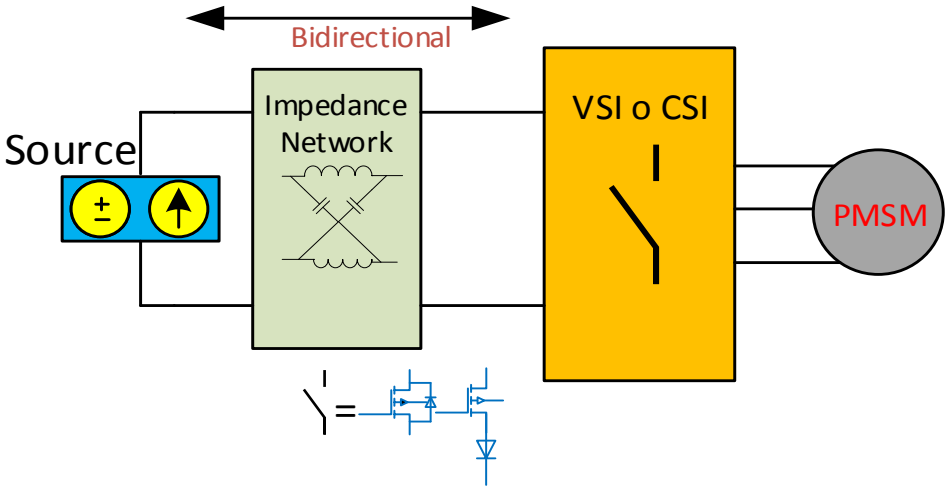

Fig.31. Schematic of power converters with impedance network for applications in traction system.

A basic network impedance is composed of linear energy storage elements, capacitors and inductors. There is also the possibility of implementing various configurations with the help of semiconductor elements such as switches and diodes [43]. For bidirectional impedance network topologies, it is necessary to know the different control strategies and modulations types for obtaining the phases, frequencies, voltage amplitude and current in the converter. A new zero switching state called Shoot-through exists in these converts. This state is caused by the short-circuiting of one, two or all three legs of the inverter [44]. These types of topologies have problems such as discontinuous current input when the ZSI is powered by voltage, high current stress in the case of current ZSI, although there are some proposals that solve these problems [45] - [46]. In the inverter output, stage is similar to a conventional voltage source inverter or current source inverter with states actives and states zeros. However, in these topologies it is incorporated an additional zero state. This state is achieved by shorting of one, two, or three legs of power converter [47]. This short circuit condition is prohibited in the conventional topologies VSI because causes its destruction. In these topologies, this condition is permissible because the network input impedance prevents short circuit in the input source [48] - [49]. The advantages of this topology is efficiency and low cost, because they require smaller inductors and capacitors when working at high frequency and they have high reliability regarding EMI emissions [50].

Several modulation techniques are proposed for use in converters with impedance networks [51]-[52]; the use of these techniques allows obtaining waveforms of current or voltage. Also, this type of converters allow the reduction of harmonics by integrating the new switching state "shoot-through" in the classical methods of modulation, which is required to achieve a minimum and effective switching semiconductor harmonic distortion. In the Fig.32, a classification of modulation techniques for power converters of two levels with impedance networks are presented and serves to meet the needs in the development of electric traction system application.

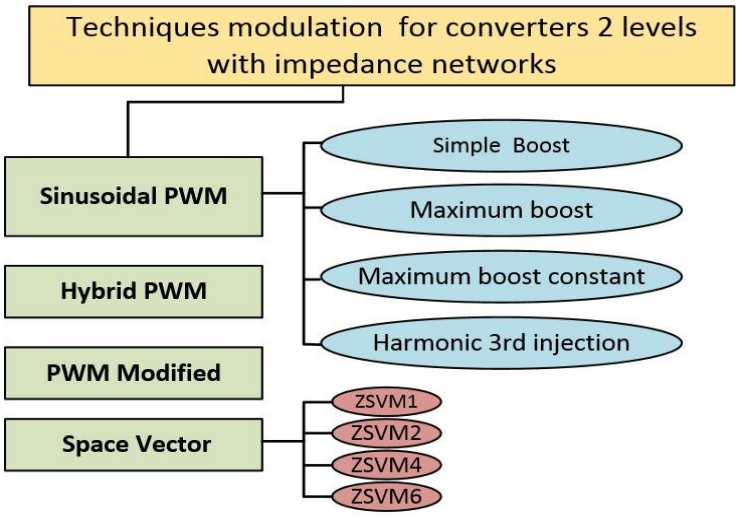

Fig.32. Classification of techniques of modulation.

The simple boost method (Fig.33) for the topologies of the Fig.16; consists in the comparing a triangular carrier signal with the sinusoidal signals or modulating system reference. Short circuit states that allow the power converter with network impedance perform the function of increasing the input voltage is by the use of two additional levels of comparison (VP + and VP-). This additional state is generated when the carrier signal is above the positive reference value VP or shoot-through signal and the modulating signal or below its negative reference signal. The modulating signal generate the shoot-through (ST) state or short-circuit and will be repeated during the application of modulation. A disadvantage of this modulation is the modulation index decreased (M) and rising state short circuit range; this increases the stress on network devices and semiconductors of the inverter [53].

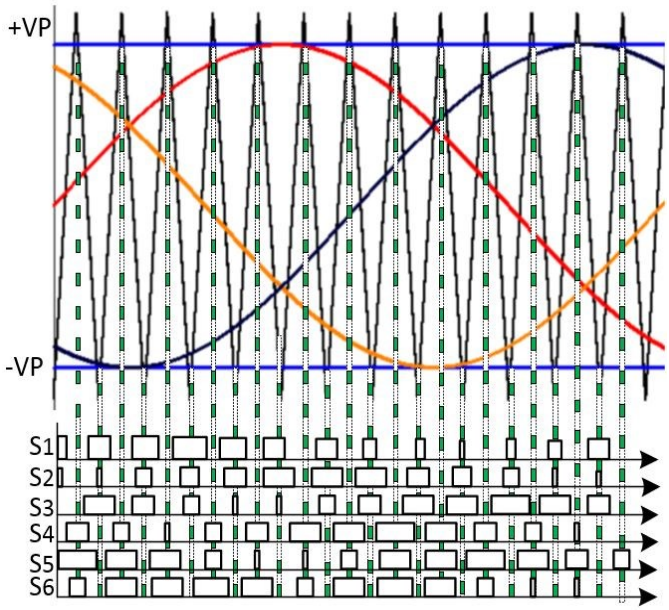

Fig.33. Simple boost method.

In this case, the duty cycle D is calculated by (9):

$$D_{op} = 1 - M \tag{9}$$

The method known as maximum boost (Fig.34) used for the topologies of the Fig 16, presented in [54] was designed to reduce stress voltage devices, and it also reduces switching losses for the output voltage compared to the single boost. The method is based on maintaining the modulation index (M) as high as possible, and the boost factor (B) as low as possible. The problem identified in this method is the time variation shoot-through state; it generates low frequency harmonics, which generates ripple in the current passive elements of the network.

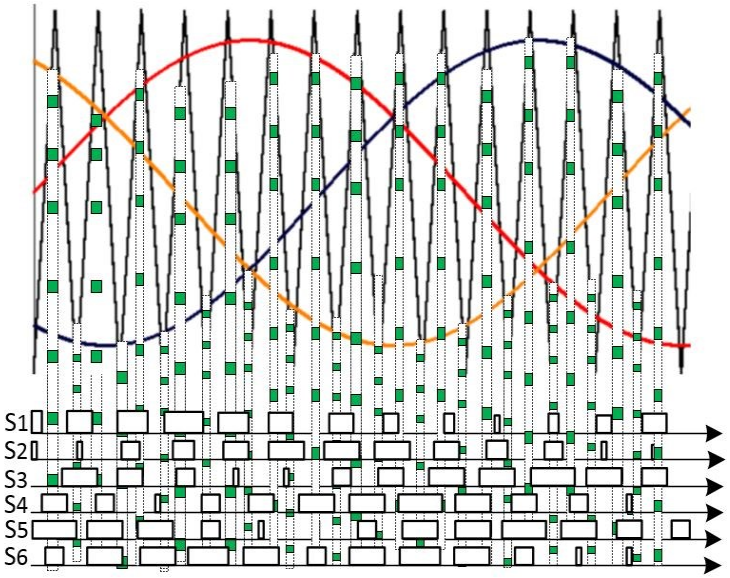

Fig.34. Maximum boost method.

The duty cycle D for this method is calculated by (10):

$$D_{op} = 1 - \frac{3\sqrt{3}M}{2\pi} \tag{10}$$

The method of maximum boost constant [55] consists in slight modification of the reference signal of the shoot-through state; using this method, a shoot-through state is obtained with a time constant through a duty cycle ratio for each switching (Fig.35). This is achieved by modifying the two additional levels of comparison VP + and VP-, the advantage of using this method is that it minimizes low frequency harmonics the generation of and current ripple in the passive elements of the network impedance [26].

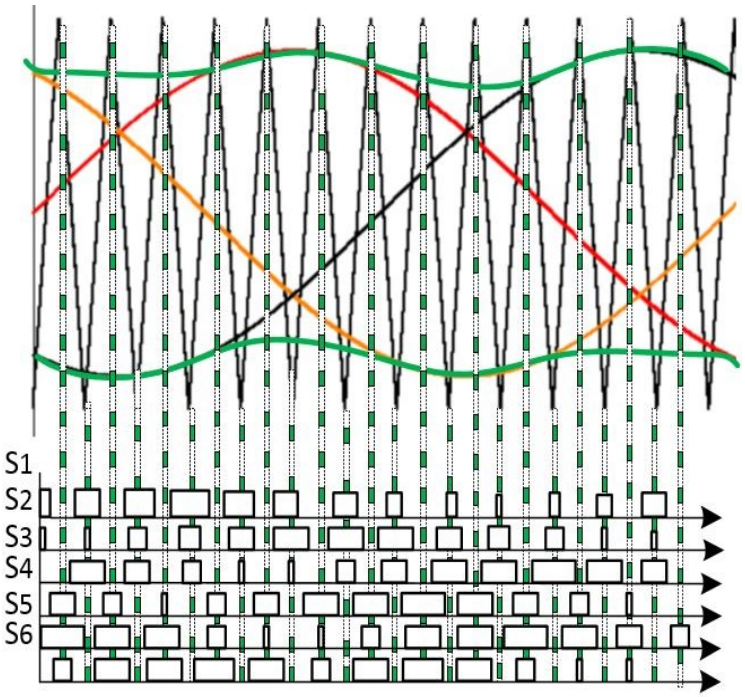

Fig.35. Maximum boost constant method.

For this method, the duty cycle ratio is calculated by (11):

$$D_{op} = 1 - \frac{\sqrt{3}M}{2} \tag{11}$$

The injection method of the third harmonic (Fig. 36) consists of the application of a range of modulation index. It extends from 1 to $2\sqrt{3}$ and third harmonic component is injected with 1/6 of the fundamental component of the magnitude of the three phases of voltages of references; the use of two additional levels comparison VP+ and VP- is necessary to obtain shoot-through states constants [53]

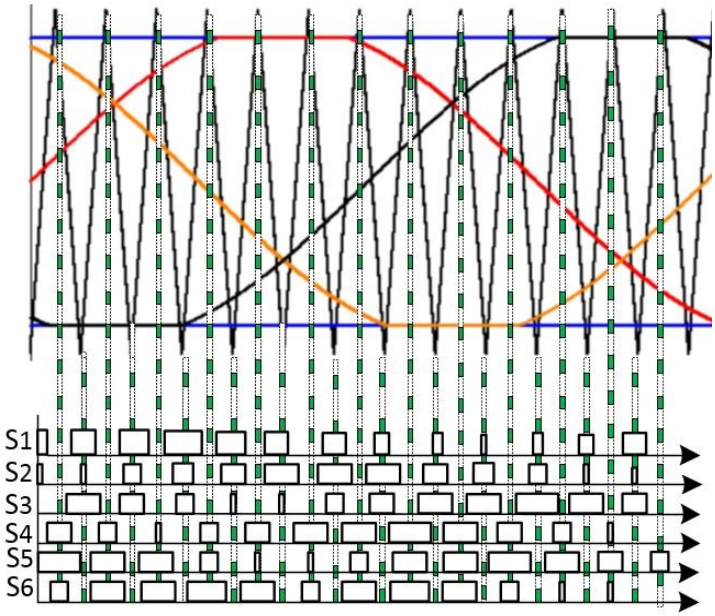

Fig.36. Method of injection of third harmonic.

The technique of space vector modulation (SVM) is a technique that is used constantly for vector control in power converters with impedance network and it presents some variations with respect to the conventional technique. This is because the presence of a new switching state called shoot-through. In [56- 58] some techniques for this type of converters are presents; its application has several advantages; the reduction of harmonics, low voltage and current stress on the passive elements and reduced losses in activation. There are three methods of space vector modulation. The first called ZSVM2 (Fig.37) where divided state while switching shoot-through (T_{sh}) into four equal parts in a cycle with a modified two-time activation [59].

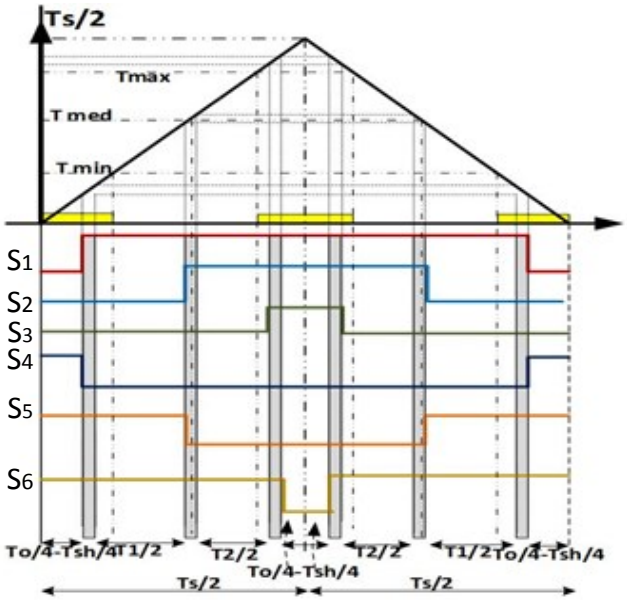

Fig.37. Modulation ZSVM2.

3.4.3 Topologies of Impedance source network for CSI.

The topologies of impedance source network used for CSI inverters are shown in the Fig.38. The first topology is the Quasi-z and the second topology is the Trans-z. This topology can increase the input voltage to meet the variable motor speed and achieve a bidirectional power flow. In addition, the impedance network allows a closed circuit for the input current during the open circuit state of the inverter and protects the switches and the inductor [60].

The second topology has the same operating principle and voltage gain regions similar to the Quasi Z topology but different stress current conditions [61].

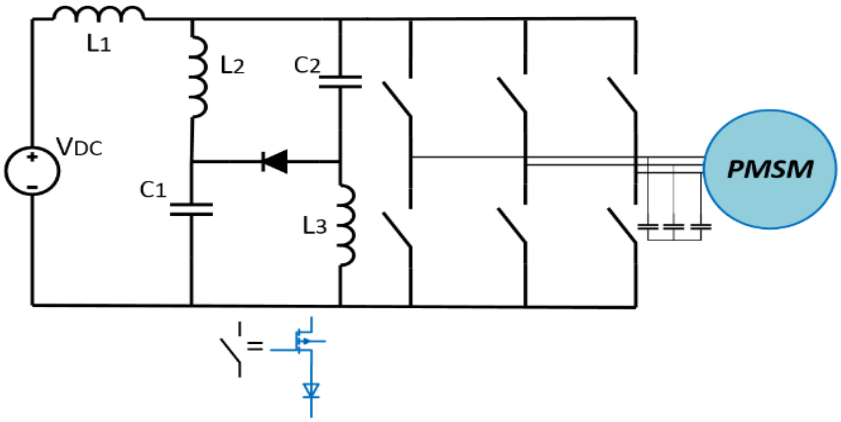

a)

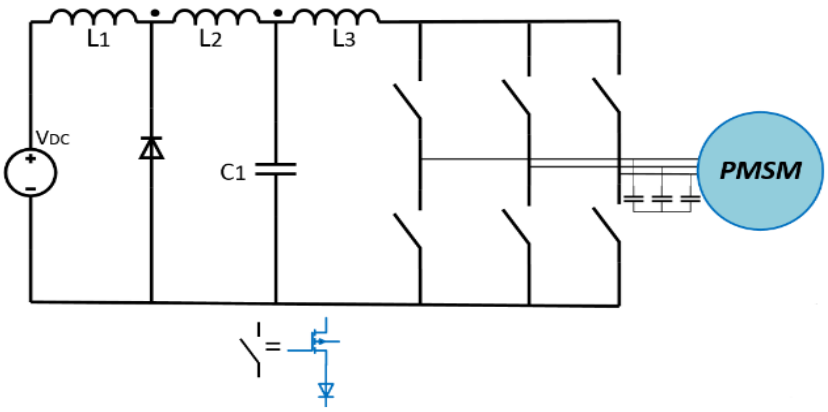

b)

Fig.38. Impedance source network topologies for CSI inverters, a) Quasi-z b) Trans-z

The topology Quasi Z has two modes of operation; continuous and discontinuous, in the continuous mode are three situations: during the first situation the inverter is in an active state and the DC link voltage V_{out} is equal to the equivalent output voltage V_{DC}, the diode is not active [62] and this situation is called active state (Fig.39a). The second mode (Fig. 39b) shows the inverter equivalent to a short circuit by turning on the upper and lower switches in the same phase leg, in two-phase legs or three phase legs together, the dc link voltage is zero and diode

is off [63]. In the third mode (Fig. 39c), called open state, the switch devices are disconnected in the inverter, which is similar to a state open, the diode is turned on and the voltage of dc link is equal to sum of voltage in each capacitor [63].

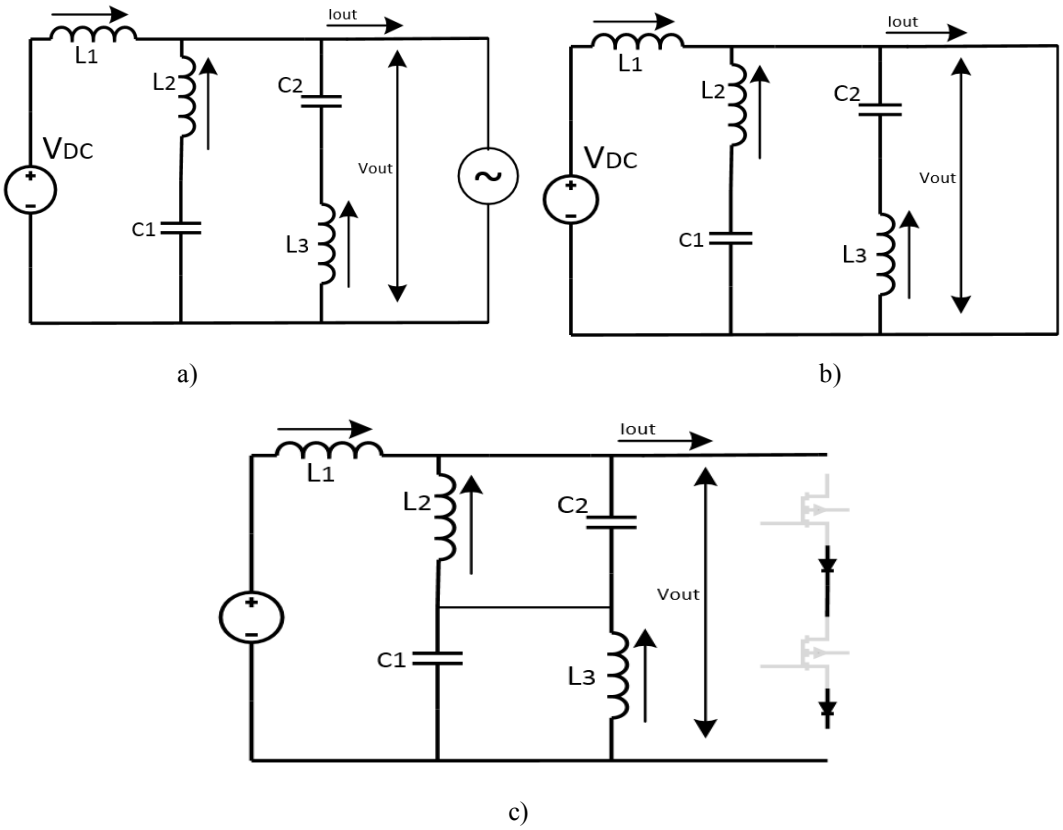

Fig.39. Modes of operation continuous in Quasi-z impedance network, a) first mode b) second mode c) third mode.

The discontinuous operation has two modes of operation. During the open state (Fig. 40a) the diode is on and the devices of inverter are disconnected; in this moment the capacitor is charging. But, in other two states the capacitor keeps discharging because the unchanged inductor current. When the second mode continuous ends, if the voltage of the capacitor decreases to a value below the output voltage at the moment that the inverter is switched to active state again the diode is working because the voltage drop is positive, but the diode of the inverter is reverse biased and this similar to an open circuit and capacitor is charged again in this new open state [62]. In the second discontinuous mode (Fig. 40b), the voltage drop in the power converter is still smaller or equal to zero and continuous in state open, and diode is off.

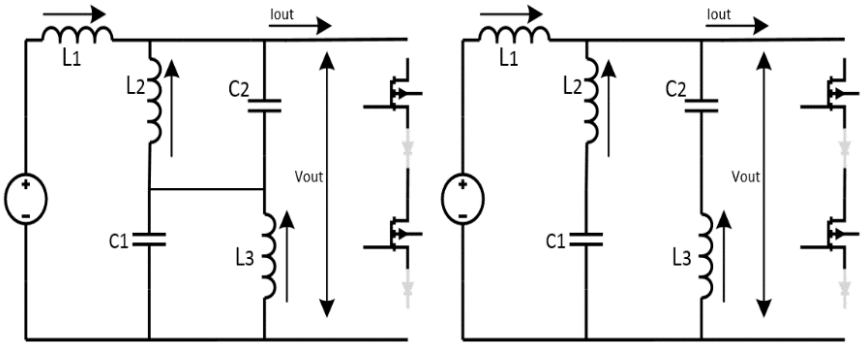

a) b)

Fig.40. Modes of operation discontinuous in Quasi-z impedance network, a) first Mode b) second mode.

The Trans-Z topology is a topology with coupling of transformer that can be represented by the circuit of Fig. 41 as seen from the inverter DC link. The topologies of impedance network Trans- Z and Trans- Quasi Z were designed to solve the problem of stress in the passive elements of the Z and Quasi Z topologies

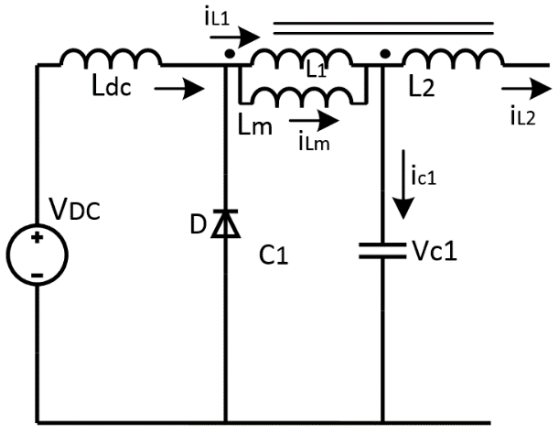

Fig. 41. Equivalent circuit of Trans-Z source inverter viewed from the DC link.

This topology has three states of operation described in Fig 38, in the first state called active (Fig.42a) the inverter work in one of the actives states, the second state (Fig. 42b) when a short circuit occurs in a leg o several of the converter, and in the third state (Fig. 42c) it is performed a shoot-through zero states [61].

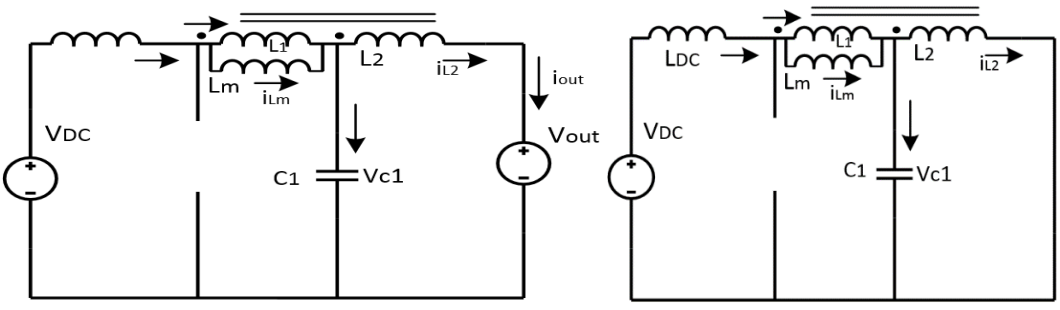

a) b)

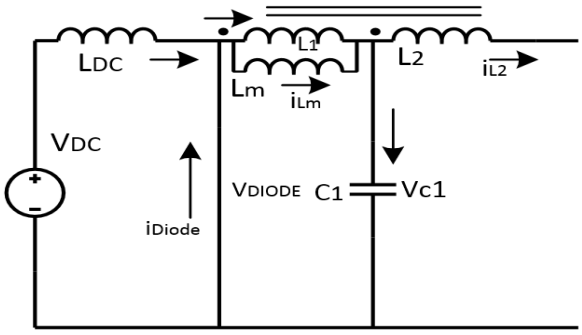

c)

Fig 42. States of operation of topology Trans-Z source inverter, a) State active; b) State Short Circuit, c) State shoot-through.

3.4.3.1 Control Techniques for Impedance Network.

For the control of these topology is important obtain a good dynamic of the power converter, this because an impedance network has a non-minimum phase behavior and can be a problem or limitation at the moment of the design of a control for the network. For the analysis of the small signal model, in this topology it is possible to work with different state variables, the input current, the current of the inductances, the voltages in the capacitors, the models obtained in this way provide a transfer function that is used for the design of the controller and also provides dynamic characteristics in the system. The circuit for small signal analysis in the topology Quasi Z is shown in Fig.43, where it is established that SD is the control variables and input voltages or capacitor the which variables to control.

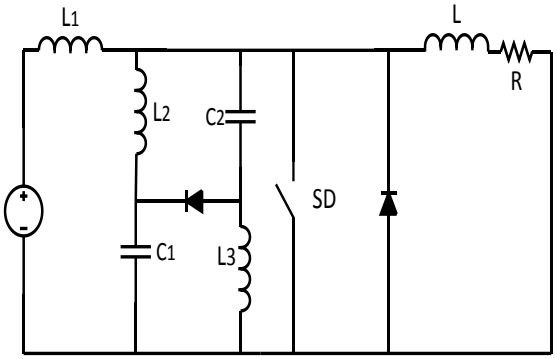

Fig.43. Quasi-Z impedance network source equivalent circuit for small signal analysis.

In the small signal analysis of this topology it is considered that the impedance network is symmetric, this means that the values of capacitance and inductance are equal (C_1=C_2 and L_1=L_2) in differents researches the authors analyze the advantages of symmetry in the network [64-66]. The voltage or current that enters the inverter can be controlled by two methods: voltage or current control, which can be direct or indirect.

The direct method, that is shown in Fig.44, improves transient response and minimizes the perturbation and facilitates the network impedance controller design.

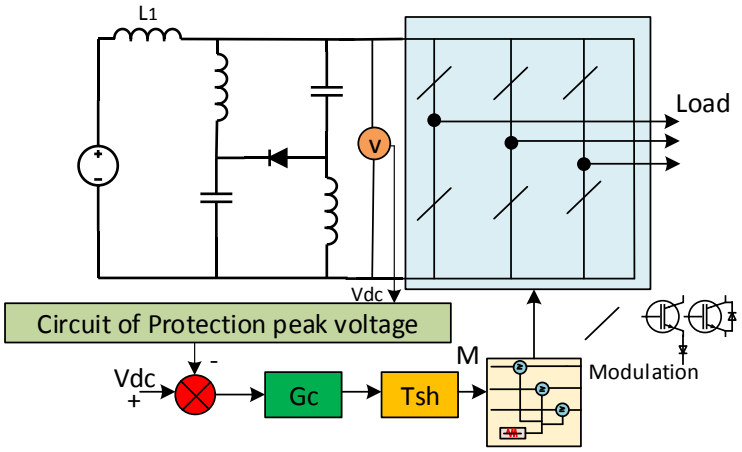

Fig.44. Quasi-Z impedance network direct control method capacitor voltage Vc.

The indirect method, shown in Fig.45, work with the capacitor voltage or current output inductor, which are measured in order to compare them to a voltage or current reference.

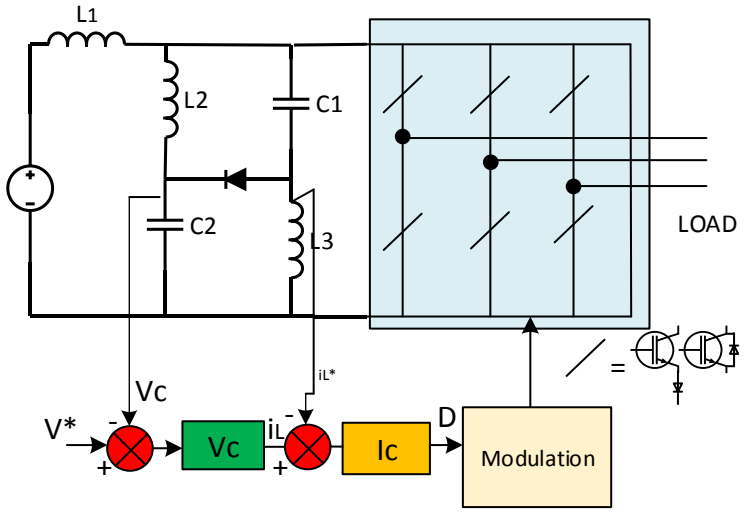

Fig.45. Quasi-Z impedance network indirect control voltage capacitor Vc and IL.

It is very important to take into consideration that when working with the method of indirect control the voltage peak can generate problems, it can become uncontrollable and this could affect the output voltage, causing greater stress to the semiconductors in the inverter and increasing distortion. One way to solve this problem is by modifying the modulation index [67].

The design of this type of controllers consists of comparing the voltage peak generated in the capacitor of the network, with a reference voltage and current peak generated in the inductor, in is very important obtained the transfer function for design a PI controller. These

are calculated based on the desired response and dynamics, with this obtains the work cycle (D) that enters the modulator [68].

When working with the direct method, the output voltage peak of the impedance network is used and the same procedure is applied, that is, obtaining the transfer function and a PI controller which now regulates the modulation index (M) [69]. In general, when designing systems with regeneration or bi-directional, the load current is considered as another state variable, this allows to reduce the disturbances in the input voltage as well as the oscillations of the controller [53].

3.4.2.2 Development of indirect control.

This sub-section present the development of a method indirect in impedance source network, the topology used for this application is the Current Fed Quasi-Z power inverter shown in Fig. 42. The devices used in the CSI power converter are Mosfet SiC to 50 kHz of switching frequency a scheme of control proposed is shown in the Fig. 46. The goal is validate the method and analyze the response of the topology of impedance network in to power converter to high frequencies of switching.

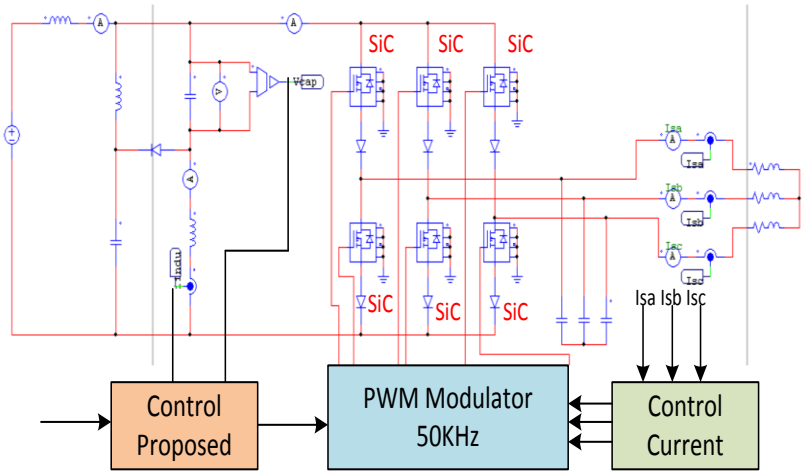

Fig.46. Topology Current Fed Quasi-Z and control proposed.

Considering that the average voltage over one switching period should be zero in steady state, V_{out} is calculated by (12):

$$V_{out} = \frac{D_A + D_{sh} + D_{op}}{D_A} = \frac{1 - 2D_{op}}{D_A} V_{in} \tag{12}$$

Similarly, considering that; the average current of the capacitors over one switching period should be zero in steady sate. I_{L1} can be calculated by (13) and (14):

$$I_{L1} = I_{L2} = \frac{D_{op}}{D_A + D_A + D_{sh}} \tag{13}$$

$$I_{L1} = I_{L2} = \frac{D_{op}}{1 - D_{op}} I_{in} \tag{14}$$

Where the D_A, D_{sh} and D_{op} are the duty cycles of the active states, shoot-through state and traditional zero state.

The differential equations that describe the system shown in Fig.30 when S_D is on and considering that $L_1 = L_2 = L_3$ and $C_1 = C_2$ can be written as (15), (16) and (17):

$$\frac{L di_L(t)}{dt} = (1 - 2D_{OP})V_C(t) - V_{out}(t)(1 - 2D_{OP}) \tag{15}$$

$$\frac{C dV_C(t)}{dt} = (2D_{OP} - 1)I_L(t) + D_{OP} I_{DC} \tag{16}$$

$$\frac{L_I di_L(t)}{dt} = (-2D_{OP})V_C(t) - rI_{DC}(t) + (V_{in} - (1 - D_{OP})V_{out}) \tag{17}$$

The system can be represented in matrix form as (18):

$$\frac{d}{dt}\begin{bmatrix} i_L \\ V_c \\ I_{DC} \end{bmatrix} = \begin{bmatrix} 0 & \frac{(1-2D_{OP})}{L} & 0 \\ \frac{(2D_{OP}-1)}{C} & 0 & \frac{D_{OP}}{C} \\ 0 & \frac{-2D_{OP}}{L_i} & \frac{-r}{L_i} \end{bmatrix} \begin{bmatrix} i_L(t) \\ V_C(t) \\ I_{DC}(t) \end{bmatrix} + \begin{bmatrix} \frac{V_{out}}{L}(1 - D_{op}) \\ 0 \\ \frac{V_{in}(1-D_{op})V_{out}}{L} \end{bmatrix} \tag{18}$$

The parameters of the impedance network and data used to obtain the transfer functions of I_L and V_c are shown in Table 5.

Table I
Parameters of impedance network.

Parameter	Value
D_{op}	0.33
$L=L_1=L_2$	50uH
L_{load}	0.47mH
$C=C_1=C_2$	660uF
V_{in}	100V
R_{load}	5Ω
Modulation Technique	Maximum Boost

Resolving (17) we obtain the transfer functions (19) and (20):

$$GV_c(s) = \frac{1.328e^{-6}s^2 - 0.0794504s - 99.96}{3e^{-11}s^3 + 5e^{-8}s^2 + 4800s + 18} \tag{19}$$

$$GI_L(s) = \frac{9.996e^{-6}s^2 - 6000.42s - 39.98}{3e^{-11}s^3 + 5e^{-8}s^2 + 4800s + 18} \tag{20}$$

With the obtained transfer function, the loop is closed by designing and implementing a PI. A diagram of the closed loop of the converter and impedance network source is presented in Fig 47.

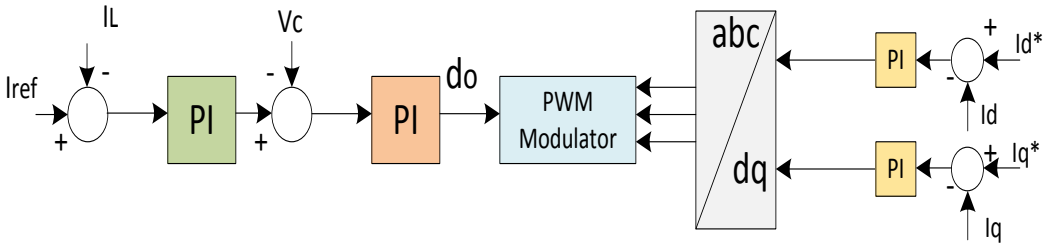

Fig.47. Close loop control of power converter.

The I_d* and I_q* are the currents of the converter after passing through a transformation. The PI control for these currents is designed to improve the response of the closed loop. For the tuning of the PI controller for the impedance network there are different methods, to minimize the time in the search of the K_p and K_i values the SiSoTools of Matlab was used, which allows faster and effective tuning when compared with the analytical methods. Moreover it can work directly with the transfer functions.

The modulation technique used is the maximum boost method (Fig.48), the duty cycle D is calculated by (21), and the index of modulation is M=0.8:

$$D_{op} = 1 - \frac{3\sqrt{3}M}{2\pi} = 1 - \frac{3\sqrt{3}*0.8}{2\pi} = 0.33 \quad (21)$$

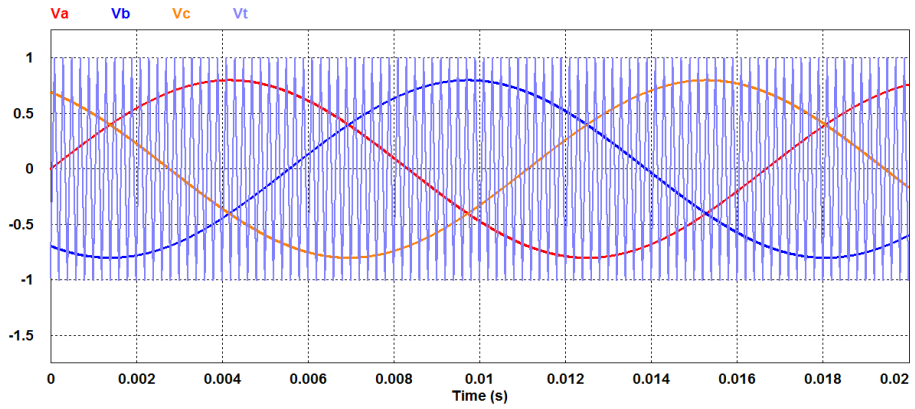

a)

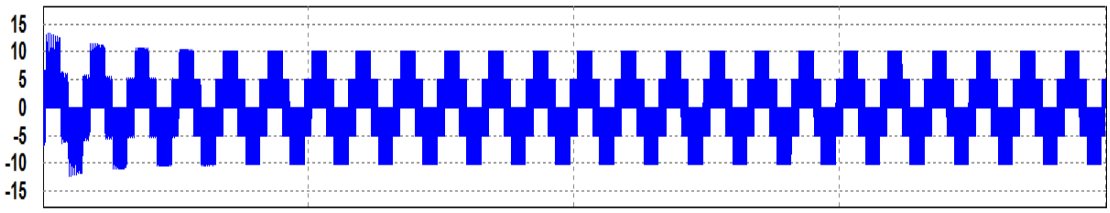

b)

Fig.48. Modulation technique. a) Signals of reference. b) PWM current output in phase A.

For the tuning of the PI controller for the impedance network, the SiSoTools of Matlab was used (Fig.49), which allows faster and effective tuning when compared with the analytical methods. Moreover it can work directly with the transfer functions.

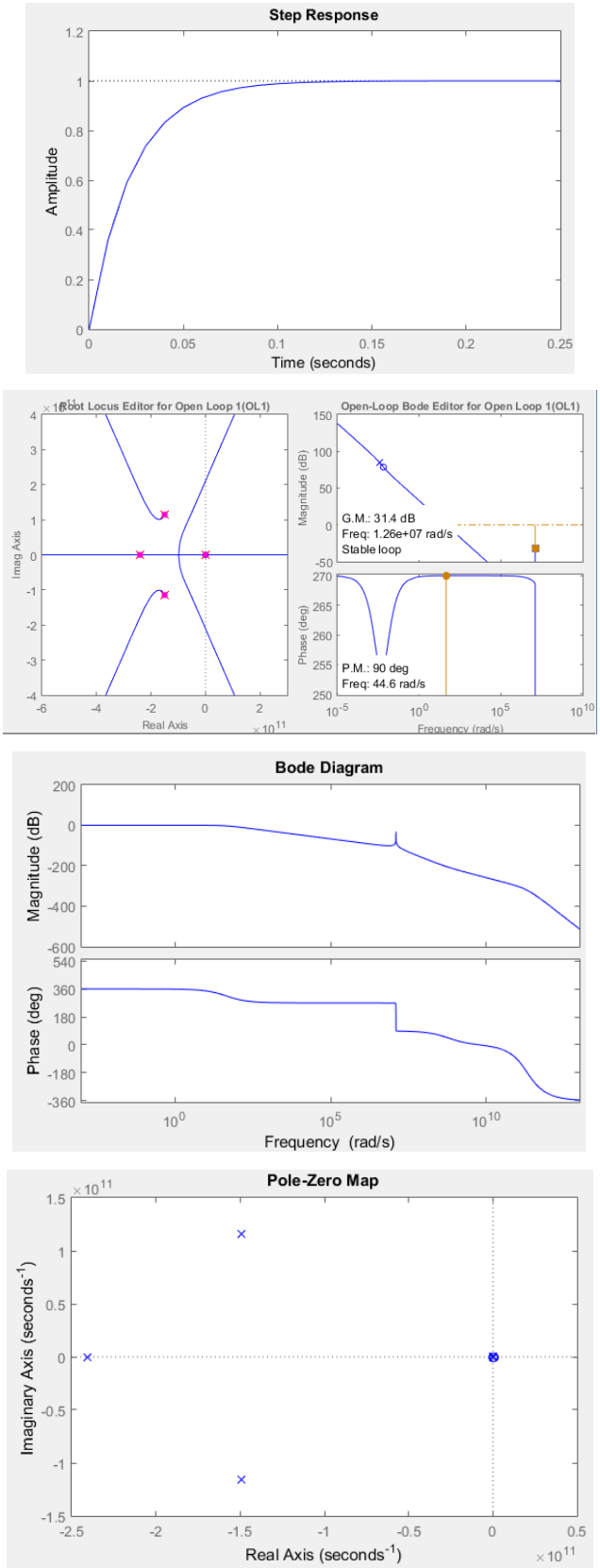

Fig.49.Tuning of PI´s control with SiSoTools.

The parameters used for the simulations are presented in the Table V. The current of output in the impedance network that enters to CSI power converter with this parameters is shown in the Fig. 50.

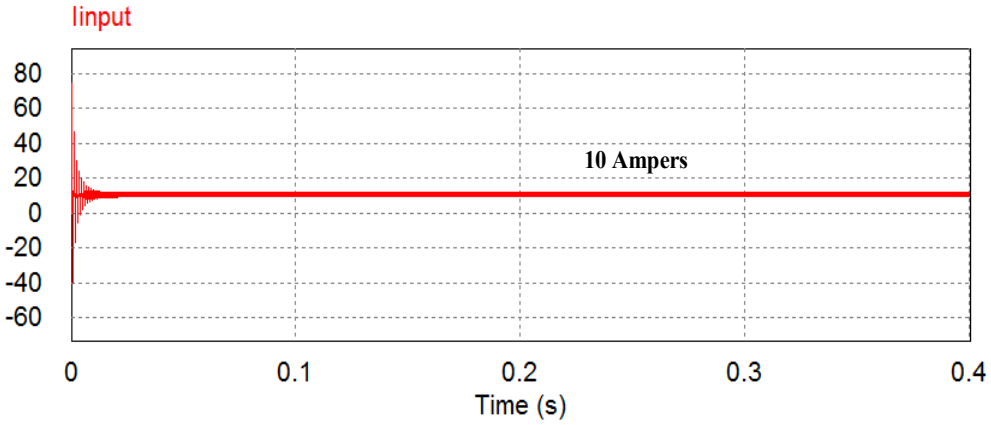

Fig.50. Current of input to CSI power converter.

The results obtained in the topology of power converter with the control proposed are shown in the Fig 51. The first part presents the sinusoidal output currents in the current source power inverter. The second part presents the behavior of current and voltage controls over the impedance network. The analisys of stress in the passive devices are shown in the Fig.52 and the stress is reduced by effects of the same control implemented in comparison with an open loop topology, this shows that the control proposed in closed loop helps to minimize these effects that can cause damage to the passive elements of the converter and allows to regulate the input current to the converter.

Table 6
Parameters for simulations for SiC Quasi-Z topology.

Parameter	Value
V_{DC}	100V
$L=L_1=L_2$	50uH
C=C1=C2	50kHz
Frequency	660uF
C filter	10uF
Mosfet SiC	SCT2450KE
Diode SiC	C3D08065I
Pi Current	P= 0.6 I=0.053
Pi voltage	P=0.8 I=0.0034
Pi of Id and Iq	P=2.2; I=0,23

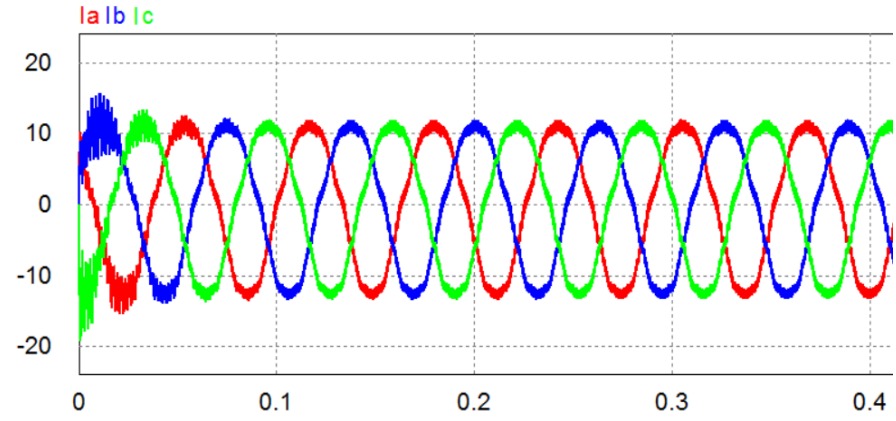

a)

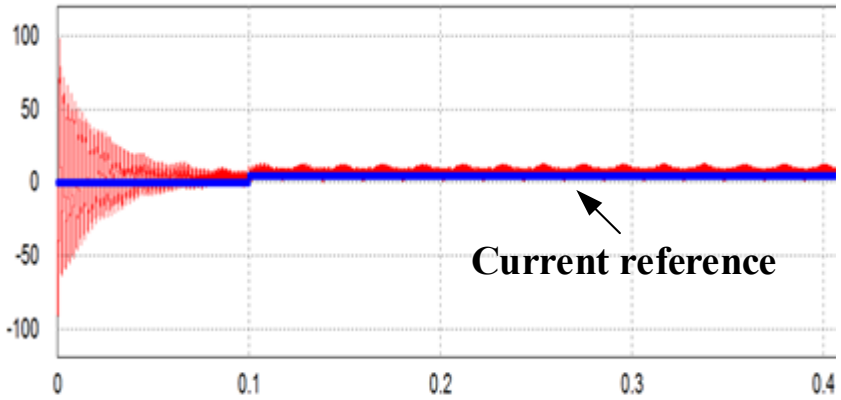

b)

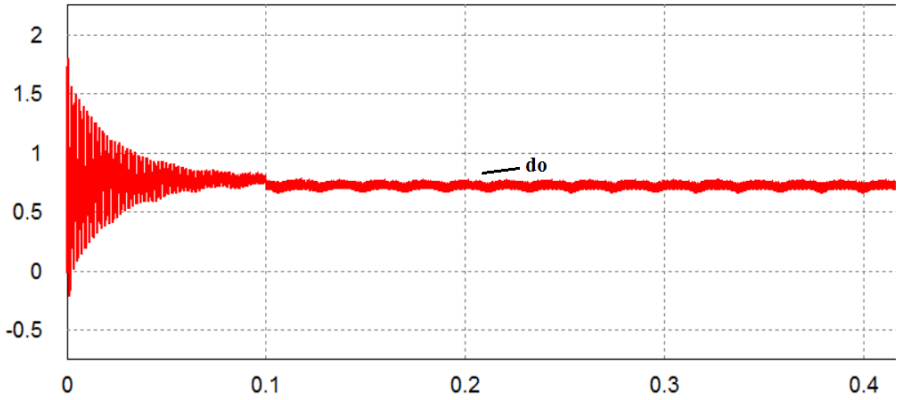

c)

Fig.51. Result of control proposed. a) Currents of output in the CSI power converter, b) Current control in impedance network source, c) Voltage control (do) in impedance source network.

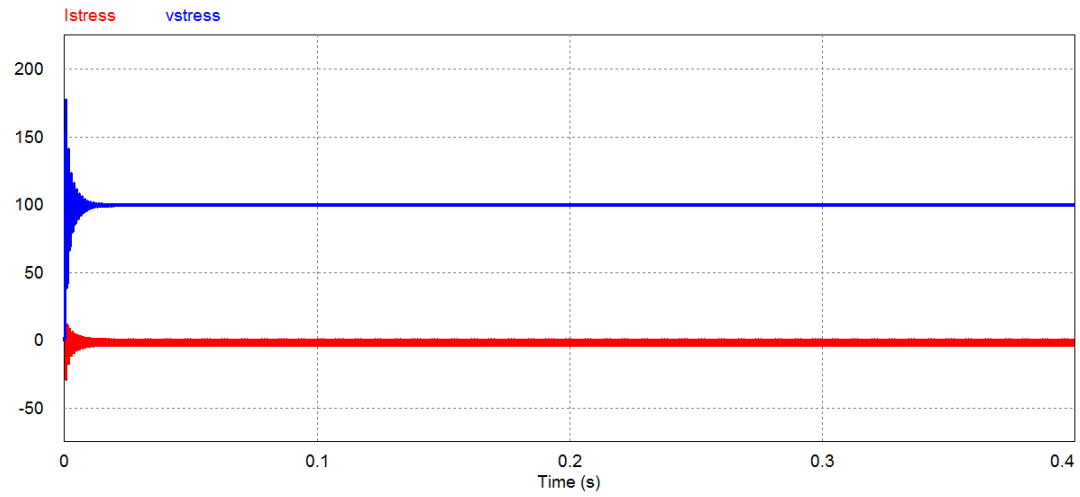

a)

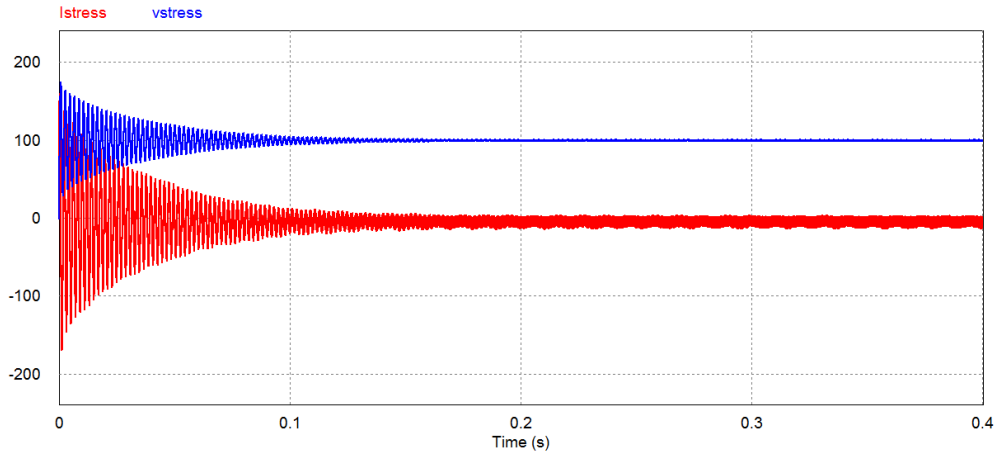

b)

Fig.52. Stress in passive devices. a) Stress in passive device in close loop control, b) Stress in passive device in open loop.

When the PI control in the impedance network is not properly tuned generates different problems and increases the distortion harmonic total THD (Fig.53) that can cause problems in the control of the load; this by the bad function of the loop of control, this effects would be a serious problem in an electric traction system for the losses that could generate.

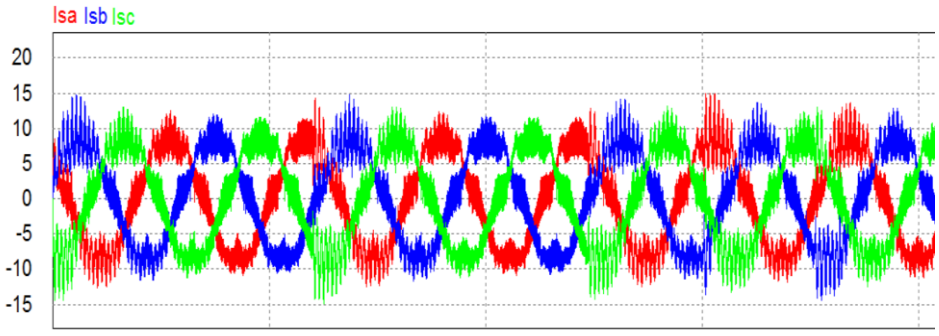

Fig.53. Results of control badly tuned.

For the Trans Z topology (Fig.54), a simulation with maximum constant boost control modulation (MCBC) is performed to analyze the stress in the passive components of the impedance network, the devices used are Mosfet SiC to 100 kHz.

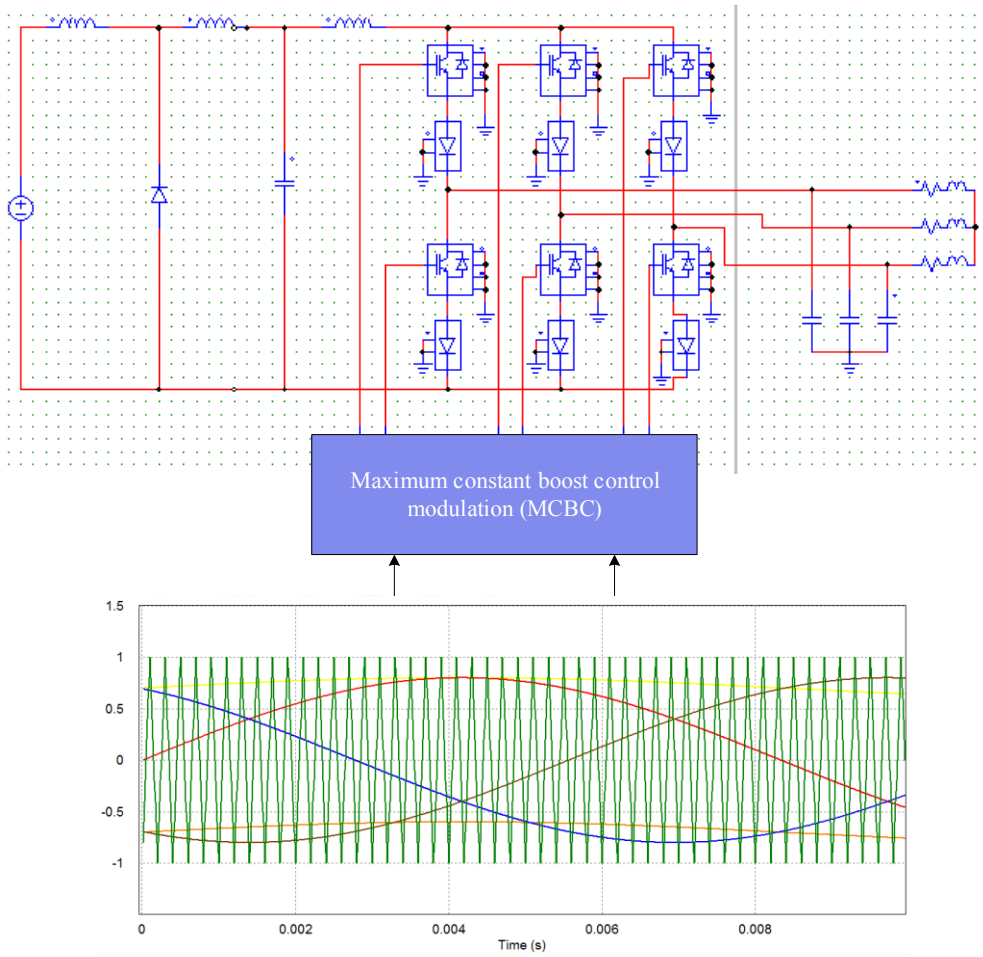

Fig.54. maximum constant boost control modulation (MCBC).

The duty cycle ratio is calculated by (22), the index of modulation M is 0.9, the signals of PWM current and voltage are presented in the Fig.55.

$$D_{op} = 1 - \frac{\sqrt{3}M}{2} = \ 1 - \frac{\sqrt{3}M}{2} = 1 - \frac{\sqrt{3}*0.9}{2} = 0.220 \qquad (22)$$

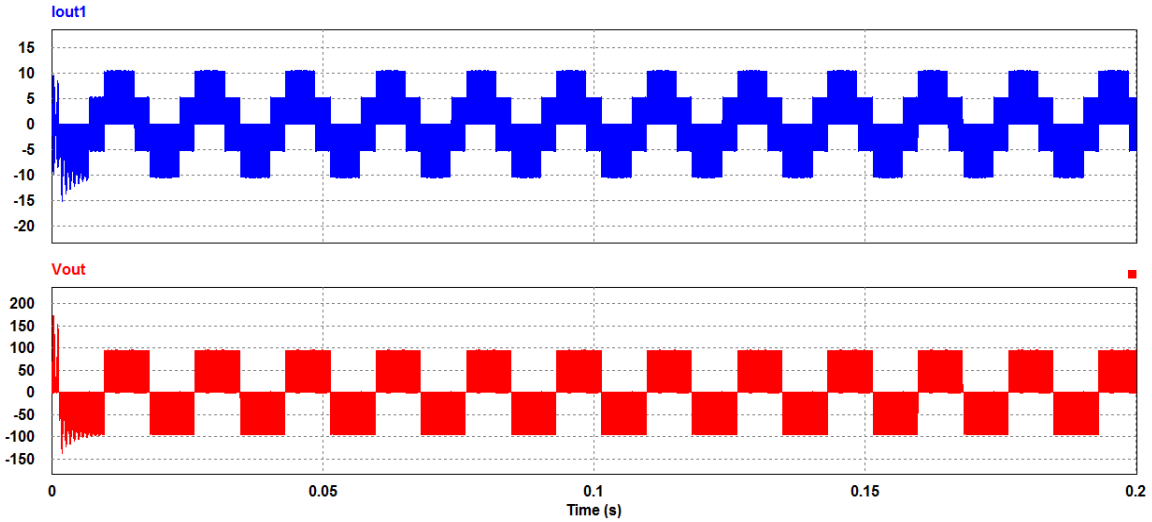

Fig.55. Signals of current and voltage in MCBC.

The parameters and values of passive devices used for the simulations are presented in the Table 7. The results obtained in the simulations are shown in the Fig. 56.

Table 7
Parameters for simulations for SiC Trans-Z topology.

Parameter	Value
V_{DC}	100V
$L=L_1=L_2$	50uH
C1	100uF
Frequency	100kHz
C filter	50uF
Rload	5Ω
Load	0.47mH
Mosfet SiC	SCT2450KE
Diode SiC	C3D08065I
PWM Technique	MCBC

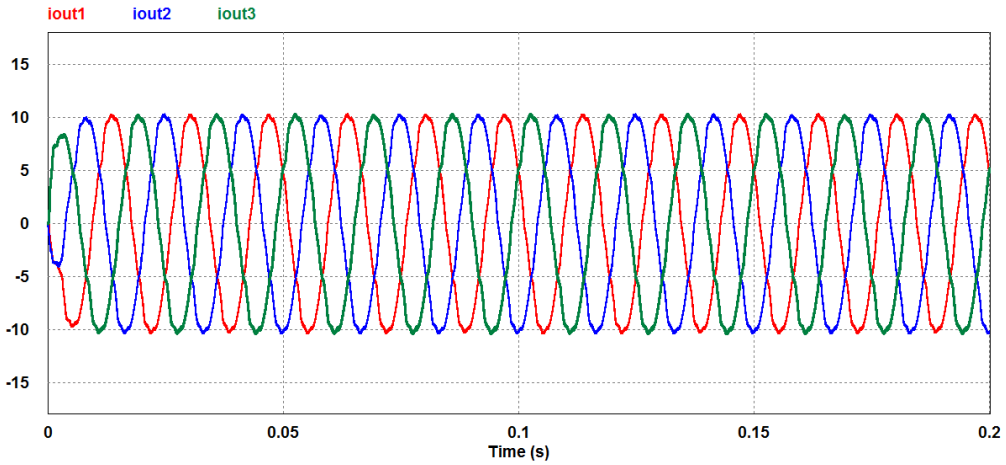

a)

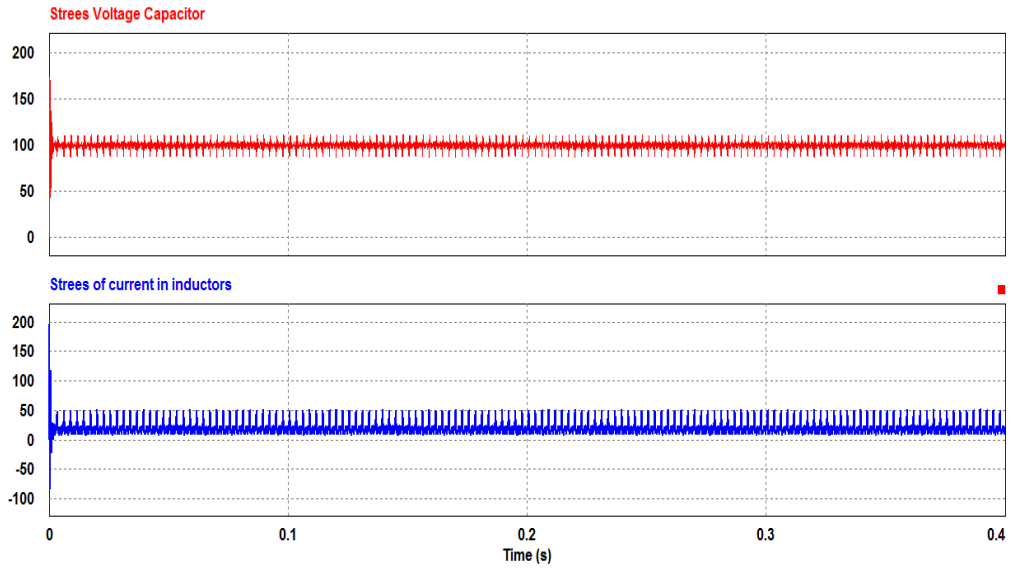

b)

Fig.56. Results in simulations. a) Current of output, b) Stress in passive device in Trans Z SiC power converter.

The analysis of stress in the passive devices of the Trans Z power converter allows to verify the behavior of the current in the inductors and the voltage in the capacitor. The study of these topologies in this first part allows to analyze their modes of operation when they are used with three-phase converters with current sources. These topologies allow solving the problem of current return in the CSI but this recharge is not constant, it happens only in instants of short times, this depends on the operating mode of the converter, therefore an optimal and constant recharge of the battery is not obtained.

3.4.4. V-I power converter.

The V-I power converter transforms the voltage of the battery to current constant as source for the inverter. The topology V-I shown in Fig.57 is composed of two interrupt and two diodes. The configuration allows the energy to be reversible or bidirectional and can work with different topologies of current source inverter (CSI), then solving the problem of bidirectional in the current source inverter.

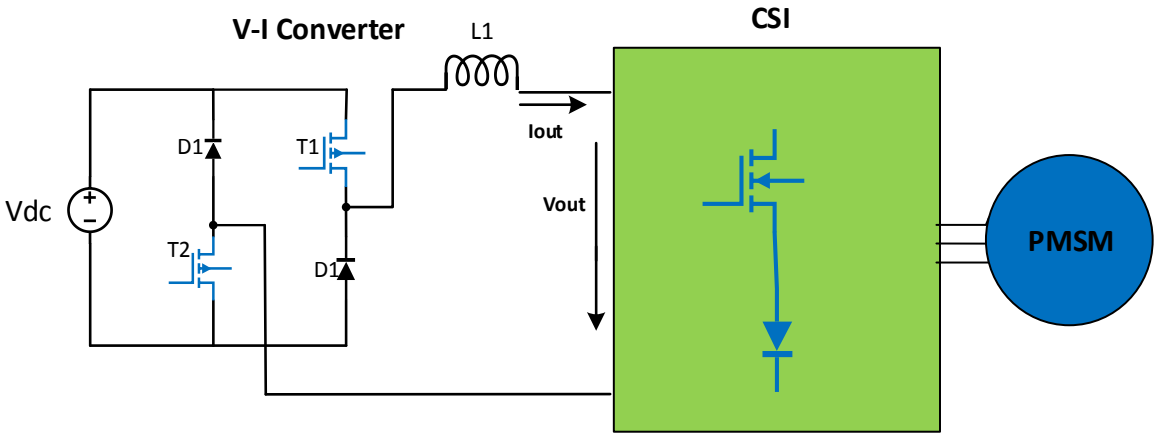

Fig.57. V-I power converter topology.

The V-I power converter operates in four modes of operations [38]. In the first mode (Fig. 58) when the mosfet T_1 and T_2 are turned on, the battery voltage is applied to the converter and charging the inductor, in this mode a current I_{out} and a voltage V_{out} are obtained being $V_S=V_{Battery}$. Current returns through the activation mosfet T_2, and the Diodes D_1, D_2 are in reverse bias therefore does not activate.

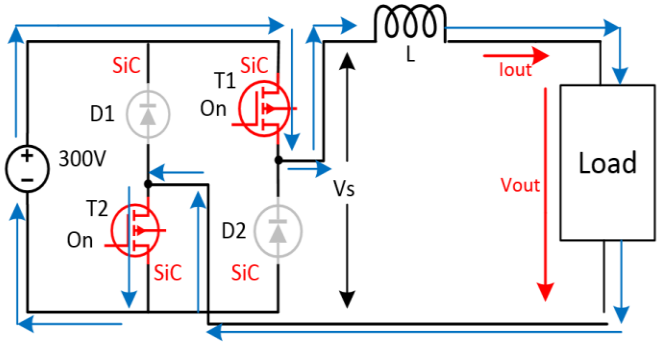

Fig 58. V-I power converter in the first mode.

In the second mode (Fig. 59) the mosfet T_1 is turned on and the T_2 is off, this disconnects the battery of the power converter and V_s=0V, and the flows of current circulate through diode D_1 [38].

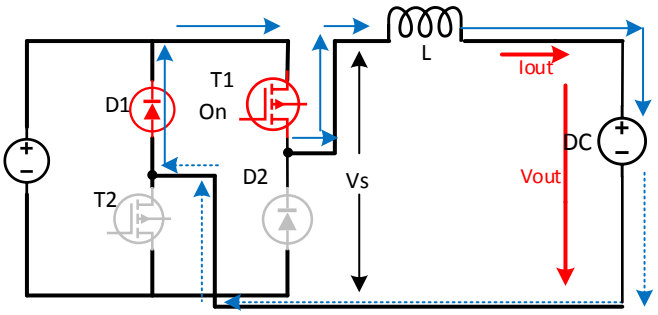

Fig 59. V-I power converter in the second mode.

In the third mode (Fig.60) the mosfet T_2 is turned on and T_1 is off; this mode disconnects the battery of the power converter and V_s=0v, and the flows of current circulate through diode D_2 [38].

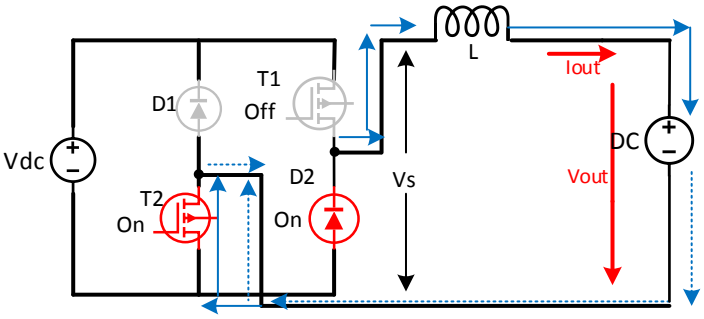

Fig 60. V-I power converter in the third mode.

In the fourth mode (Fig. 61) the mosfet are turned off and the current flows through the diodes D_1 and D_2; this mode is implemented in the case of the current converter returns to recharge the high voltage battery $Vs=-V_{Battery}$ [38].

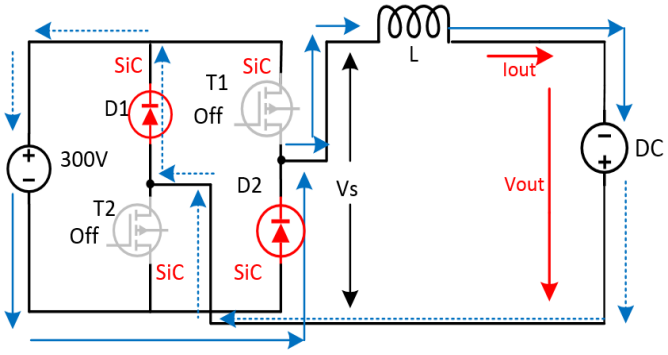

Fig 61. V-I power converter in the fourth mode.

The model dynamic of V-I converter is governed by (20):

$$L\frac{dI_{DC}(t)}{dt} = V_S(t) - V_{in}(t) \tag{23}$$

Where the output voltage, V_S, of the V-I converter can take three values: the battery voltage ($V_S = V_{Battery}$) when the V-I converter operates in first state, $V_S = 0$ when T_1 or T_2 are OFF, and $V_S = -V_{Battery}$ for charging the battery in fourth state. To maintain a desired level of the dc choke current, the V-I converter alternates between first state and On-Off of T_1 or T_2 in the motoring operation mode considering the load an electric motor, as shown in Fig. 62.

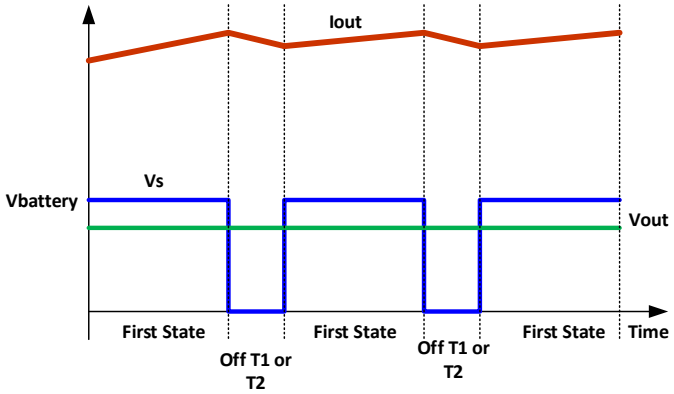

Fig. 62. V-I operation in first state motoring.

The V-I converter minimizes the problem of energy recovery in the CSI topology, the recovery is constant and not at intervals as with the topologies described in the previous section. The use of this topology allows controlling the input current to regulate at a constant level, and for doing this the implementation of a control for the output current is necessary depending on a desired reference and the design characteristics in power.

3.4.4.1 Design of control of current for V-I power converter.

The design of the control of current of output in the V-I converter consists in regulating and minimizing the current ripple for stabilize the value of output current. For the analisys and design of current control the two scenarios of the first and the fourth modes are analyzed.

The circuit shown in the Fig. 63, represents the equivalent circuit in the first mode, a flow of current and voltage are generated when a load RLC is connected. Also for the analysis they are considered internal resistance of the SiC mosfet (R_{ds}=R_{on}), inductance (RL) and capacitance (RC).

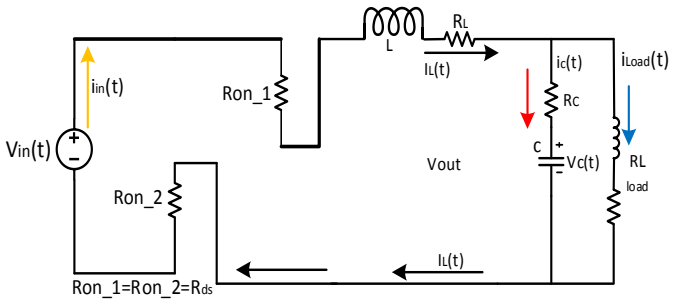

Fig. 63. Equivalent first mode circuit.

In function of this circuit the equations of system are described in (21), (22), (23), (24):

$$V_{in}(t) = V_{Ron_1} + V_L + V_{OUT} + V_{RL} + V_{Ron\_2} \tag{24}$$

$$V_{in}(t) = R_{on_1} I_L(t) + L\frac{di_L(t)}{dt} + R_L I_L(t) + V_{out} + R_{on_2} I_L(t) \tag{25}$$

$$V_{in}(t) = 2R_{ds} I_L(t) + L\frac{di_L(t)}{dt} + R_L I_L(t) + V_{out} \tag{26}$$

$$L\frac{di_L(t)}{dt} = V_{in}(t) - 2R_{ds} I_L(t) - R_L I_L(t) - V_{out} \tag{27}$$

The value of V_{out} can be expressed in terms of R_{load} and R_C by the equation (25):

$$V_{out} = \frac{R_{Load}R_c}{R_{Load}+R_c} i_L(t) + \frac{R_{Load}}{R_{Load}+R_c} V_c(t) \tag{28}$$

Substituting (25) into (24) we have the equations (26):

$$L\frac{di_L(t)}{dt} = V_{in}(t) - 2R_{ds} I_L(t) - R_{Load} I_L(t) - \frac{R_{Load}R_c}{R_{Load}+R_c} i_L(t) - \frac{R_{Load}}{R_{Load}+R_c} V_c(t) \tag{29}$$

Resolving the system we obtained (27)-(28)

$$L\frac{di_L(t)}{dt} = V_{in}(t) - \left[2R_{ds} + R_{Load} + \frac{R_{Load}R_c}{R_{Load}+R_c}\right] I_L(t) - \frac{R_{Load}}{R_{Load}+R_c} V_c(t) \tag{30}$$

$$\frac{di_L(t)}{dt} = \frac{V_{in}(t)}{L} - \left[\frac{2R_{ds}+R_{Load}+\frac{R_{Load}R_c}{R_{Load}+R_c}}{L}\right] I_L(t) - \frac{\frac{R_{Load}}{R_{Load}+R_c}}{L} V_c(t) \tag{31}$$

The equation that is obtained from the output circuit it is given by (29), (30), (31):

$$\boldsymbol{C\frac{dV_C(t)}{dt} = V(t) - I_L(t)} \tag{32}$$

$$\mathbf{C}\frac{\mathbf{dV_C(t)}}{\mathbf{dt}} = \frac{\mathbf{R_{Load}}}{\mathbf{R_{Load}+R_c}}\mathbf{I_L(t)} - \frac{\mathbf{1}}{\mathbf{R_{Load}+R_c}}\mathbf{V_c(t)} \quad (33)$$

$$\frac{dV_C(t)}{dt} = \frac{\frac{R_{Load}}{R_{Load}+R_C}}{C}I_L(t) - \frac{\frac{1}{R_{Load}+R_C}}{C}V_c(t) \quad (34)$$

Resolving the system we can set the equation of state space model (35), (36):

$$\boldsymbol{X(t) = AX(t) + B} \quad (35)$$

$$\boldsymbol{Y(t) = CX(t) + D} \quad (36)$$

The equations (34) and (35) can be expressed in in the matrix form:

$$\begin{bmatrix} \frac{di_L(t)}{dt} \\ \frac{dV_C(t)}{dt} \end{bmatrix} = \begin{bmatrix} \frac{2R_{ds}+R_L+\frac{R_{Load}R_c}{R_{Load}+R_c}}{L} & -\frac{\frac{R_{Load}}{R_{Load}+R_c}}{L} \\ \frac{\frac{R_{Load}}{R_{Load}+R_c}}{C} & -\frac{1}{\frac{R_{Load}+R_c}{C}} \end{bmatrix} \begin{bmatrix} I_L(t) \\ V_c(t) \end{bmatrix} + \begin{bmatrix} \frac{1}{L} \\ 0 \end{bmatrix} V_{in}(t) \quad (37)$$

$$\begin{bmatrix} \frac{V_o(t)}{dt} \\ I_{in}(t) \end{bmatrix} = \begin{bmatrix} \frac{R_{Load}R_c}{R_{Load}+R_c} & \frac{R_{Load}}{R_{Load}+R_c} \\ 1 & 0 \end{bmatrix} \begin{bmatrix} I_L(t) \\ V_c(t) \end{bmatrix} + \begin{bmatrix} 0 \\ 0 \end{bmatrix} V_{in}(t) \quad (38)$$

The parameters and data used to obtain the transfer functions of the system are shown in Table 8.

Table VII
Parameters for calculated transfer function.

Parameter	Value
V_{DC}	300 V
Inductance L	20mH
Resistencia inductance RL	0.15Ω
Capacitor C	100uF
ESR capacitor	0.05 Ω
Rload	10 Ω
L load	1mH
Rds Mosfet	40m Ω

Resolving (37) and (38) by state space model we obtain the transfer functions on the current of output (39):

$$I_{out}(s) = \frac{10s+1.5e^4}{s^2+1503s+1.144e^5} \quad (39)$$

For the tuning of PI control, the Matlab PID tuner tool is used, the tool the tool allows to quickly obtain the value of the constants K_p and K_i for the control proposed. (Fig.64).

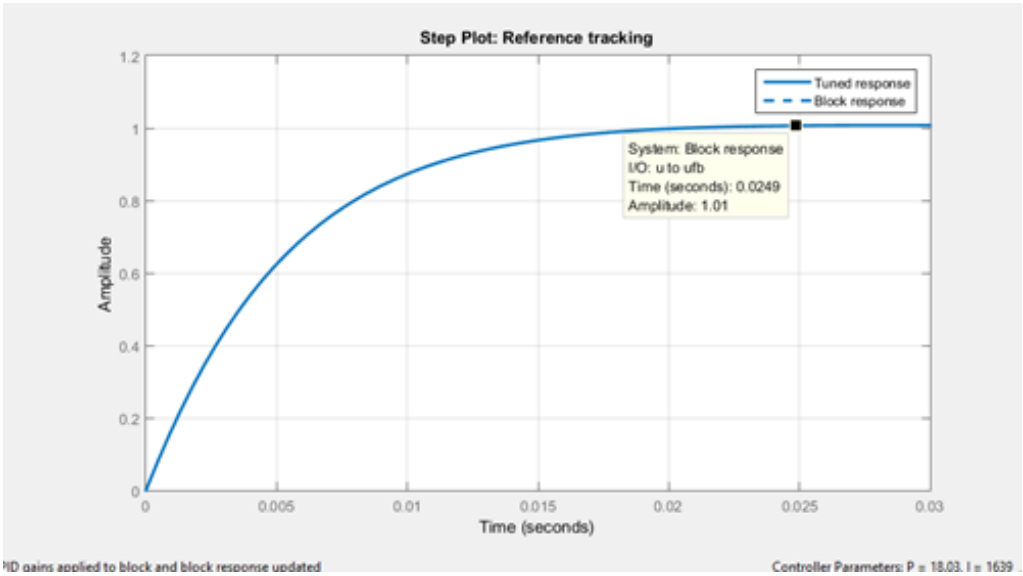

a)

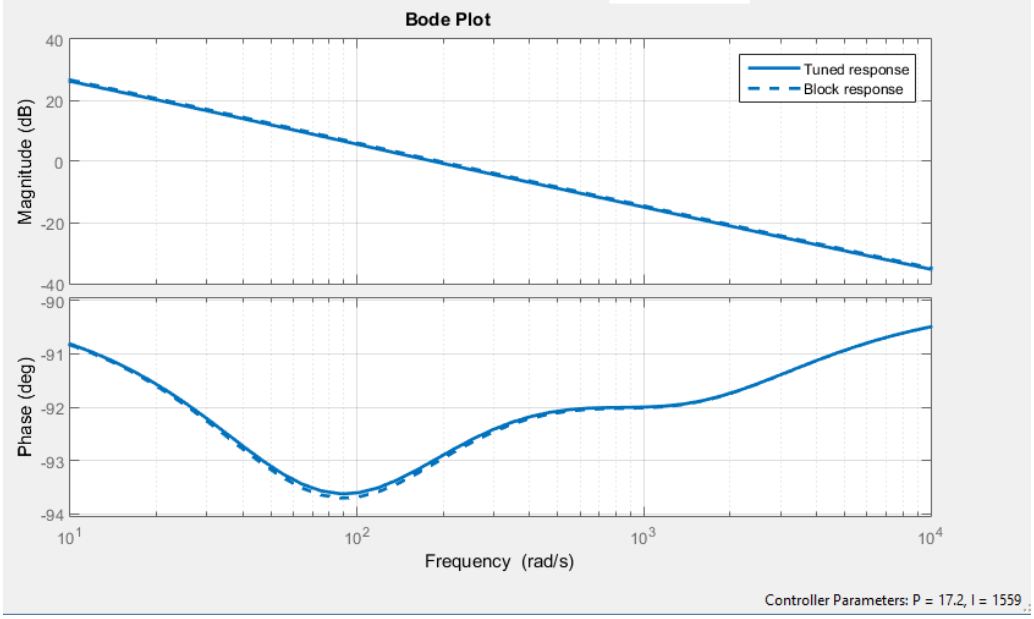

b)

Fig. 64. Tuner tool, tuning of PI a) Step plot response, b) Bode plot response.

The values of the constants Kp and Ki obtained by this method are shown in the Fig 65.

Controller Parameters

	Tuned	Block
P	17.1953	18.0261
I	1559.4961	1639.4073
D		
N		

Performance and Robustness

	Tuned	Block
Rise time	0.0109 seconds	0.0104 seconds
Settling time	0.0173 seconds	0.0165 seconds
Overshoot	0.704 %	0.749 %
Peak	1.01	1.01
Gain margin	Inf dB @ NaN rad/s	Inf dB @ NaN rad/s
Phase margin	87 deg @ 185 rad/s	87 deg @ 194 rad/s
Closed-loop stability	Stable	Stable

Fig. 65. Values of Kp and Ki tuning.

The signals of reference and control of the response in the design of PI control for the transfer function (36) are shown in the Fig.66.

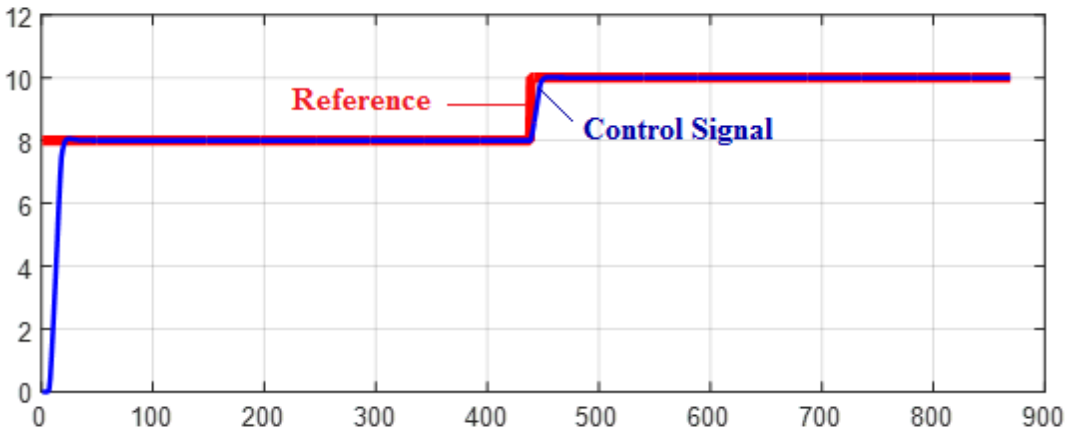

Fig. 66. Signals of reference and control.

Implementing control in close loop on the converter topology converter V-I in Simulink (Fig.67) are obtained the results shown in Fig (68).

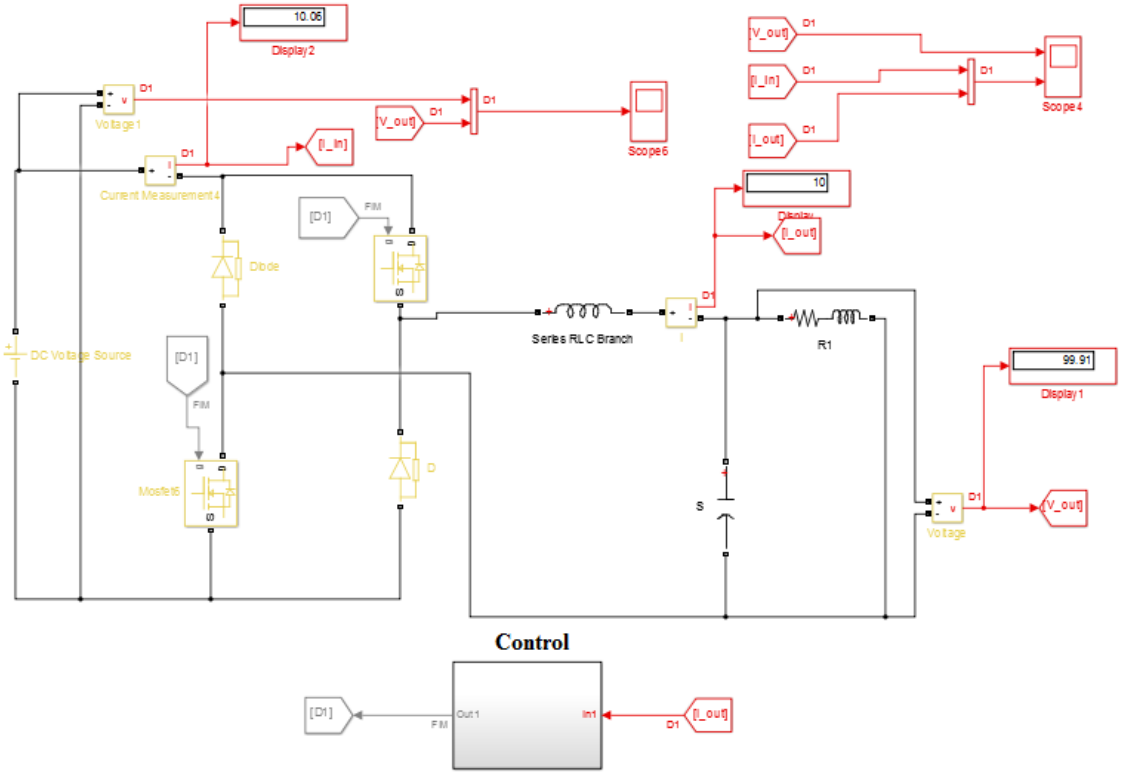

Fig. 67. V-I power converter in Simulink, close loop.

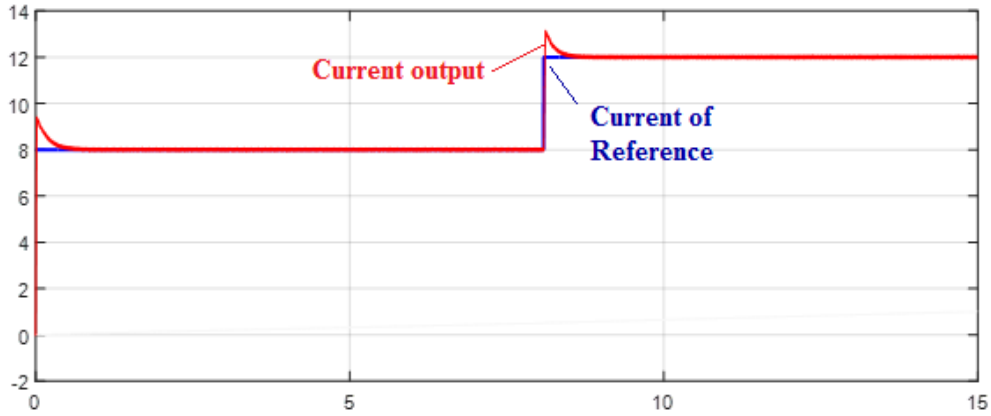

a)

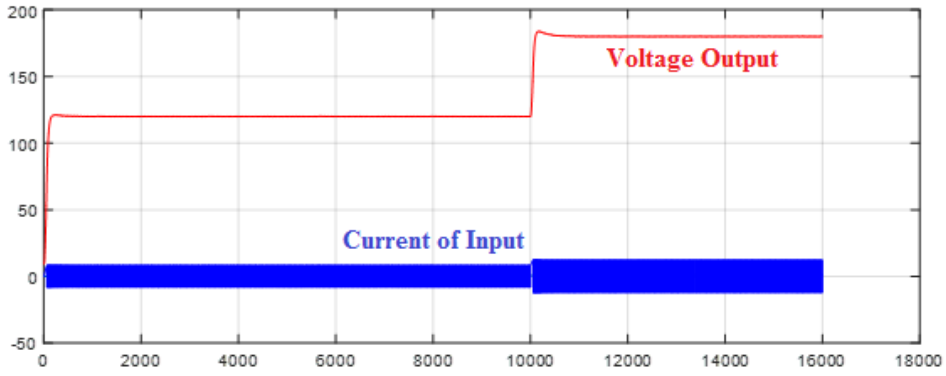

b)

Fig. 68. Results in simulation of V-I power converter, a) Current of output response to control, b) Voltage output and current of input in the V-I converter.

The circuit shown in the Fig. 69, represent the equivalent circuit in the fourth mode, this situation analyzes the flow of the current when it returns to the battery.

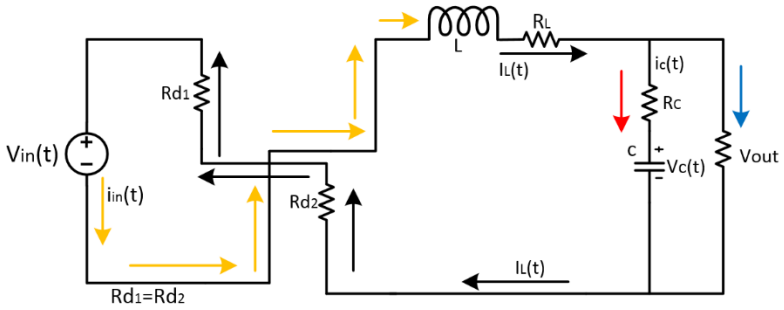

Fig. 69. Equivalent circuit fourth mode.

$$-V_{in}(t) = V_L - V_o - V_{D1} \tag{40}$$

$$-V_{in}(t) = -L\frac{di_L(t)}{dt} - R_L I_L(t) - 2(R_d I_L(t)) - V_{out} \tag{41}$$

$$-V_{in}(t) = -L\frac{di_L(t)}{dt} - R_L I_L(t) - 2(R_d I_L(t)) - \left(\frac{R_{Load}R_c}{R_{Load}+R_c} i_L(t) + \frac{R_{Load}}{R_{Load}+R_c} V_c(t)\right) \tag{42}$$

$$-V_{in}(t) = -L\frac{di_L(t)}{dt} - R_L I_L(t) - 2(R_d I_L(t)) - \frac{R_{Load}R_c}{R_{Load}+R_c} i_L(t) - \frac{R_{Load}}{R_{Load}+R_c} V_c(t) \tag{43}$$

$$\frac{di_L(t)}{dt} = \frac{V_{in}(t)}{L} - \left[\frac{R_L+2R_d+\frac{R_{Load}R_c}{R_{Load}+R_c}}{L}\right] i_L(t) - \frac{\frac{R_{Load}}{R_{Load}+R_c}}{L} V_c(t) \tag{44}$$

In the analysis in the circuit of output are obtained the equations (41)-(42):

$$C\frac{dV_C(t)}{dt} = V(t) - I_L(t) \tag{45}$$

$$\frac{\mathbf{dV_C(t)}}{\mathbf{dt}} = \frac{\frac{\mathbf{R_{Load}}}{\mathbf{R_{Load}+R_c}}}{\mathbf{C}} \mathbf{I_L(t)} - \frac{\frac{\mathbf{1}}{\mathbf{R_{Load}+R_c}}}{\mathbf{C}} \mathbf{V_c(t)} \tag{46}$$

The differential equations of the system in matrix form are expressed in (47) and (48):

$$\begin{bmatrix} \frac{di_L(t)}{dt} \\ \frac{\mathbf{dV_C(t)}}{\mathbf{dt}} \end{bmatrix} = \begin{bmatrix} \frac{2R_d+R_L+\frac{R_{Load}R_c}{R_{Load}+R_c}}{L} & -\frac{\frac{R_{Load}}{R_{Load}+R_c}}{L} \\ \frac{\frac{R_{Load}}{R_{Load}+R_c}}{C} & -\frac{\frac{1}{R_{Load}+R_c}}{C} \end{bmatrix} \begin{bmatrix} I_L(t) \\ V_c(t) \end{bmatrix} + \begin{bmatrix} \frac{1}{L} \\ 0 \end{bmatrix} V_{in}(t) \tag{47}$$

$$\begin{bmatrix} \frac{V_o(t)}{dt} \\ I_{in}(t) \end{bmatrix} = \begin{bmatrix} \frac{R_{Load}R_c}{R_{Load}+R_c} & \frac{R_{Load}}{R_{Load}+R_c} \\ 1 & 0 \end{bmatrix} \begin{bmatrix} I_L(t) \\ V_c(t) \end{bmatrix} + \begin{bmatrix} 0 \\ 0 \end{bmatrix} V_{in}(t) \tag{48}$$

Solving the system in the same way as the previous analysis and considering the Rd of the diodes you get the transfer function (49):

$$I_{out}(s) = \frac{800s+4.4e^6}{s^2+26460s+1.241e^8} \quad (49)$$

3.4.5 Study comparative.

This section details a comparative study between the bidirectional topologies for CSI presented in the previous section. The objective is to be able to analyze the advantages and disadvantages of each one in order to select the best performance and operation at high operating frequencies.

The Dc-Dc full bridge topology have four transistors Mosfets, the use of this topology allows the regeneration of current to the battery, this recirculation of current is constant for this it must be active transistors T1 and T4 (Fig. 70). For the two operating situations it is necessary to switch at least two transistors, this would increase the power losses and the efficiency of the system would be reduced. In addition, a control is required for the operating situation.

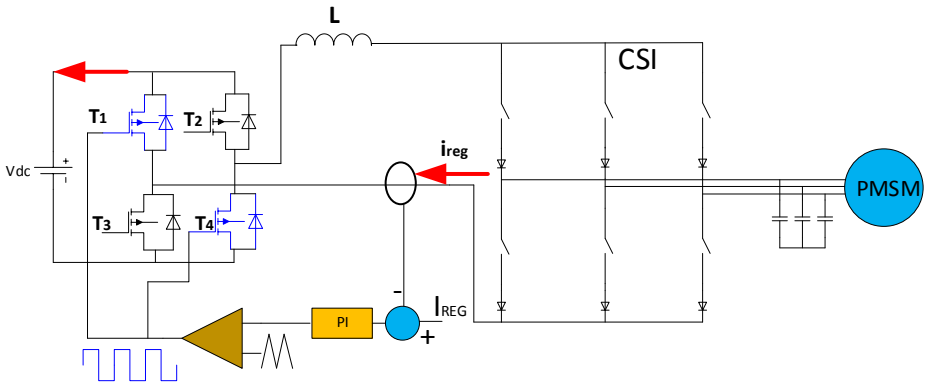

Fig. 70. DC-DC full bridge topology in situation of current of regeneration.

But this topology could work at higher switching frequency ranges through the use of silicon carbide devices, the use of this technology would allow to improve the design and size of the input coil. To establish a relation of frequency inductance and to consider it for the design, the equation (50) allows us to find an approximate value of it.

$$L_{dc} = \frac{\Delta I * V_{dc}}{2\pi f_{sw} I_{dcmax}} \quad (50)$$

Where ΔI is the ripple current; V_{dc} is the voltage of input, f_{sw} is the switching frequency and I_{dcmax} is the current maxima of output. The Fig 71 shown the relation frequency/inductance for values of 0.4 of current ripple, 300V of input and 20 Amperes of current out for a range of 5 kHz to 100 kHz; while the frequency is increasing the value of the inductance is reduced, this allows to design a smaller and more compact coil.

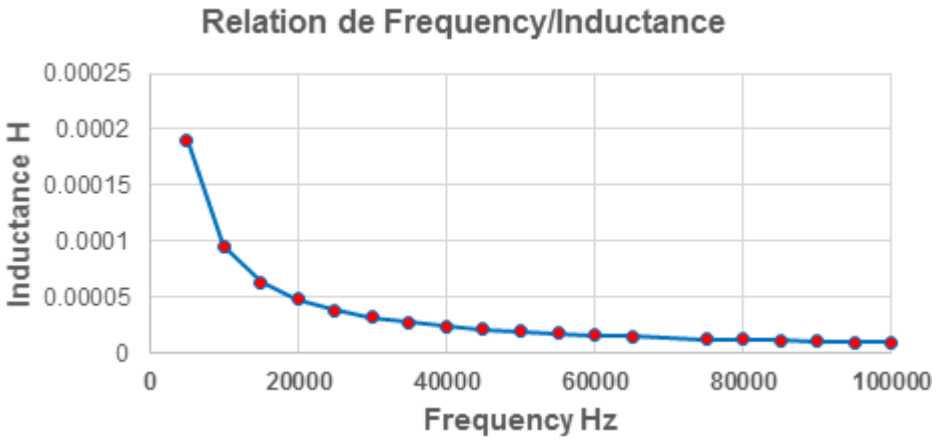

Fig. 71. Relation of frequency/ inductance.

The use of impedance networks in topologies of power converters in applications of electric traction systems help to overcome the problems and limitations of voltage and current that frequently occurs in the VSI and CSI topologies detailed in the previous section. These topologies are formed by storage elements of linear energy, capacitors and inductors, in the quasi Z and trans Z topologies previously analyzed, the use of SiC devices in the CSI inverters (Fig.72) allows to work with a higher frequency of switching, this helps the design and reduction of size of the passive elements of the network, which generates a great advantage.

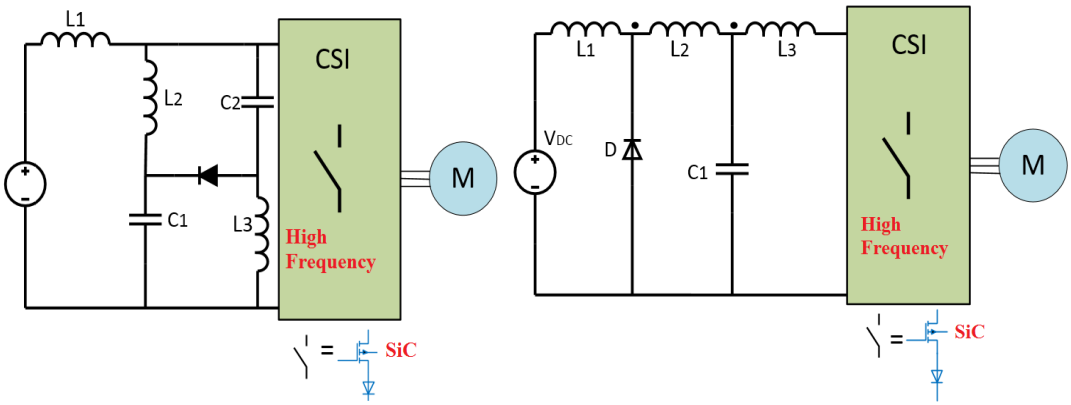

a) b)

Fig. 72. Impedance network source in SiC Inverters. a) SiC Quasi Z, b) SiC Trans z.

For the design of passive elements is considered the state of continuous in the two modes of operations in the expression (51)

$$D_{op} + D_{nop} = 1 \tag{51}$$

Where D_{op} is the duty radio in first mode and D_{nop} is the duty radio in second mode. If the impedance network is symmetric, we have L_2=L_3 and C_1=C_2 the values of currents in the devices are the expressions (52),(53),(54)

$$I_{out} = I_{L1} + I_{L2} + I_{L3} \tag{52}$$

$$I_{L2} = I_{L3} = \frac{D_{op}}{1-2D_{op}} I_{L1} \tag{53}$$

$$I_{out} = I_{L1} + I_{L2} + I_{L3} = \frac{1}{1-2D_{op}} I_{L1} \tag{54}$$

The capacitance is calculated by (55):

$$C_1 = C_2 = \frac{(1-D_{op})D_{op}}{M} \frac{2\sqrt{2}I_{Lrms}}{\sqrt{3}\Delta V_c f_s} \tag{55}$$

Where f_s is the switching frequency of switching of power converter and D_{op} is the duty cycle in the continuous mode. For the design and calculation of L_1, L_2 and L_3 the current of ripple is about 25-30% of the inductor current and can be calculated by (56) and (57),

$$L_2 = L_3 = \frac{V_{in}D_{op}}{30\%I_{L2}f_s} \tag{56}$$

$$L_1 = \frac{V_{in}D_{op}}{30\%I_{L1}f_s} \tag{57}$$

Calculating the values of C_1, C_2, L_1, L_2 and L_3, using the analysis described above and are presented in Table 9.

Table 9
Values of inductances and capacitors.

Parameter	Value Calculated
V_{DC}	100 V
Capacitors C_1=C_2	165.66uF
L_2=L_3	50uH
L_1	51.52uH
IL_1	22 A
IL_2= IL_3	21.35A
Dop	0.33

The relation of capacitor and inductance rms current and the Dop is shown in the Fig. 73.

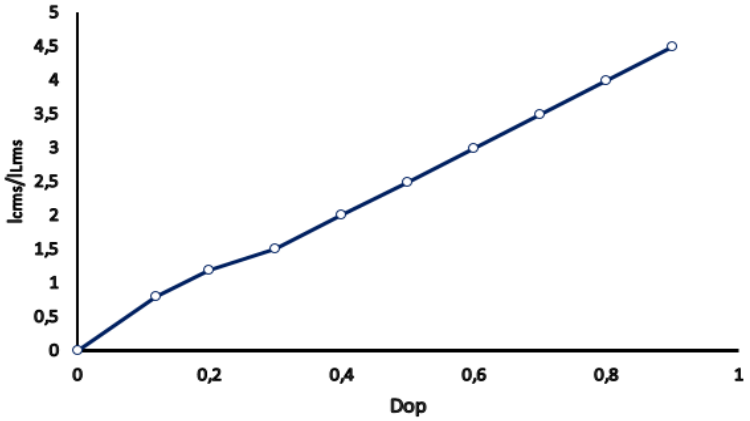

Fig. 73. Relation of Capacitor-Current rms Current vs Dop

In order to obtain the approximate size and volume of the inductors, the core geometry approach is utilized [28], for determining the size and volume of the inductors are necessary several values and constants that are detailed in Table 10.

Table 10
Constants and parameter use for analysis of size and volume

Parameter	Quasi Z SiC	Trans Z SiC
Magnetic Core Type	T125-26	RM-14
Frequency of Switching	100 kHz	100 kHz
Inductance L	50uH	50uH
MLT Length per turn	6.20 cm	7.20 cm
Ac Sectional area	1.340cm^2	1.880cm^2
Wa core window area	5.808cm^2	2.561cm^2
BT Saturation of Core	0.5T	0.5T
Ku winding fill factor	0.4	0.4
μ0 Permeability [H/m]	4π x10 $^{-7}$	4π x10 $^{-7}$
ρ wire resistivity	2.3x10^{-6}	2.3x10^{-6}

Most of these constants are obtained by tables of the coil manufacturers and used for calculated the core geometric constant (58):

$$K_g = \frac{A_c^2 W_a}{MLT} \tag{58}$$

The air gap length l_g is the relation (59):

$$l_g = \frac{\mu_0 I_{max}}{B_{max} A_c} \text{x} 10^6 \tag{59}$$

The number of turns is calculated by (60):

$$n = \frac{L I_{max}}{B_{max} A_c} \text{x} 10^4 \tag{60}$$

For evaluating the wire size, the wire cross-sectional area Aw is limited by the available core window (61):

$$A_w = \frac{K_u W_A}{n} \tag{61}$$

With this value select the AWG and actual winding resistance is calculated by (62):

$$R = \frac{\rho n(MLT)}{A_w} \tag{62}$$

With the analysis the magnetic core is established, the weight and volume estimation can be done with the data provided in the datasheet. The results of analysis for two topologies are present in the Table 11.

Table 11
Results of analisys of volume and weight.

Parameter	Quasi Z SiC	Quasi Z Si	Trans Z SiC	Trans Z Si
Core geometric Constant Kg	1.68cm^5	5.77 cm^5	1.25cm^5	4.52 cm^5
Air gap length lg	1.125 cm	2.18 cm	0.401 cm	0.459 cm
Number of turns	44	174	60	180
Winding resistance	11.8mΩ	179.2 mΩ	58.4mΩ	45.7 mΩ
AWG	24	18	22	20
Volume	0.015 L	0.094L	0.020 L	0.037L
Weight	0.114 Kg	0.96 Kg	0.148 Kg	0.495 Kg

The Fig. 74 shows a comparison between the impedance network source SiC topologies to 100 kHz and conventional topologies with silicon device to 20 kHz in function of the weight.

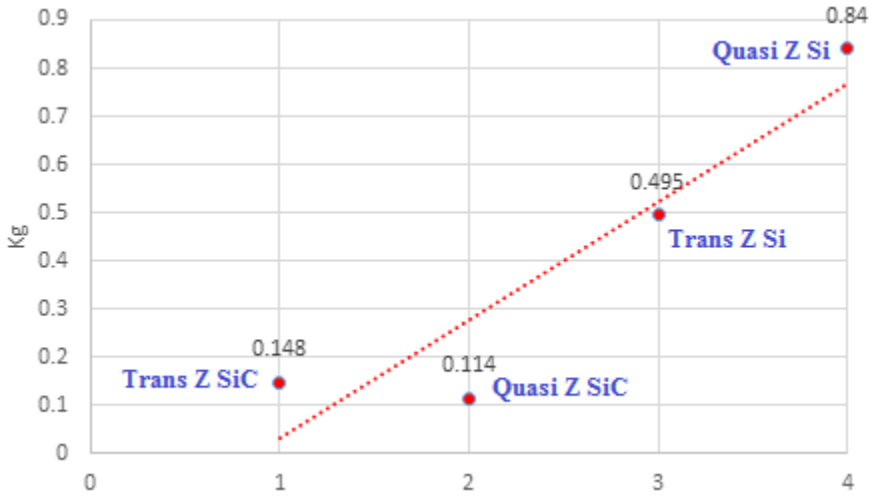

Fig. 74 Comparisson of weigh between SiC topologies vs Si topologies.

These results show that by increasing the frequencies in this type of topology, a reduction in the size of the passive elements of the network is obtained, this improves the design of the converters in size and weight, making them more compact. These converters still present problems such as discontinuous current input, this generates stress situations in the passive components. Besides the fundamental problem is the recovery of energy that is instantaneous and in short times and it is not continuous, this implies that the system does not reach a high efficiency, for this reason these topologies are considered as emerging within the traction systems electric.

For the analysis of power losses in impedance network, the losses in a chokes or inductors are from the following sources, hysteresis loss, copper or winding loss and Eddy current loss.

The hysteresis loss is due to the materials intrinsic properties due to the energy used to align and re-align the magnetic domains. The general form of the losses per unit volume $P_{m,sp}$ is calculated by (63):

$$P_m = kf^a(B_{ac})^d \tag{63}$$

Where k, a and d are constants depending of type of material, for this case is ferrite. Eddy current loss from the circulating currents within the magnetic materials due to differential in flux voltage inside the cores itself [28]. These losses are high dependent upon the thickness of the walls of the cores. The Eddy current loss per unit of volume can be calculated by (64):

$$P_{EC} = \frac{d^a \omega^2 B^d}{24\rho_{core}} \tag{64}$$

The copper or winding loss. This is also dependent on the wire size, switching frequency, etc. Skin effect and proximity effect will contribute to this loss. The copper or winding loss per unit of volume by (65):

$$P_{core} = J_{rms}^2 \rho_{cu} \tag{65}$$

Where J_{rms} is the I_{rms}/Ac. The power losses by conduction and switching in the SiC diode are calculated by (66) and (67):

$$P_{cond} = I_{d\_rms}^2 R_d + I_0 V_d \tag{66}$$

$$P_{sw} = Q_c V_o f_s \tag{67}$$

Where Io is the output current, V_d and R_d are the equivalent resistance and forward voltage drop at given junction temperature of the SiC Schottky diode. Q_c is the total Schottky diode junction charge at specified voltage, V_o is the output voltage, and f_s is the converter switching frequency.

The power losses in Quasi Z impedance network (Fig. 75) with SiC devices are shown in the Table 12 and are they are compared with a conventional topology quasi z with Si devices.

Table 12
Core Losses in Impedance Network and power losses in diode.

Parameter	Quasi Z SiC (100 kHz)	Quasi Z Si (20 kHz)
Hysteresis Losses	1.151mW/cm^3	8.95 mW/cm^3
Eddy current loss	3.89mW/cm^3	7.12W/ cm^3
Copper or winding loss	33.09 W/cm^3	44.34 W/cm^3
Total Core Losses	**33.095041W/cm^3**	**51.46 W/cm^3**
Conduction Diode	4.65 W	3.97 W
Switching Diode	0.826W	2.71 W

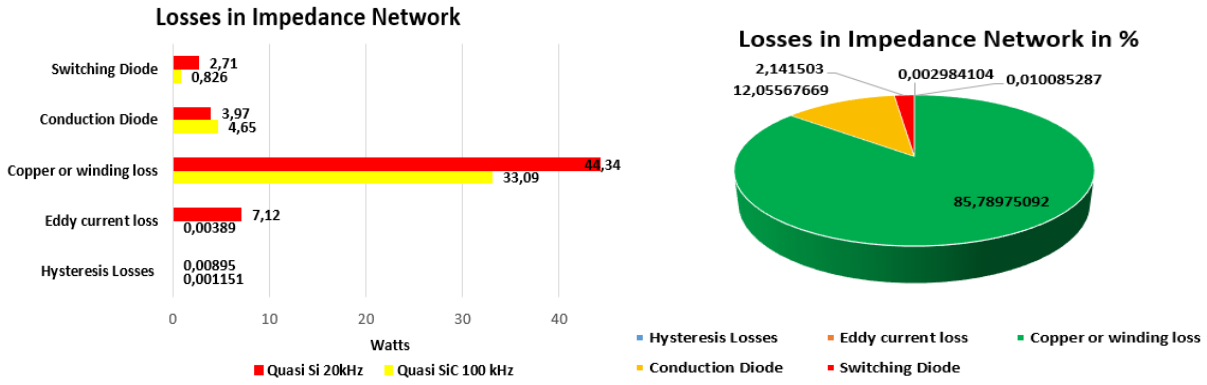

Fig. 75. Losses in Impedance Network.

For the power losses in the CSI converter the important rule is that there must always be at least one switch forward biased in each half bridge of the converter [27]. The loss of conduction Pc of mosfet and diode are expressed as (68) and (69).

$$P_{cond\_mosfet} = R_{ds(on)} I_{DC}^2 \tag{68}$$

$$P_{cond\_diode} = I_{d\_rms}^2 R_d + I_0 V_d \tag{69}$$

Where the R_{ds} is the Resistencia on of Mosfet SiC, I_{DC} is the current of input in the converter; I_0 is the output current in the power converter V_d and R_d are the equivalent resistance and forward voltage drop at given junction temperature of the SiC Schottky diode; I_{d_rms} is the RMS current of the boost diode over one line cycle at given input voltage, output voltage and load current.

The Mosfet and diode switching power losses can be calculated with the expression (70):

$$P_{sw} = \frac{6}{2\pi} f_{sw}(E_{On} + E_{OFF} + E_{OFFD}) \frac{V_{DC}}{i_{REF}} \frac{I_{DC}}{V_{REF}} \qquad (70)$$

The power losses in the topologies of power converters quasi Z and Trans Z with SiC devices in percentages are shown in the Fig 76 and Table 13, also are compared with conventional silicon topologies at low switching frequency.

Table 13
Power Losses in Impedance Network SiC topologies vs Si topologies

Features and Power Losses	**Quasi Z SiC 100kHz**	**Quasi Z Si 10 kHz**	**Trans Z SiC 10kHz**	**Trans Z Si 10kHz**
Vdc	100 V	100 V	100 V	100 V
Transistors	SCT30N120	IRG7PH30K	SCT30N120	IRG7PH30K
Voltage and Current	1200v, 45A	1200v, 25A	1200v, 45A	1200v, 25A
R_{ds}	90mΩ		90mΩ	
Operation Junction Temperature	200^{0}C	100^{0}C	200^{0}C	100^{0}C
Thermal Resistance	0.65^{0}C/W	0.7 ^{0}C/W	0.65^{0}C/W	0.7 ^{0}C/W
Turn on Energy E_{on}	500µJ	850 µJ	500µJ	850 µJ
Turn off Energy E_{off}	350 µJ	750 µJ	350 µJ	750 µJ
Diodes	SCS220KC	FFH60UP60S	SCS220KC	FFH60UP60S
Conduction Mosfets	31.92w	42.32w	66.72w	119.04w
Conduction Diodes	21.12w	37.76w	44.76w	66.94w
Switching Mosfets	12.82w	5.266w	14.308w	8.5w
Switching Diodes	8.46w	7.62w	11.82w	10.8w
Total Power Losses	**74.32w**	**92.96w**	**137.60w**	**205.28w**

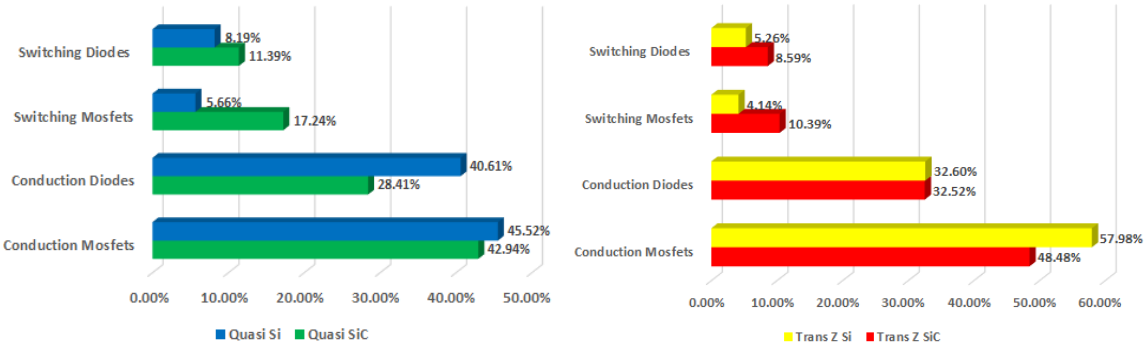

Fig. 76 Power Losses CSI power converters.

In this way it is demonstrated that the use of SiC devices reduces the power losses in this type of converter topologies. In addition, to general expectation was demonstrated in the design of passive devices with the volume and size reduction by the application of SiC devices to high frequency of switching. This optimization would improve the efficiency of the system but the main drawback remains the lack of continuous energy recovery that for these types of topologies is in short times being an intermittent recharge.

Regarding the converter V-I topology (voltage-current), which has the operation presented in the previous section, it is formed by 2 switches (Fig. 77), two diodes and a choke coil; the switches are turned on when it is necessary to transform the source feedback into current for the CSI, this current has to be constant and therefore a current control is necessary. The diodes work when energy is recovered, this recovery is constant and continuous this generates a great advantage over the other topologies analyzed.

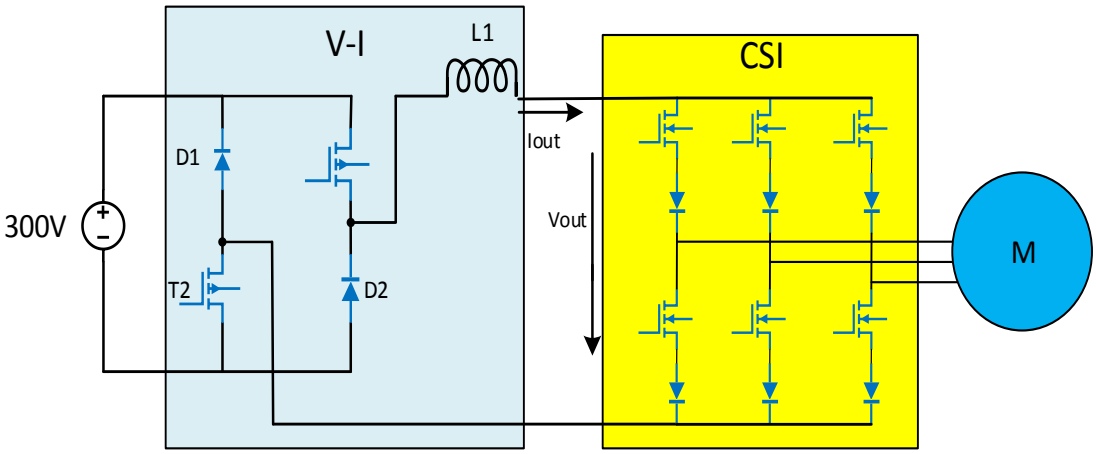

Fig. 77 V-I CSI power converter topology.

The V-I topology has certain advantages:

- This topology works with semiconductor devices, which can be conventional silicon or silicon carbide, the use of SiC devices increases the possibility of working at higher switching frequency.
- If working at higher switching frequencies, there is the possibility of reducing the size and value of the passive elements in this case of the choke coil.
- The regeneration of the current is constant and at all times and only depends on the conduction of the two diodes. The diodes do not need any type of control they are only used to direct the current for the return to the battery.
- The power losses could be reduced when SiC devices are used, this would improve the efficiency of the traction system, besides the power density and temperature is improved, the SiC components work at higher current and temperature ranges.
- The V-I converter works with a frequency independent of the CSI, this can be varied according to the needs, this generates an advantage at the time of design since increasing the frequency allows to reduce the ripple in the input current to the converter (Fig.78)

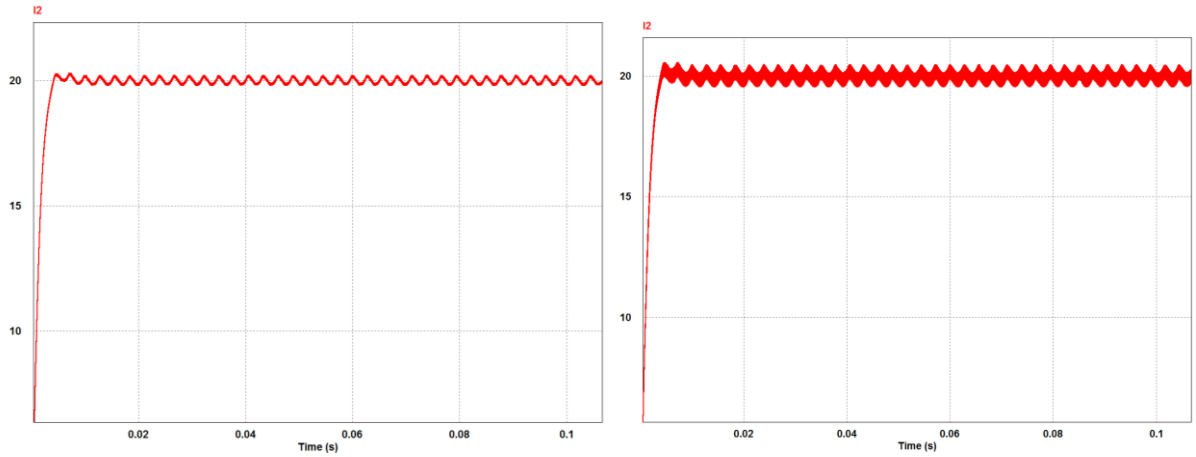

a) b)

Fig. 78 Current output ripple a) V-I frequency 80 kHz, b) V-I frequency 10 kHz

The power losses by conduction and switching of this topology with SiC devices are presented in Table 14. Also in the Fig 79 shows a comparison of the power losses with conventional silicon topologies. For the power losses the equations (68) - (69) and (70) presented in the previous analysis are used.

Table 14
Power losses in V-I SiC power converter

Features and Power Losses	**V-I Converter SiC 80kHz**	**CSI SiC 100kHz**	**V-I Si 5kHz**	**CSI Si 10kHz**
Vdc	300 V	300 V	300 V	300 V
Transistors	SCT3040KL	SCT3040KL	IXGH40N60	IXGH40N60
Voltage and Current	1200v, 55A	1200v, 55A	1200v, 45A	1200v, 25A
R_{ds}	40mΩ	40mΩ		
Diodes	GB50SLT12	GB50SLT12	ISL9R3060G	ISL9R3060G
Conduction Mosfets	54.62w	123.6w	55.16w	214.04w
Conduction Diodes	7.68w	35.34w	12.7w	42.28w
Switching Mosfets	16.96w	72.1w	14.68w	17.76w
Switching Diodes	16.88w	38.64	11.6w	27.3w
Power Losses	**96.14w**	**269.68w**	**97.14w**	**301.38w**
Total Power Losses	**365.82w**		**398.52w**	

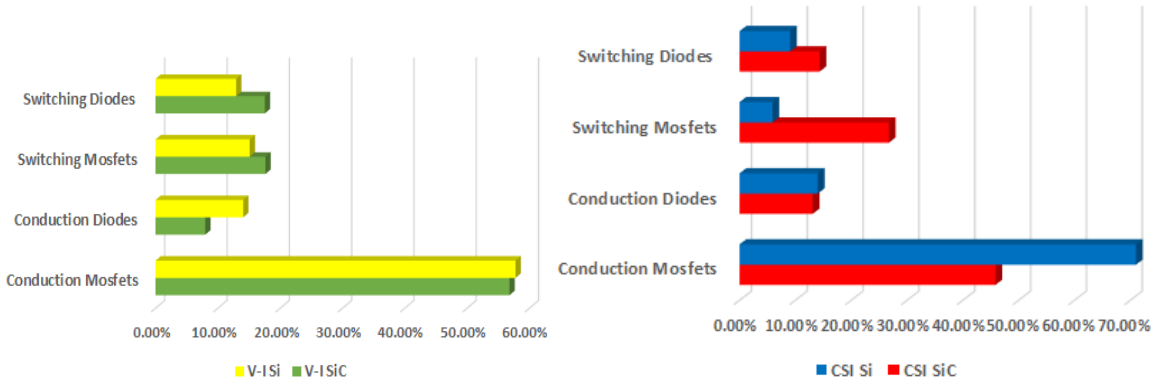

Fig. 79. Comparisson of power losses in V-I CSI SiC power converter.

This topology has many advantages in comparison with others studied, this allows a recovery of energy at all times which solves the problems detected in the other topologies and also you can apply some control technique of easy implementation, which makes it very interesting for application in an electric traction system

A comparative study of all bidirectional topologies presented, the analysis is presented in Table 15 and focuses on the number of active and passive devices, advantages and disadvantages detected, this with the purpose of selecting the best performance and most efficiency, for its implementation.

Table 15
Comparative Study

Features	Dc-Dc	Quasi Z	Trans Z	V-I
No. of Mosfets	4	0	0	2
No. Diodes	0	1	1	2
No. of Capacitors	0	2	2	0
No. of Inductors	1	3	3	1
Energy Recovery	Continuous	Discontinuous	Discontinuous	Continuous
Buck Boost	No	Yes	Yes	Yes
Stress in passive devices	No	Yes	Yes	No
Reduce of Size of passive	Yes only with SiC devices	Yes only with SiC devices	Yes only with SiC devices	Yes only with SiC devices
Power Losses	High	Low	Low	Low
Control	Complex	Complex	Very complex	Easy
Efficiency	Low	Moderate	Low	High
High Frequency	Yes	Yes	Yes	Yes

By performing a weighting (Fig.80) you can establish the topology with the highest performance and to be used, for this situation is the V-I power converter.

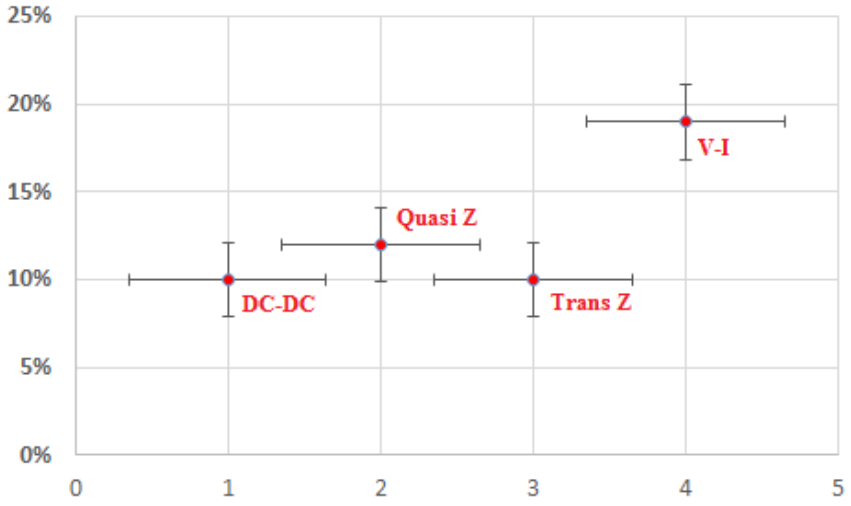

Fig. 80. Topology weighting.

3.5 Conclusions

This chapter presents the operation mode of a bidirectional CSI converter topology plus the modulation techniques and their implementation. In addition, an analysis of the operation of different topologies of bidirectional Dc-Dc converters used in CSI topologies is presented.

Different topologies are discussed, different analysis of their operation is carried out, determining the advantages and disadvantages of each of the selected topologies, especially in the recovery of energy to solve the problem of the CSI power converter topology.

The main contribution is to show the advantages provided by SiC devices in this type of converter topologies for applications in electric traction systems with the aim of improving efficiency, size and volume.

Based on all the analysis implemented and the comparisons made, it is concluded that the DC-DC V-I bidirectional topology has the highest performance and it allows improving the efficiency of the system to be implemented.

3.6 References

[1] Zhiqiao Wu; Gui-Jia Su, "High-performance permanent magnet machine drive for electric vehicle applications using a current source inverter," Industrial Electronics, 2008. IECON 2008. 34th Annual Conference of IEEE, vol., no., pp.2812,2817, 10-13 Nov.2008.

[2] Gui-Jia Su; Lixin Tang, "Current source inverter based traction drive for EV battery charging applications," Vehicle Power and Propulsion Conference (VPPC), 2011 IEEE , vol., no., pp.1,6, 6-9 Sept. 2011.

[3] D. Lusignani, D. Barater, G. Franceschini, G. Buticchi, M. Galea and C. Gerada, "A high-speed electric drive for the more electric engine," 2015 IEEE Energy Conversion Congress and Exposition (ECCE), Montreal, QC, 2015, pp. 4004-4011.

[4] I. Koch, F. Hinrichsen and W. R. Canders, "Application of SiC-JFETs in current source inverter topologies," 2005 European Conference on Power Electronics and Applications, Dresden, 2005, pp. 7 pp.-P.7.

[5] J. Martin, A. Bier, S. Catellani, L. G. Alves-Rodrigues and F. Barruel, "A high efficiency 5.3kW Current Source Inverter (CSI) prototype using 1.2kV Silicon Carbide (SiC) bi-directional voltage switches in hard switching," PCIM Europe 2016; International Exhibition and Conference for Power Electronics, Intelligent Motion, Renewable Energy and Energy Management, Nuremberg, Germany, 2016, pp. 1-8.

[6] Power Electronic Converters, DC-AC Conversion – Guy Seguier, Francis Labrique 1993 eBook ISBN 9783642503221.

[7] Xupeng Fang; Mingjie Zhu; Zhiqiao Chen; Jie Liu; Xinwei Zhao, "Current-fed Z-source inverter modulation," in Electrical Machines and Systems (ICEMS), 2011 International Conference on , vol., no., pp.1-6, 20-23 Aug. 2011.

[8] Keliang Zhou; Danwei Wang, "Relationship between space-vector modulation and three-phase carrier-based PWM: a comprehensive analysis [three-phase inverters]," in Industrial Electronics, IEEE Transactions on, vol.49, no.1, pp.186-196, Feb 2002.

[9] M. S. A. Dahidah, G. Konstantinou and V. G. Agelidis, "A Review of Multilevel Selective Harmonic Elimination PWM: Formulations, Solving Algorithms, Implementation and Applications," in IEEE Transactions on Power Electronics, vol. 30, no. 8, pp. 4091-4106, Aug. 2015.

[10] S. Huang, D. C. Pham, K. Huang and S. Cheng, "Space vector PWM techniques for current and voltage source converters: A short review," 2012 15th International Conference on Electrical Machines and Systems (ICEMS), Sapporo, 2012, pp. 1-6.

[11] E. R. C. da Silva, E. C. dos Santos and B. Jacobina, "Pulsewidth Modulation Strategies," in IEEE Industrial Electronics Magazine, vol. 5, no. 2, pp. 37-45, June 2011.

[12] X. Guo, D. Xu and B. Wu, "Four-Leg Current-Source Inverter With a New Space Vector Modulation for Common-Mode Voltage Suppression," in IEEE Transactions on Industrial Electronics, vol. 62, no. 10, pp. 6003-6007, Oct. 2015.

[13] M. I. Masoud, A. S. Abdelkhalik and R. Al-Abri, "Vector controlled five-phase PWM-CSI induction motor drive fed from controlled three-phase PWM current source rectifier," 7th IET International Conference on Power Electronics, Machines and Drives (PEMD 2014), Manchester, 2014, pp. 1-6.

[14] M. A. Elgenedy, A. Abdel-Khalik, A. Elserougi, S. Ahmed and A. M. Massoud, "A new five-phase to three-phase back-to-back current source converter based wind energy conversion system," 2013 7th IEEE GCC Conference and Exhibition (GCC), Doha, 2013, pp. 193-198.

[15] M. I. Masoud and A. S. Abdel-Khalik, "Vector controlled five-phase PWM-CSI induction motor drive," 4th International Conference on Power Engineering, Energy and Electrical Drives, Istanbul, 2013, pp. 258-264.

[16] D. Xu and B. Wu, "Multilevel Current Source Inverters with Phase Shifted Trapezoidal PWM," 2005 IEEE 36th Power Electronics Specialists Conference, Recife, 2005, pp. 2540-2546.

[17] B. Wu, S. B. Dewan and G. R. Slemon, "PWM-CSI inverter for induction motor drives," Conference Record of the IEEE Industry Applications Society Annual Meeting,, San Diego, CA, USA, 1989, pp. 508-513 vol.1.

[18] A. Agarwal and V. Agarwal, "FPGA Realization of Trapezoidal PWM for Generalized Frequency Converter," in IEEE Transactions on Industrial Informatics, vol. 8, no. 3, pp. 501-510, Aug. 2012.

[19] D. C. Pham, S. Huang and K. Huang, "Modeling and simulation of current source inverters with space vector modulation," 2010 International Conference on Electrical Machines and Systems, Incheon, 2010, pp. 320-325.

[20] H. Gao, S. Das, B. Wu, M. Pande and D. Xu, "A space vector modulation based direct torque control scheme for a current source inverter fed induction motor drive," IECON 2015 - 41st Annual Conference of the IEEE Industrial Electronics Society, Yokohama, 2015, pp. 001307-001312.

[21] M. S. A. Dahidah, G. Konstantinou and V. G. Agelidis, "A Review of Multilevel Selective Harmonic Elimination PWM: Formulations, Solving Algorithms, Implementation and Applications," in IEEE Transactions on Power Electronics, vol. 30, no. 8, pp. 4091-4106, Aug. 2015.

[22] P. Saranya and V. Rajini, "Selective harmonic elimination in three-phase Current Source Inverter- A generalized approach," 2011 International Conference on Emerging Trends in Electrical and Computer Technology, Tamil Nadu, 2011, pp. 358-363.

[23] Y. Zhang and Y. W. Li, "Investigation and Suppression of Harmonics Interaction in High-Power PWM Current-Source Motor Drives," in IEEE Transactions on Power Electronics, vol. 30, no. 2, pp. 668-679, Feb. 2015.

[24] A. Schonung and H. Stemmler, ‘‘Static frequency changers with subharmonic control in conjunction with reversible variable speed a.c. drives,’’ Brown Boweri Rev. , vol. 51, no. 8/9, Aug./Sept. 1964,pp. 555–577.

[25] J. Espinoza and G. Joos, "On-line generation of gating signals for current source converter topologies," Industrial Electronics, 1993. Conference Proceedings, ISIE'93 - Budapest., IEEE International Symposium on, Budapest, Hungary, 1993, pp. 674-678.

[26] D. Rathnakumar, J. LakshmanaPerumal and T. Srinivasan, "A new software implementation of space vector PWM," Proceedings. IEEE SoutheastCon, 2005., 2005, pp. 131-136.

[27] . R. Jardan, S. B. Dewan, and G. Slemon, ‘‘General analysis of three-phase inverters,’’ IEEE Trans. Ind. Applicat, vol. 5, no. 6, pp. 672–679, 1969.

[28] A. Busse and J. Holtz, ‘‘Multiloop control of a unity power factor fast-switching AC to DC converter,’’ in Conf. Rec. IEEE Power Electronics Specialists Conf. (PESC’82) , 1982, pp. 171 –179.

[29] Y. W. Li, B. Wu, D. Xu and N. Zargari, "Space Vector Sequence Investigation and Synchronization Methods for PWM Modulation of a High Power Current Source Rectifier," 2007 IEEE Power Electronics Specialists Conference, Orlando, FL, 2007, pp. 2841-2847.

[30] S. A. Azmi, G. P. Adam and B. W. Williams, "New modulation strategy for three-phase current source inverters," 4th International Conference on Power Engineering, Energy and Electrical Drives, Istanbul, 2013, pp. 1110-1115.

[31] Longcheng Tan, Yaohua Li, Ping Wang and Wei Xu, "The application of neurocomputing on space vector modulation for current source converters," 2008 IEEE International Conference on Industrial Technology, Chengdu, 2008, pp. 1-4.

[32] J. Holtz, M. Höltgen and J. O. Krah, "A Space Vector Modulator for the High-Switching Frequency Control of Three-Level SiC Inverters," in IEEE Transactions on Power Electronics, vol. 29, no. 5, pp. 2618-2626, May 2014.

[33] S. Sridharan and P. T. Krein, "Performance and efficiency enhancement of induction machine drives: Duality-based approach to VSI and CSI control," 2013 IEEE 14th Workshop on Control and Modeling for Power Electronics (COMPEL), Salt Lake City, UT, 2013, pp. 1-8.

[34] K. Taniguchi and H. Irie, "Trapezoidal Modulating Signal for Three-Phase PWM Inverter," in IEEE Transactions on Industrial Electronics, vol. IE-33, no. 2, pp. 193-200, May 1986.

[35] J. N. Chiasson, L. M. Tolbert, K. J. McKenzie and Zhong Du, "A complete solution to the harmonic elimination problem," in IEEE Transactions on Power Electronics, vol. 19, no. 2, pp. 491-499, March 2004.

[36] J. R. Wells, B. M. Nee, P. L. Chapman and P. T. Krein, "Selective harmonic control: a general problem formulation and selected solutions," in IEEE Transactions on Power Electronics, vol. 20, no. 6, pp. 1337-1345, Nov. 2005.

[37] S. Yang, F. Z. Peng, Q. Lei, R. Inoshita and Z. Qian, "Current-fed quasi-Z-source inverter with voltage buck-boost and regeneration capability," 2009 IEEE Energy Conversion Congress and Exposition, San Jose, CA, 2009, pp. 3675-3682.

[38] G. J. Su and L. Tang, "Current source inverter based traction drive for EV battery charging applications," 2011 IEEE Vehicle Power and Propulsion Conference, Chicago, IL, 2011, pp. 1-6.

[39] F. Gao, P. C. Loh, F. Blaabjerg and D. M. Vilathgamuwa, "Five-Level Current-Source Inverters With Buck–Boost and Inductive-Current Balancing Capabilities," in IEEE Transactions on Industrial Electronics, vol. 57, no. 8, pp. 2613-2622, Aug. 2010.

[40] O. Hegazy, J. Van Mierlo and P. Lataire, "Design and control of bidirectional DC/AC and DC/DC converters for plug-in hybrid electric vehicles," 2011 International Conference on Power Engineering, Energy and Electrical Drives, Malaga, 2011, pp. 1-7.

[41] R. Priewasser, M. Agostinelli, C. Unterrieder, S. Marsili and M. Huemer, "Modeling, Control, and Implementation of DC–DC Converters for Variable Frequency Operation," in IEEE Transactions on Power Electronics, vol. 29, no. 1, pp. 287-301, Jan. 2014.

[42] Siwakoti, Y.P.; Fang Zheng Peng; Blaabjerg, F.; Poh Chiang Loh; Town, G.E., "Impedance-Source Networks for Electric Power Conversion Part I: A Topological Review," in Power Electronics, IEEE Transactions on, vol.30, no.2, pp.699-716, Feb. 2015 doi: 10.1109/TPEL.2014.

[43] Yamashita, N.; Asano, M.; Yamanaka, M.; Koizumi, H., "A Z-source inverter accepting rapid reverse current flow," in TENCON 2010 – 2010 IEEE Region 10 Conference , vol., no., pp.48-53, 21-24 Nov. 2010 TENCON.2010.

[44] F. Z. Peng, “Z-source inverter,” IEEE Trans. Ind. Appl., vol. 39, pp.504-510, Mar/Apr 2003.

[45] P. C. Loh, C. J. Gajanayake, D. M. Vilathgamuwa, and F. Blaabjerg, “Evaluation of resonant damping techniques for Z-source current-type inverter,” IEEE Trans. Power Electron., vol. 23, no. 4, pp. 2035–2043, Jul. 2008.

[46] Karimi, R.; Koeneke, T.; Kaczorowski, D.; Werner, T.; Mertens, A., "Low voltage and high power DC-AC inverter topologies for electric vehicles," Energy Conversion Congress and Exposition (ECCE), 2013 IEEE, vol., no., pp.2805, 2812, 15-19 Sept. 2013.

[47] Shuai Jiang; Dong Cao; Peng, F.Z., "High frequency transformer isolated Z-source inverters," Applied Power Electronics Conference and Exposition (APEC), 2011 Twenty-Sixth Annual IEEE , vol., no., pp.442,449, 6-11 March 2011.

[48] Ding Li; Poh Chiang Loh; Miao Zhu; Feng Gao; Blaabjerg, F., "Generalized Multicell Switched-Inductor and Switched-Capacitor Z Source Inverters," Power Electronics, IEEE Transactions on, vol.28, no.2, pp.837, 848, Feb. 2013.

[49] H. Xu, F. Peng, L. Chen and X. Wen, “Analysis and design of Bidirectional Z-source inverter for electrical vehicles,” in Proc. IEEE Applied Power Electronics Conference and Exposition, Austin, TX, Feb. 2008, pp. 1252-1257.

[50] Hegazy, O.; Barrero, R.; Van Mierlo, J.; Lataire, P.; Omar, N.; Coosemans,T., "An Advanced Power Electronics Interface for Electric Vehicles Applications,” Power Electronics, IEEE Transactions on , vol.28, no.12, pp.5508,5521, Dec. 2013.

[51] Q. Lei, F. Z. Peng and S. Yang, "Discontinuous operation modes of current-fed Quasi-Z-Source inverter," 2011 Twenty-Sixth Annual IEEE Applied Power Electronics Conference and Exposition (APEC), Fort Worth, TX, 2011, pp. 437-441.

[52] Q. Lei, D. Cao and F. Z. Peng, "Novel Loss and Harmonic Minimized Vector Modulation for a Current-Fed Quasi-Z-Source Inverter in HEV Motor Drive Application," in IEEE Transactions on Power Electronics, vol. 29, no. 3, pp. 1344-1357, March 2014.

[53] Y. P. Siwakoti, F. Z. Peng, F. Blaabjerg, P. C. Loh, G. E. Town and S. Yang, "Impedance-Source Networks for Electric Power Conversion Part II: Review of Control and Modulation Techniques," in IEEE Transactions on Power Electronics, vol. 30, no. 4, pp. 1887-1906, April 2015.

[54] F. Z. Peng, M. Shen and Z. Qian, "Maximum boost control of the Zsource inverter," Power Electronics Specialists Conference, 2004. PESC 04. 2004 IEEE 35th Annual, 2004, pp. 255-260 Vol.1.

[55] Miaosen Shen, Jin Wang, A. Joseph, Fang Zheng Peng, L. M. Tolbert and D. J. Adams, "Constant boost control of the Z-source inverter to minimize current ripple and voltage stress," in IEEE Transactions on Industry Applications, vol. 42, no. 3, pp. 770-778, May-June 2006.

[56] U. S. Ali and V. Kamaraj, "A novel space vector PWM for Z-source inverter," Electrical Energy Systems (ICEES), 2011 1st International Conference on, Newport Beach, CA, 2011, pp. 82-85.

[57] E. R. C. da Silva, E. C. dos Santos and B. Jacobina, "Pulsewidth Modulation Strategies," in IEEE Industrial Electronics Magazine, vol. 5, no. 2, pp. 37-45, June 2011

[58] Q. Lei, D. Cao and F. Z. Peng, "Novel SVPWM switching pattern for high efficiency 15KW current-fed quasi-Z-source inverter in HEV motor drive application," 2012 Twenty-Seventh Annual IEEE Applied Power Electronics Conference and Exposition (APEC), Orlando, FL, 2012, pp. 2407-2420.

[59] Y. Liu, B. Ge, H. Abu-Rub and F. Z. Peng, "Overview of Space Vector Modulations for Three-Phase Z-Source/Quasi-Z-Source Inverters," in IEEE Transactions on Power Electronics, vol. 29, no. 4, pp. 2098-2108, April 2014.

[60] F. E. Alfaris and S. Bhattacharya, "A current-fed quasi Z-source inverter with SiC power modules for EV/HEV applications," 2017 IEEE Energy Conversion Congress and Exposition (ECCE), Cincinnati, OH, 2017, pp. 5445-5452.

[61] W. Qian, F. Z. Peng and H. Cha, "Trans-Z-Source Inverters," in IEEE Transactions on Power Electronics, vol. 26, no. 12, pp. 3453-3463, Dec. 2011.

[62] Q. Lei, S. Yang, F. Z. Peng and R. Inoshita, "Application of current-fed quasi-Z-Source Inverter for traction drive of hybrid electric vehicles," 2009 IEEE Vehicle Power and Propulsion Conference, Dearborn, MI, 2009, pp. 754-760.

[63] D. Cao, Q. Lei and F. Z. Peng, "Development of high efficiency current-fed quasi-Z-source inverter for HEV motor drive," 2013 Twenty-Eighth Annual IEEE Applied Power Electronics Conference and Exposition (APEC), Long Beach, CA, 2013, pp. 157-164.

[64] A. Battiston, J. P. Martin, E. H. Miliani, B. Nahid-Mobarakeh, S. Pierfederici and F. Meibody-Tabar, "Comparison Criteria for Electric Traction System Using Z-Source/Quasi Z-Source Inverter and Conventional Architectures," in IEEE Journal of Emerging and Selected Topics in Power Electronics, vol. 2, no. 3, pp. 467-476, Sept. 2014.

[65] J. Anderson and F. Z. Peng, "Four quasi-Z-Source inverters," 2008 IEEE Power Electronics Specialists Conference, Rhodes, 2008, pp. 2743-2749.
[66] Y. Li and F. Z. Peng, "AC small signal modeling, analysis and control of quasi-Z-Source Converter," Power Electronics and Motion Control Conference (IPEMC), 2012 7th International, Harbin, China, 2012, pp. 1848-1854.

[67] G. Sen and M. E. Elbuluk, "Voltage and Current-Programmed Modes in Control of the Z-Source Converter," in IEEE Transactions on Industry Applications, vol. 46, no. 2, pp. 680-686, March-April 2010.

[68] O. Ellabban, J. V. Mierlo and P. Lataire, "Control of a bidirectional Z Source Inverter for hybrid electric vehicles in motoring, regenerative braking and grid interface operations," Electric Power and Energy Conference (EPEC), 2010 IEEE, Halifax, NS, 2010, pp. 1-6.

[69] F. Guo, L. Fu, C. H. Lin, C. Li, W. Choi and J. Wang, "Development of an 85-kW Bidirectional Quasi-Z-Source Inverter With DC-Link Feed-Forward Compensation for Electric Vehicle Applications," in IEEE Transactions on Power Electronics, vol. 28, no. 12, pp. 5477-5488, Dec 2013.

4.

Method of optimization for the topologies V-I and CSI converters with SiC devices

This chapter is dedicated to the search of a method of optimization for the synchronization of the two topologies of converters chosen, i.e., the bidirectional V-I and current source inverter. The method seeks to optimize total harmonic distortion THD of the output currents and to improve efficiency for future implementation in an electric traction system.

The method involves an effective selection of the switching frequencies and the phase angle for the carrier signals present in each converter topology

Several issues are discussed such as the operation modes of the topologies analyzed at the level of switching frequencies and optimal synchronization, and the phase angles required between carrier signals to obtain a reduction in harmonic distortion in the PWM output current.

CONTENTS:

4.1 Introduction

The use of power converters with a current source for electric traction systems has not had a high growth within the industry. This is due to problems that have been detected such as energy recovery and an ideal current source that have contributed to this topology not being consolidated [1].

Several studies have been carried out to analyze the possible impact of the topology of current source inverter in electric traction systems. Some of these studies present solutions for the problems detected [2]-[3]. In general, the majority of investigations implement different types of topologies of DC-DC converters for energy recovery, but none of them focuses on the search for a suitable adaptation and synchronization between the topology that makes current source and the inverter topology CSI.

On the other hand, investigations have been presented to minimize power losses and improve of the efficiency [4]; the topology most analyzed for electric traction systems is the voltage source inverter topology (VSI), but everyone use the conventional silicon devices and works to low frequency. The results obtained under these features of operation shown that the total harmonic distortion (THD) and power losses are high.

In [5] the authors present the topology of CSI with a power converter V-I that controls the stabilization of the current of input and the recovery of the current for the battery of high voltage. For the implementation of this topology they are used insulated gate bipolar transistors (IGBTs) with reverse-blocking (RB) capability to low frequency of switching, 15 kHz for V-I power converter and 7.5 kHz for CSI. The result shows that the THD is high and the technique of modulation used is the simple signals of carrier without shift angle.

To improve the V-I current source inverter topology is necessary analyzed differents topics, firstly the frequencies of operations in each power converter, and secondly the phase angle between signals carriers of V-I power converter and CSI inverter, to finalize analyzing the type of modulation technique of best performance.

The research present in [6] analyze a control technique to minimize the effects of ripple on the output current of the V-I thereby improving the efficiency of the electric motor at high speeds controlled by CSI by using conventional silicon devices. The result in simulations shows the THD is higher and the frequency of operation of the converters is not detailed.

The main objective of this chapter is to find a suitable method that allows to synchronize effectively the two topologies of converters to obtain an optimization in the THD of the output currents and efficiency of the system. For this, SiC devices are selected that allow increasing the frequency of operation of the converters and improve their functionality. The search for the optimization method for this topology involves a series of processes and steps that must be considered and explained in the following sections of this chapter.

4.2 Method Proposed.

Various authors indicated that the CSI topology is ideal for operating at high frequency, allowing the input inductor converter and the output filter capacitors be reduced in size [7-8]. Certain advantages compared to the VSI topology are described in [9-10] as the high voltage capability, the auto short-circuits protection, and the sinusoidal output voltage due to the effect of the output filter AC capacitors.

The topology proposed for the implementation of the method uses a V-I converter to regulate and control of the current input and three-phase CSI inverter that generates the three-phase currents of output, the two topologies haven Mosfet and diodes SiC devices (Fig.81).

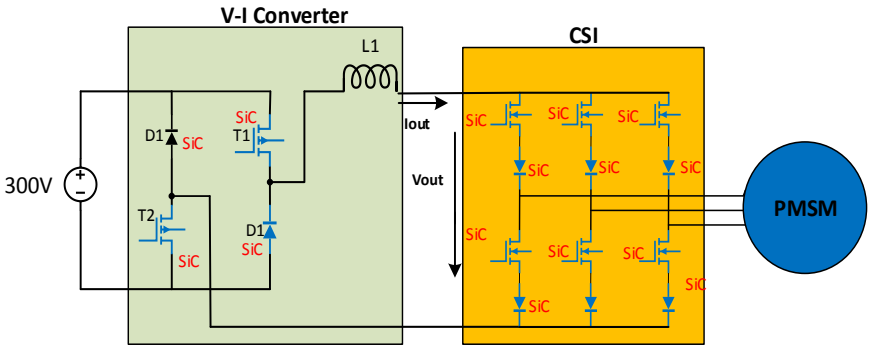

Fig.81. Topology proposed for the analysis.

The configuration allows the bidirectionality of the energy flows. In the first state (Fig.2), the SiC Mosfets T_1 and T_2 are turned on and under this condition; the battery voltage is applied to the converter and charges the inductor. In this mode a current I_{out} and a voltage V_{out} are obtained. Current returns through of CSI and the load by the activation of SiC Mosfet T_2, the Diodes D_1, and D_2 are in reverse bias therefore they are not activated Fig.82.

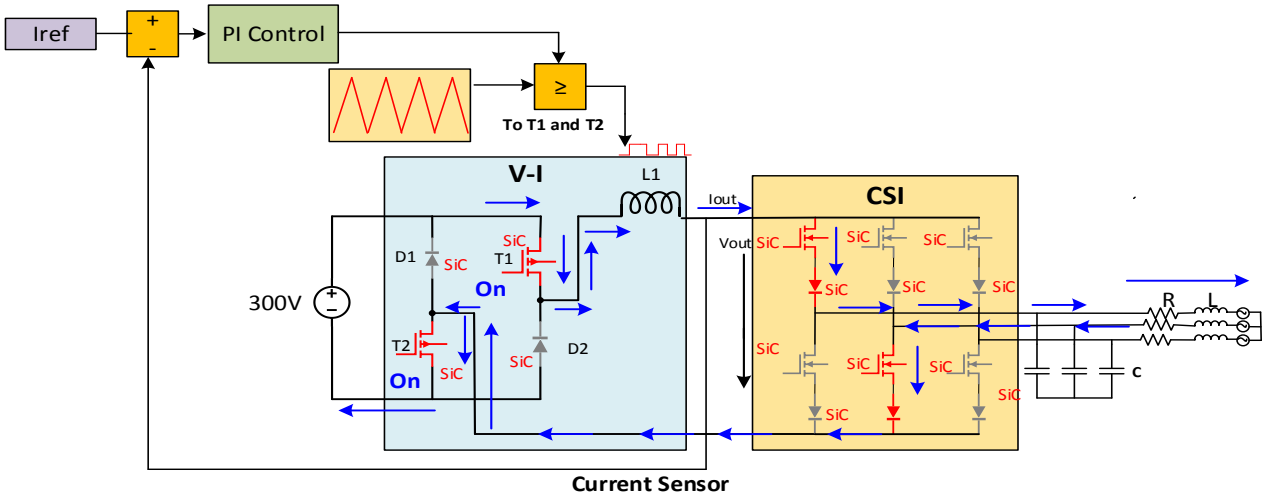

Fig.82. Topology proposed for the analysis fist state.

For the activation of T_1 and T_2 is necessary PI control which is compared with a carrier signal that has a certain frequency and as a result the pulses that turn the transistors on and off are obtained in order to obtain a regulated current. The error is obtained by comparing a current reference signal with the current output signal through a current sensor

In the second state (Fig. 83) the Mosfets are turned off and the current flows through the diodes D_1 and D_2, this mode can be implemented in the case when the current converter return energy to recharge the high voltage battery V_{out}=-$V_{Battery}$.

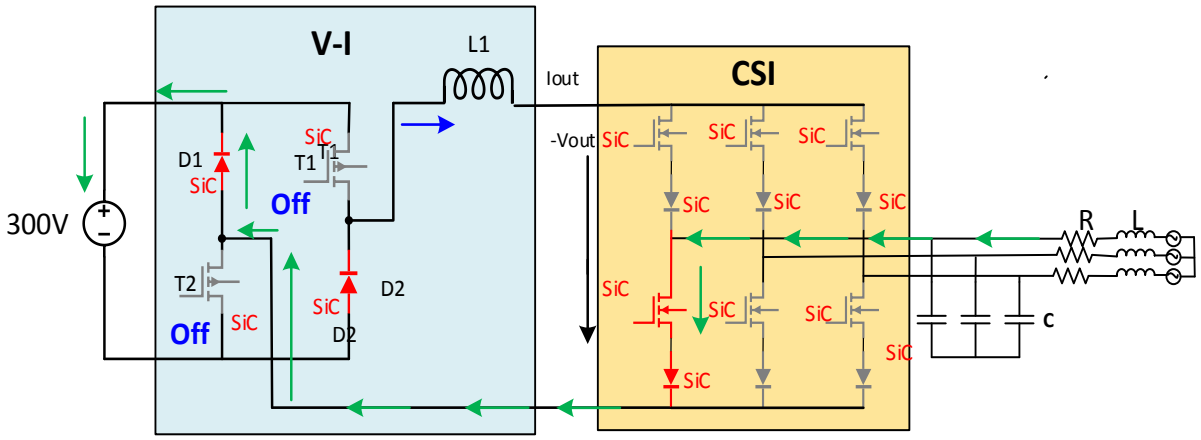

Fig.83. Topology proposed for the analysis state of recovery.

The CSI inverter is switched by a PWM modulator, which generates different signals that are responsible for turning on the six SiC transistors of the CSI (Fig.84). The modulator consists of a carrier signal that provides the switching frequency of the transistors and three sinusoidal modulating signals.

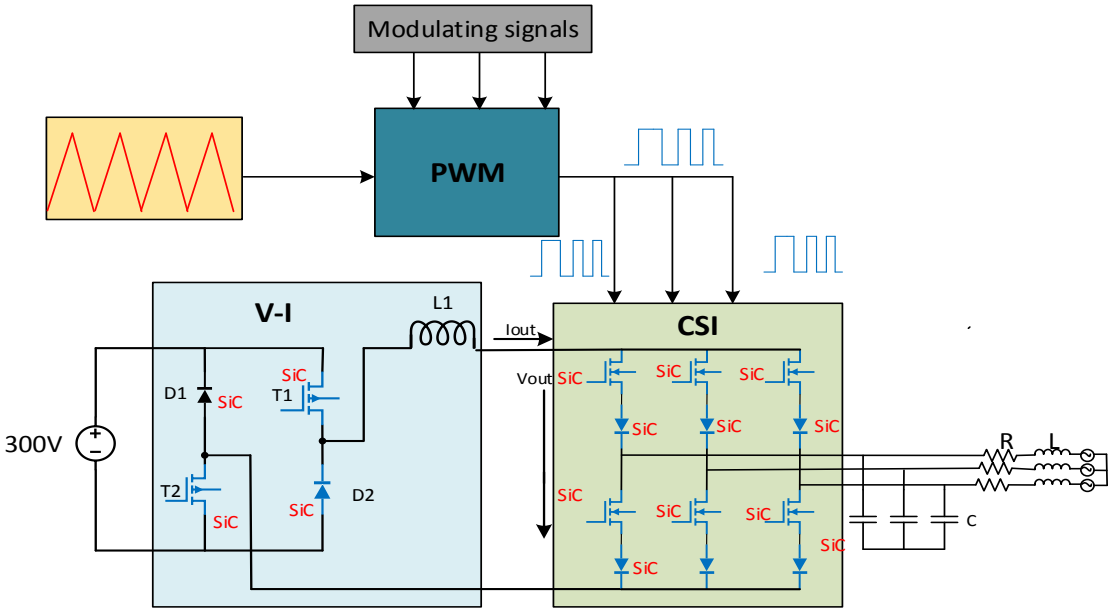

Fig.84. CSI inverter modulator PWM.

These two converter topologies can operate independently, each can take a given frequency value and a phase angle of each carrier signal. If an analysis is made with different angle conditions and leaving the frequency of the CSI fixed and varying the frequency of the V-I, different THD values are obtained for each situation; for example the Fig. 85 shown the results for F_{vi}= 5 kHz to 90 kHz, f_{csi}=90 kHz and phase angle 0 to 180°.

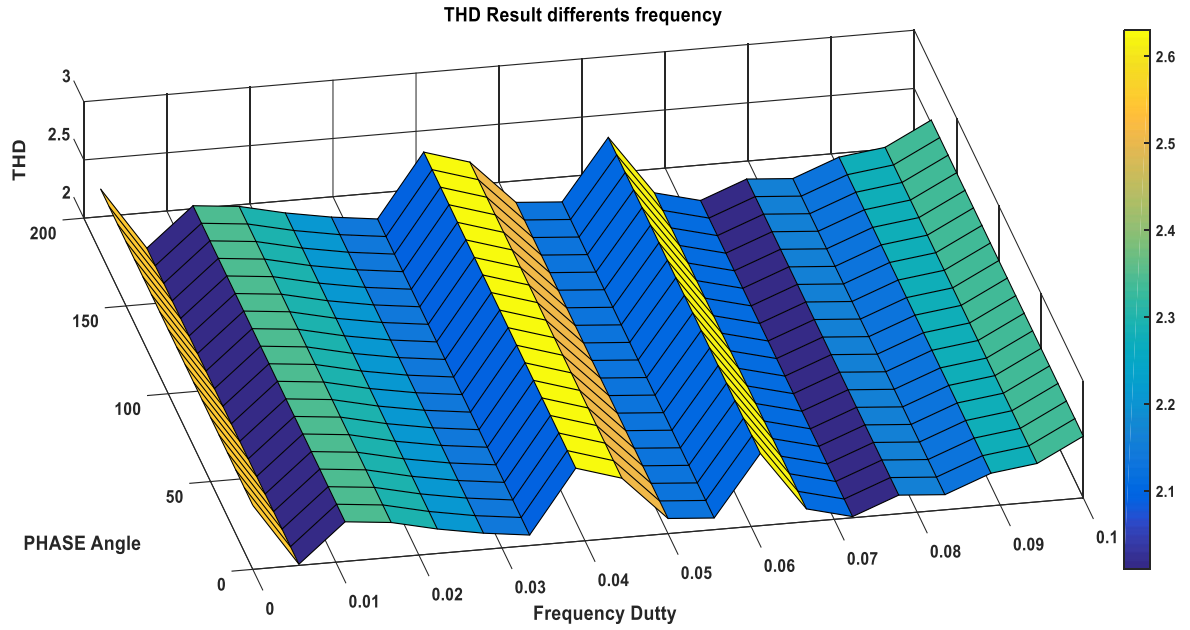

Fig.85. Surface with THD results for Fvi= 5 kHz to 90 kHz, fcsi=90 kHz and phase angle 0 to 180°.

If the results are analyzed, it is observed that there are areas where the THD is reduced to different frequency values and angles between the carrier signals of each topology. Based on these results we can establish that the search for a method that allows obtaining the values of operating frequencies of each converter and the angle of lag between the carrier signals with the purpose of reducing the THD is necessary to obtain an improvement in the efficiency of the analyzed topology.

The proposed methodology has two parts: the first part consists in implementing a control to regulate the output current of the V-I converter. To do that, the carrier signal A is compared with the control to regulate the input current to the CSI, the carrier A signal indicates the switching frequency for the V-I converter.

The second part consist in search the best frequency of operation in the V-I converter and CSI inverter, also seeks the best angle of phase between the carrier signal A and B for the purpose of obtaining a reduction in the THD of current output signals. The carrier B signal is used for modulation technique in the CSI inverter to thus synchronize the two topologies. The scheme of the method proposed is shown in the Fig.86.

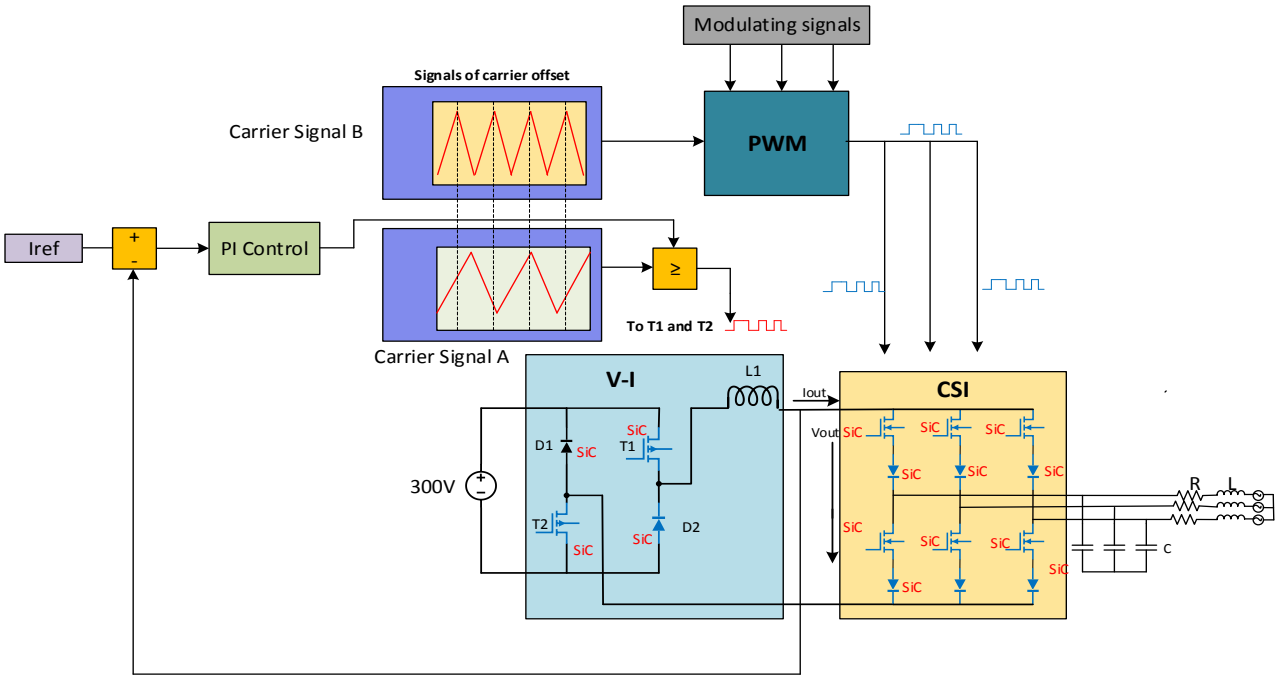

Fig.86. Schematic of operation and method proposed.

For the control of current of input in the V-I converter is necessary the implementation on PI control. The equations of the system were detailed in the previous chapter, The system of the V-I converter is expressed in its differential equations (71) - (72) input and output.

$$L\frac{di_L(t)}{dt} = V_{in}(t) - 2R_{ds}I_L(t) - R_L I_L(t) - V_{out} \tag{71}$$

$$\frac{dV_C(t)}{dt} = \frac{\frac{R_{Load}}{R_{Load}+R_c}}{C} I_L(t) - \frac{\frac{1}{R_{Load}+R_c}}{C} V_c(t) \tag{72}$$

For resolve the system, we can set the equation of state space model (73), (74):

$$\boldsymbol{X(t) = AX(t) + B} \tag{73}$$

$$\boldsymbol{Y(t) = CX(t) + D} \tag{74}$$

Expressing the equations in the matrix function, we have:

$$\begin{bmatrix} \frac{di_L(t)}{dt} \\ \frac{dV_C(t)}{dt} \end{bmatrix} = \begin{bmatrix} \frac{2R_{ds}+R_L+\frac{R_{Load}R_c}{R_{Load}+R_c}}{L} & -\frac{\frac{R_{Load}}{R_{Load}+R_c}}{L} \\ \frac{\frac{R_{Load}}{R_{Load}+R_c}}{C} & -\frac{\frac{1}{R_{Load}+R_c}}{C} \end{bmatrix} \begin{bmatrix} I_L(t) \\ V_c(t) \end{bmatrix} + \begin{bmatrix} \frac{1}{L} \\ 0 \end{bmatrix} V_{in}(t) \tag{75}$$

$$\begin{bmatrix} \frac{V_o(t)}{dt} \\ I_{in}(t) \end{bmatrix} = \begin{bmatrix} \frac{R_{Load}R_c}{R_{Load}+R_c} & \frac{R_{Load}}{R_{Load}+R_c} \\ 1 & 0 \end{bmatrix} \begin{bmatrix} I_L(t) \\ V_c(t) \end{bmatrix} + \begin{bmatrix} 0 \\ 0 \end{bmatrix} V_{in}(t) \tag{76}$$

The value of the inductance for this case is calculated with the expression (77). The values and parameters used for the solution of the system are presented in Table 16.

$$L = \frac{\Delta i V i}{2\pi f_{sw} I_{dc}} \tag{77}$$

Where Δ_i is the ripple current V_{dc} is the input voltage, fsw is the frequency of switching and I_{dc} is the maximum current of input to V-I.

Table 16
Parameters for calculated and solve the system.

Parameter	Value
V_{DC}	100 V
fsw	35 kHz
I_{dc}	10 A
Inductance L	5mH
Resistencia inductance RL	0.15Ω
Capacitor C	15uF
ESR capacitor	0.05 Ω
Rload	5 Ω
L load	1.5mH
Rds Mosfet	40m Ω

The transfer function of the current of output obtained by solving the system is the expression (78).

$$I_{out}(s) = \frac{200s+1.092e^7}{s^2+54670s+1.744e^7} \tag{78}$$

For the tuning of PI control the auto-tuning tool of the PID block of Simulink is used the results are shown in the Fig. 87 and Table 17.

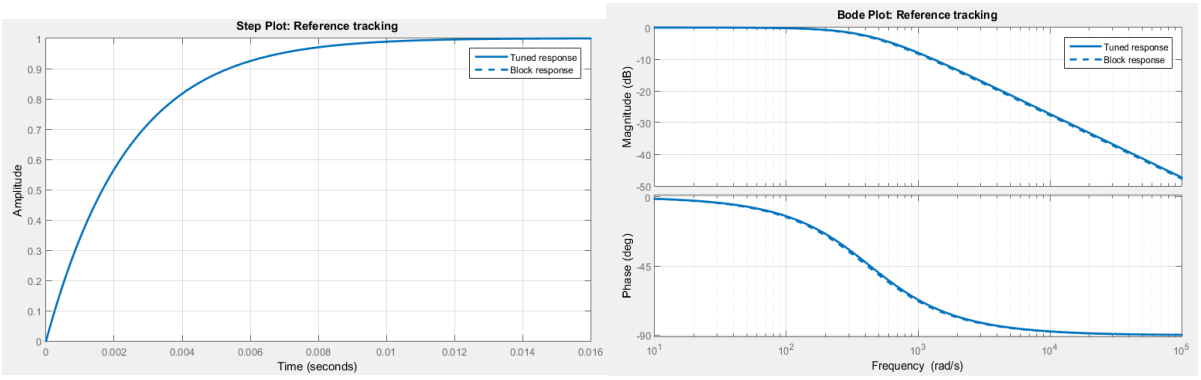

Fig.87. Tuning of PI control for V-I converter.

Table 17.
PI tuning results.

Parameter	Value
Kp	2.05769580834167
Ki	696.186624758197
Rise time	0.00488 s
Settling time	0.00838 s
Overshoot	0.0198%
Peak	1
Phase margin	89 deg @ 439 rad/s

For the implementation of the control, it is necessary to design the topologies of converters in Matlab-Simulink and with the help of the library simscape and simpower system, the topologies are built (Fig 88).

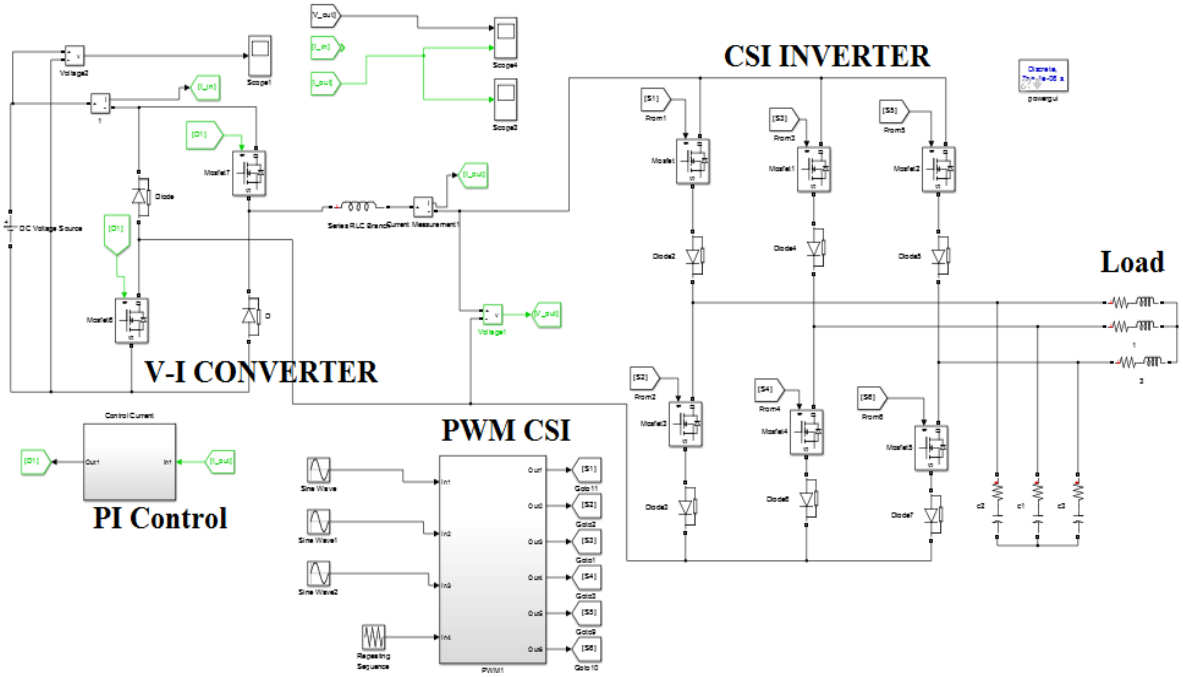

Fig.88. Schematic topologies V-I converter and CSI implemented in Simulink.

The block of the controller Pi (Fig.89) consists of capturing the signal of the output current of the V-I and comparing it with a reference, the error enters the block PI which has the constants kp and ki. The output signal of the PI is then compared with a carrier signal; this signal is the triangular shape and serves to supply the frequency for the switching of the transistors. As a result of the comparison, a pulsating signal is obtained that is distributed to each V-I transistor.

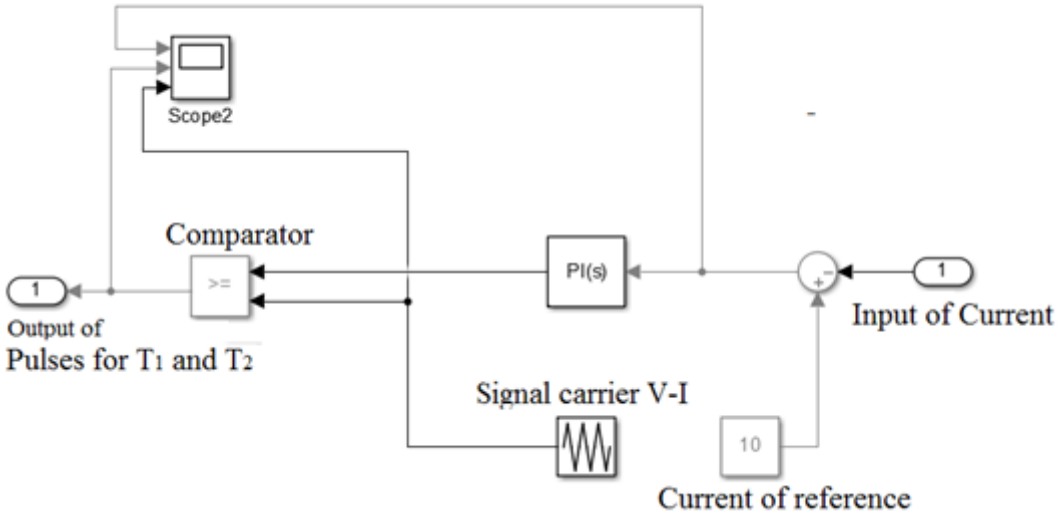

Fig.89. PI control block.

The implementation of the output current control of the V-I converter generates the simulation results presented in Fig 90.

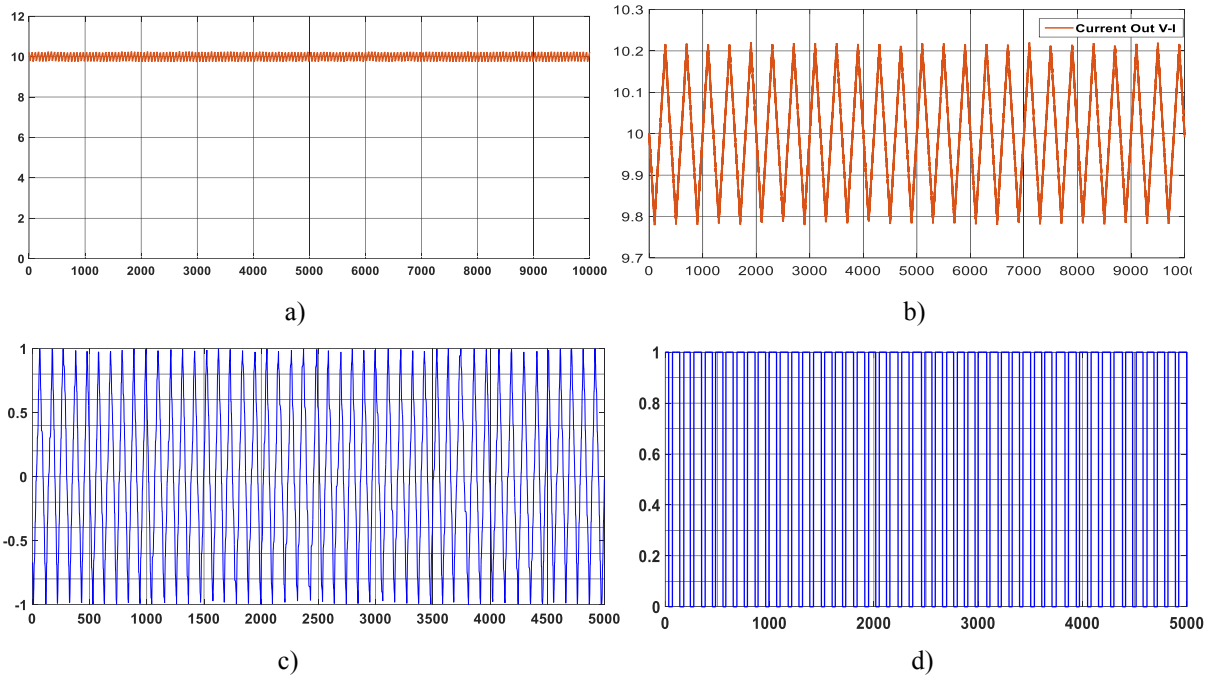

Fig.90. Simulations results in V-I converter, a) Current of output with 10 amperes of set point, b). Zoom of the current of output, c) Signal carrier of V-I converter, d) Signals of pulses in the output of the control for transistors.

Once the control has been implemented, the next stage of the proposed method is to find the optimum operating frequencies between the two topologies, to start an analysis we establish the three rules expressed in (79).

$$f_s = \begin{cases} f_{s(vi)} = f_{s(csi)} \\ f_{s(vi)} = 2f_{s(csi)} \\ 2f_{s(vi)} = f_{s(csi)} \end{cases} \tag{79}$$

The first step is to select a frequency fs in a random range of 5 kHz to 100 kHz, the first rule assigns the same switching frequency value to the V-I converter ($f_{s(vi)}$) and to the CSI inverter ($f_{s(csi)}$). The second ruler indicates that the value of the switching frequency of the CSI is the double that of the V-I converter and third ruler indicates that the switching frequency of V-I converter is the double of the CSI (Fig.91). For each rule an analysis of THD is made, the result that obtains the lowest THD between the three rules is the condition that is used to continue to the next step.

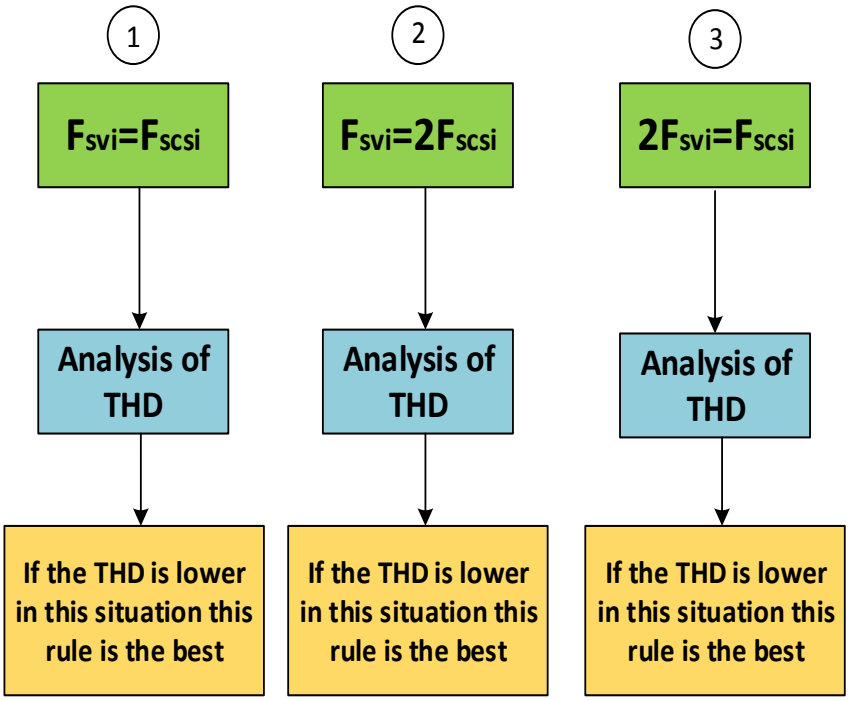

Fig.91. Rules and conditions for selection of frequency.

For the development of the second part, with the rule selected and with lower THD, we proceed to perform an analysis of the phase angles. This analysis consists of defining the two carrier signals of each converter (signal carrier A and B) and offset between two signals carriers in a range from 0 ° to 180 ° grades, the carrier signal of the V-I is considered as the reference signal (Fig. 92).

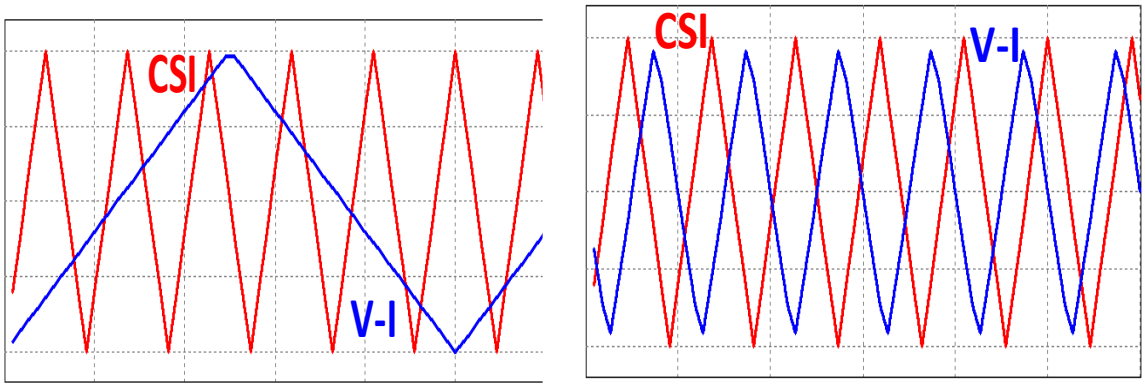

Fig 92. Signals carriers to different frequencies and angles. a) Fs (csi) =30 kHz, Fs (v-i) =15 kHz, angle=0°; b) Fs(csi)=30 kHz, Fs(v-i)=30 kHz, angle=90°.

For each angle shift condition, a THD analysis is performed, if a THD reduction is obtained in any of these situations, the method can be validated in that phase shift situation and at the switching frequencies previously analyzed (Fig.93).

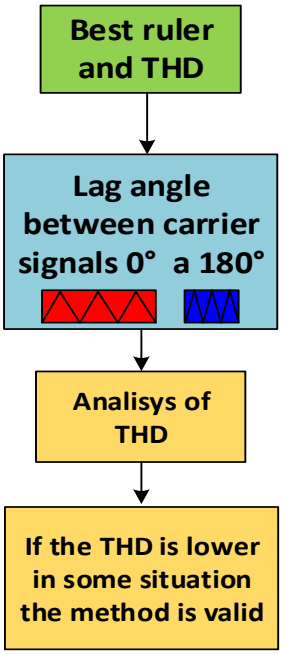

Fig 93. Second part of method.

At the end of the proposed method it can be stated that the topologies are synchronized in a way that the minimum harmonic distortion is obtained. The following would be to perform an analysis of power losses and efficiency of the topologies considering the frequency and phase angle values obtained previously.

4.3 CSI Operation.

The CSI inverter is composed of six SiC power Mosfet and six diodes schottky connected in series, a load resistive-inductive and three capacitors of filter. The six transistors are activated using a PWM modulation technique for CSI. The function of the CSI is to direct the current coming from the input source in this case of the V-I converter (Fig.94). The use of this topology has many advantages such as ruggedness to over current, short circuit protection, better efficiency in motor control, better filter design compared to VSI topology, voltages and sinusoidal currents which means less voltage dv/dt in the insulation of the machine [11-13].

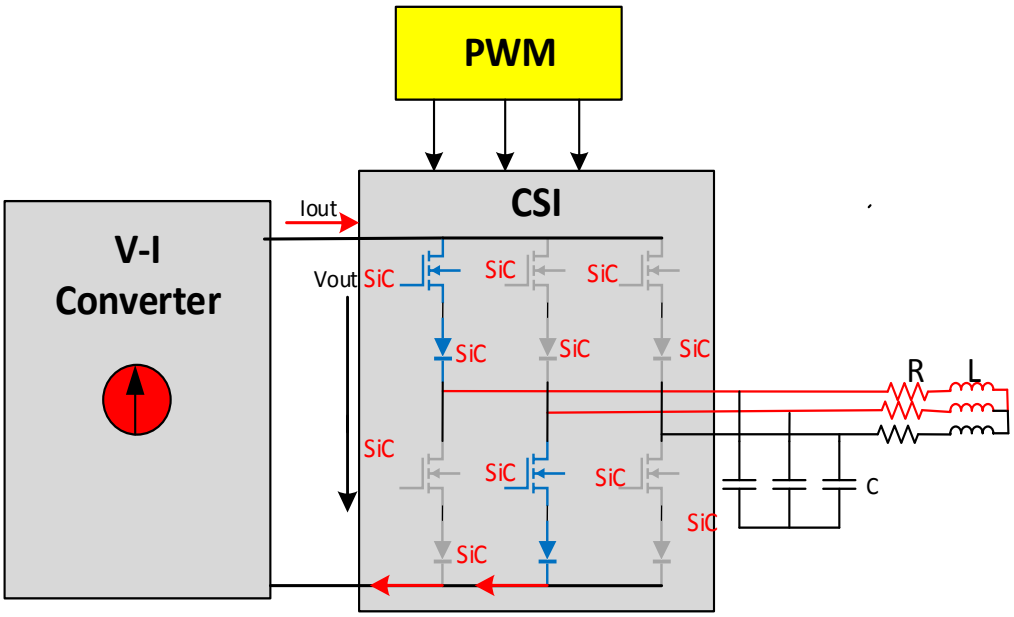

Fig 94. CSI inverte SiC topology.

For the correct operation of the inverter, although switching is simple in this type of converter, the use of a modulation technique is very important. In general, the modulation techniques are focused on drives for VSI inverters, , the few works presented on PWM modulations for CSI presented in [14-15] indicate that it is a topology with little implementation, this is a factor in our favor so it can be contribute a little more about this topology.

The PWM technique implemented for CSI allows the switching of transistors, in a converter with a current source it must always be conducting at least two transistors that can be from two different branches or from the same branch (short circuit), this condition is allowed in the CSI for the protections that it incorporates. If there is an open circuit or none of the transistors is activated generates a high voltage that can damage the components or a short circuit in the filter capacitors to the output.

For the operation of the CSI converter of our analysis, we use the PWM technique on-line generation of carrier based gating three-phase signal that is studied in [16-17]. This technique incorporates a digital control stage for the generation of pulses that is analyzed in the following subsection.

4.3.1 PWM Technique

For the implementation of the modulation technique, it is important to consider the following conditions:

- The transistors must operate as long as an open circuit on the Dc-Dc bus is avoided, otherwise the output capacitors will be short-circuited or the switches will be damaged.
- Only two switches will be activated at any time. If there are more than two waveforms of the PWM current, they cannot be defined, since the current distribution will depend on the nature of the load. This condition is naturally satisfied when using line-by-line patterns.

It is also important to define the modulation index m, which is the relation between the peak amplitude A of the sinusoidal wave and the amplitude of the triangular signal amplitude A_m in the expression (80).

$$m = \frac{A}{A_m} \tag{80}$$

The proposed technique allows the online generation of activation patterns for a three-phase power source configuration an analog / digital combined circuit is implemented. It consists of four stages that are shown in Fig 95.

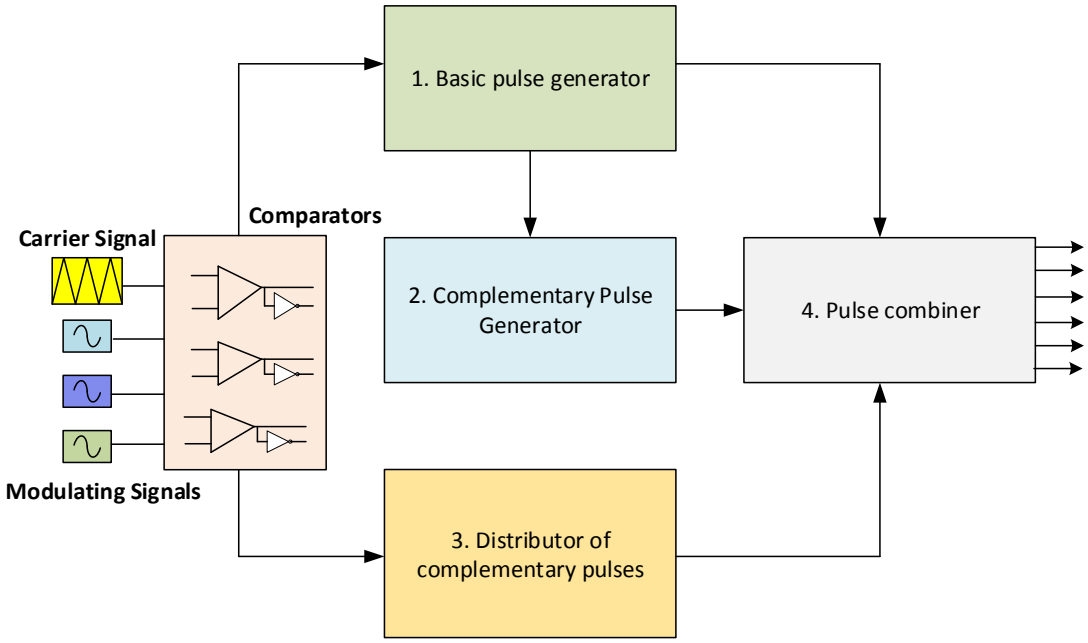

Fig 95. Gating signals generators stages.

The first block is called the basic pulse generator and it is responsible for generating the basic PWM pulses P1 (Fig.96) and combining and generating a basic sequence P2. This sequence does not guarantee the continuity of the current in the Dc-Dc link.

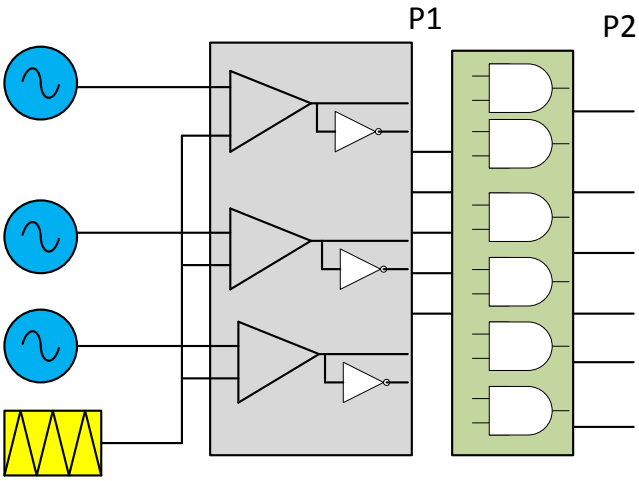

Fig 96. Block basic pulser generator, Basic PWM (P1).

The second block is denominated generator of complementary pulses, this block guarantees the continuity of link current Dc-Dc by generating a pulse output to the upper and lower circuit breakers in the same branch (short circuit) (Fig.97). These pulses find a route for the Dc-Dc bus current, while the short circuit has no harmful effect because the Dc link bus is controlled.

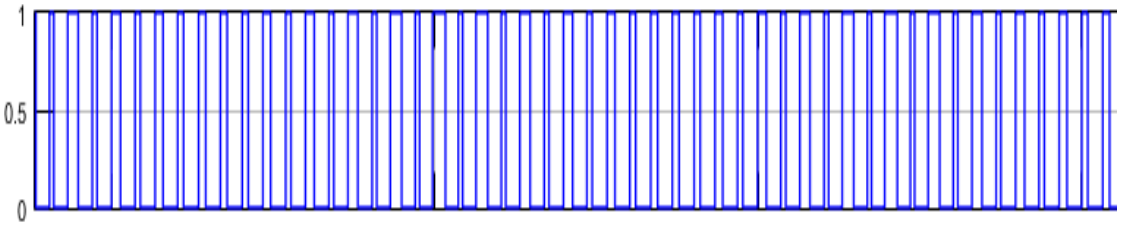

Fig 97. Block basic pulser generator.

The third block called the short-circuit pulse distributor guarantees the equitable distribution of the load current between the switches. It generates a pulse every 60 ° in half cycle for each phase to guarantee an equitable distribution of the current (Fig. 98). The input to this block are the modulating signals with an established format. The output are signals that are located in the center of the driving range for a given switch.

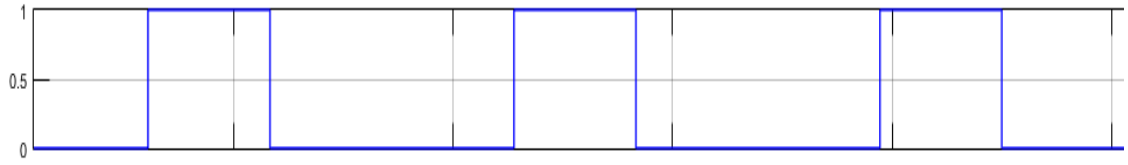

Fig 98. Short-circuit pulse distributor.

For the implementation, the reference signals are combined, in this case the modulating signals are used that use a defined combination and pass through a comparator where these signals are combined to finally obtain the pulse described above (Fig.99).

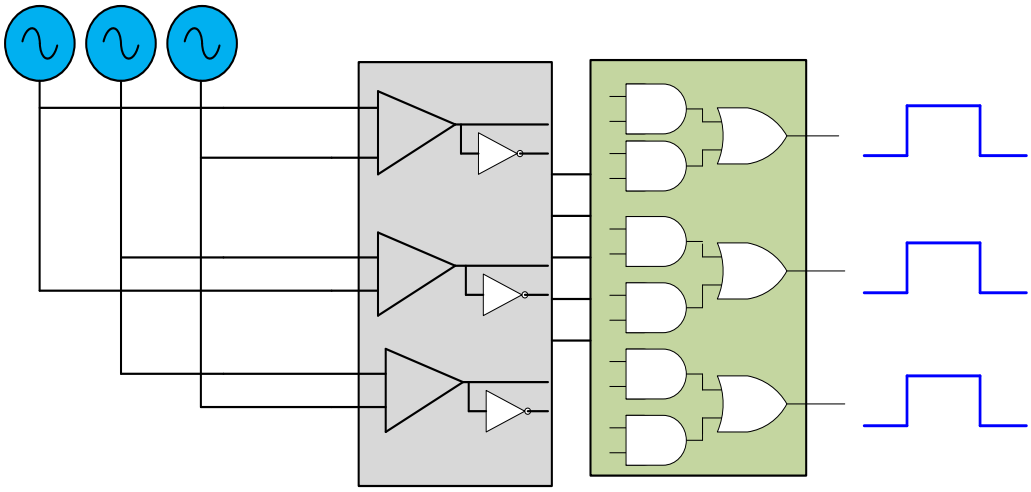

Fig 99. Elements of block short-circuit pulse distributor.

The fourth block called combiner of pulses creates a complementary pulse generator signal that is distributed equally between the three branches of the converter using the complementary signals of the pulse distributor generated in block two (Fig 100).

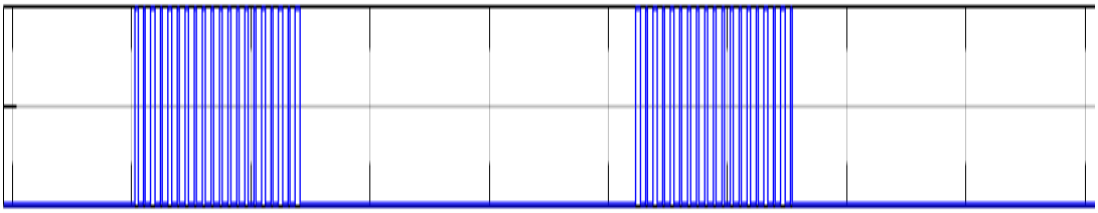

Fig 100. Complementary pulse generator signal.

The results are added to the output of the basic pulse generator (one block) to form the appropriate activation signals for switches (Fig 101).

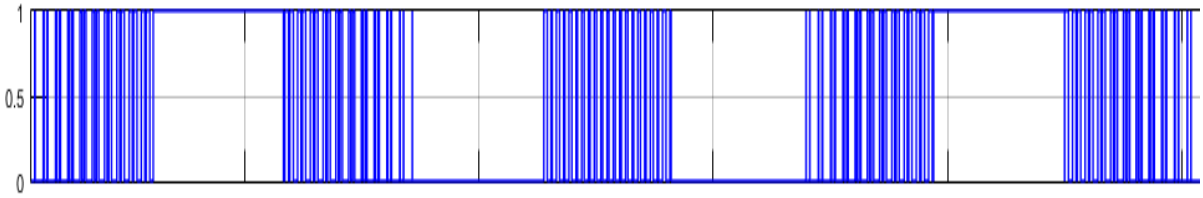

Fig 101. Output signals for gating of switches.

The scheme and circuit of the modulation technique to be implemented for the development of the present study is shown in Fig. 102.

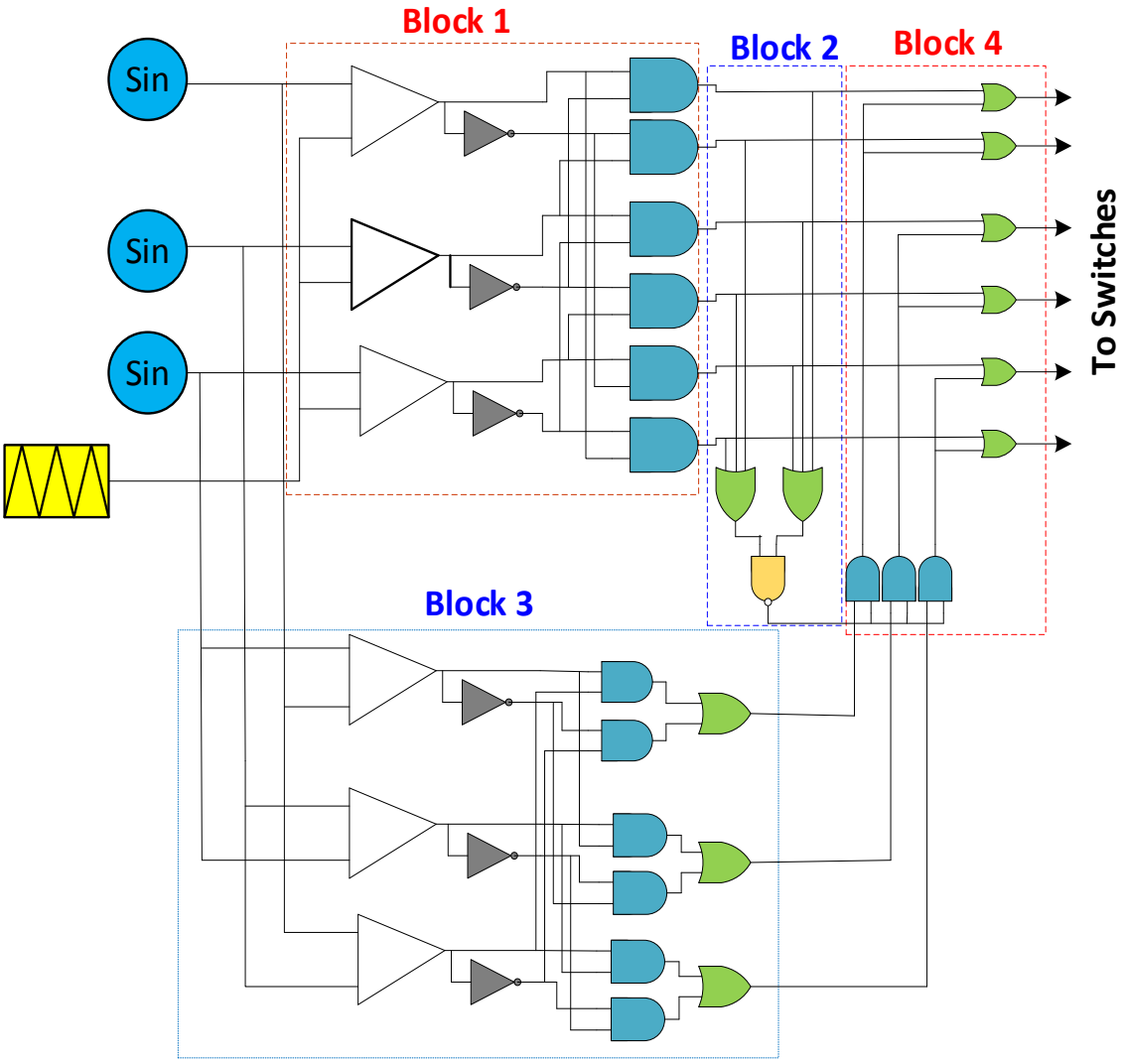

Fig 102. Schematic on PWM modulation technique for CSI.

The modulation technique analyzed and selected for the drive of the CSI inverter is called PWM online generator. It complies with all the rules previously described, it is also easy to implement in a digital system. The Simulink system model PWM is built in the Fig.103a , with the help of the simscape library. The system has the three modulating signals and the carrier signal as well as the respective outputs to the switches. The model box contains all the blocks previously analyzed as well as the entire digital system composed of logic gates and their respective connections (Fig 103b).

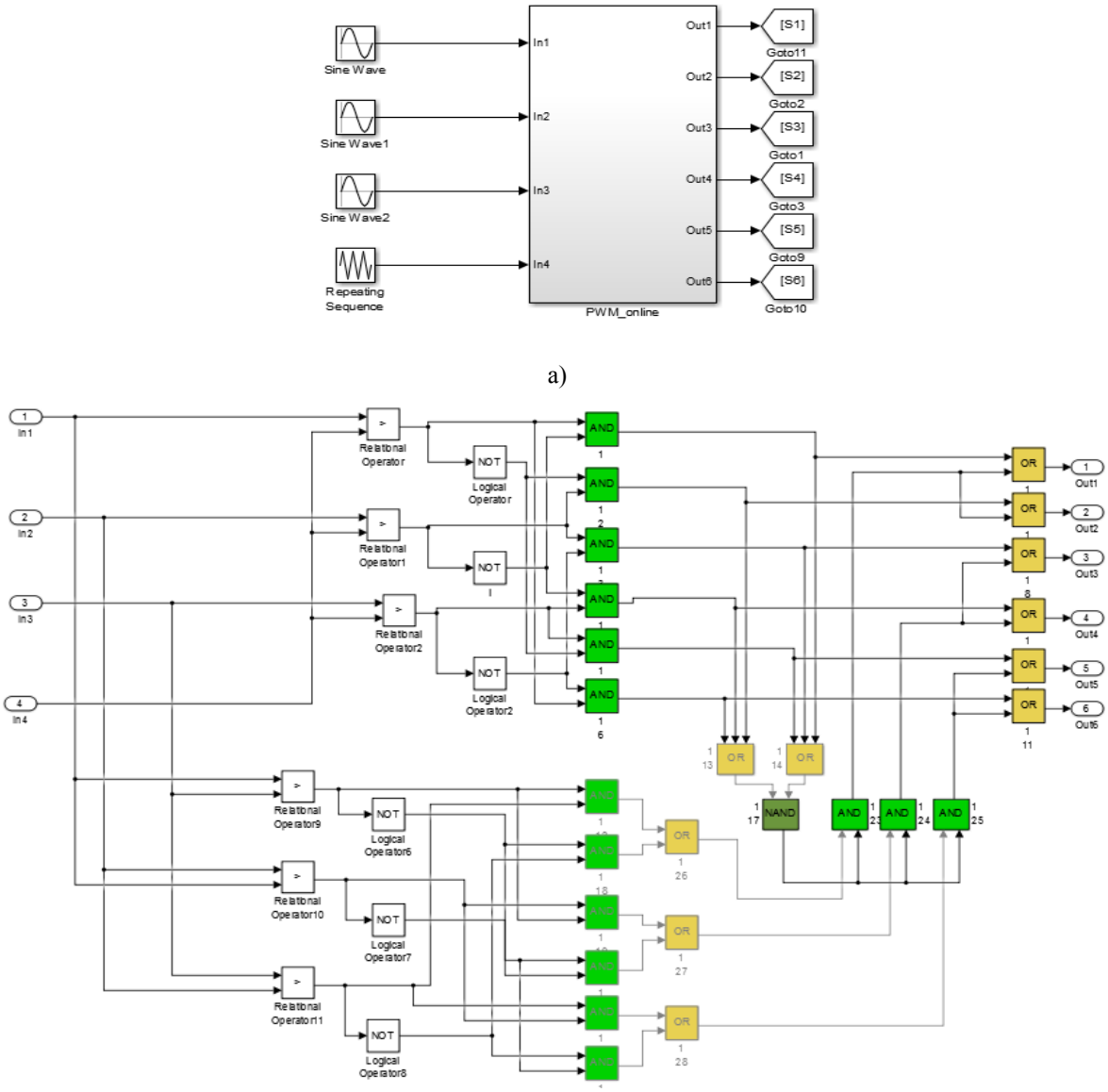

Fig 103. Simulink model system PWM. a) System box control, b) Circuit and schematic description.

To check the Simulink model, different simulations are carried out under several parameters that are presented in the Table 18.

Table 18
Parameters of simulation for PWM technique.

Parameter	Value
Situation A	
Current of Input	5 A
Frequency of switching	15 kHz
Index modulation	0.8
Situation B	
Current of Input	15 A
Frequency of switching	70 kHz
Index modulation	0.8

The figure 104 shows the results for situation A and B, the output PWM currents are obtained and it is observed that they comply with the input current condition supplied by the V-I converter.

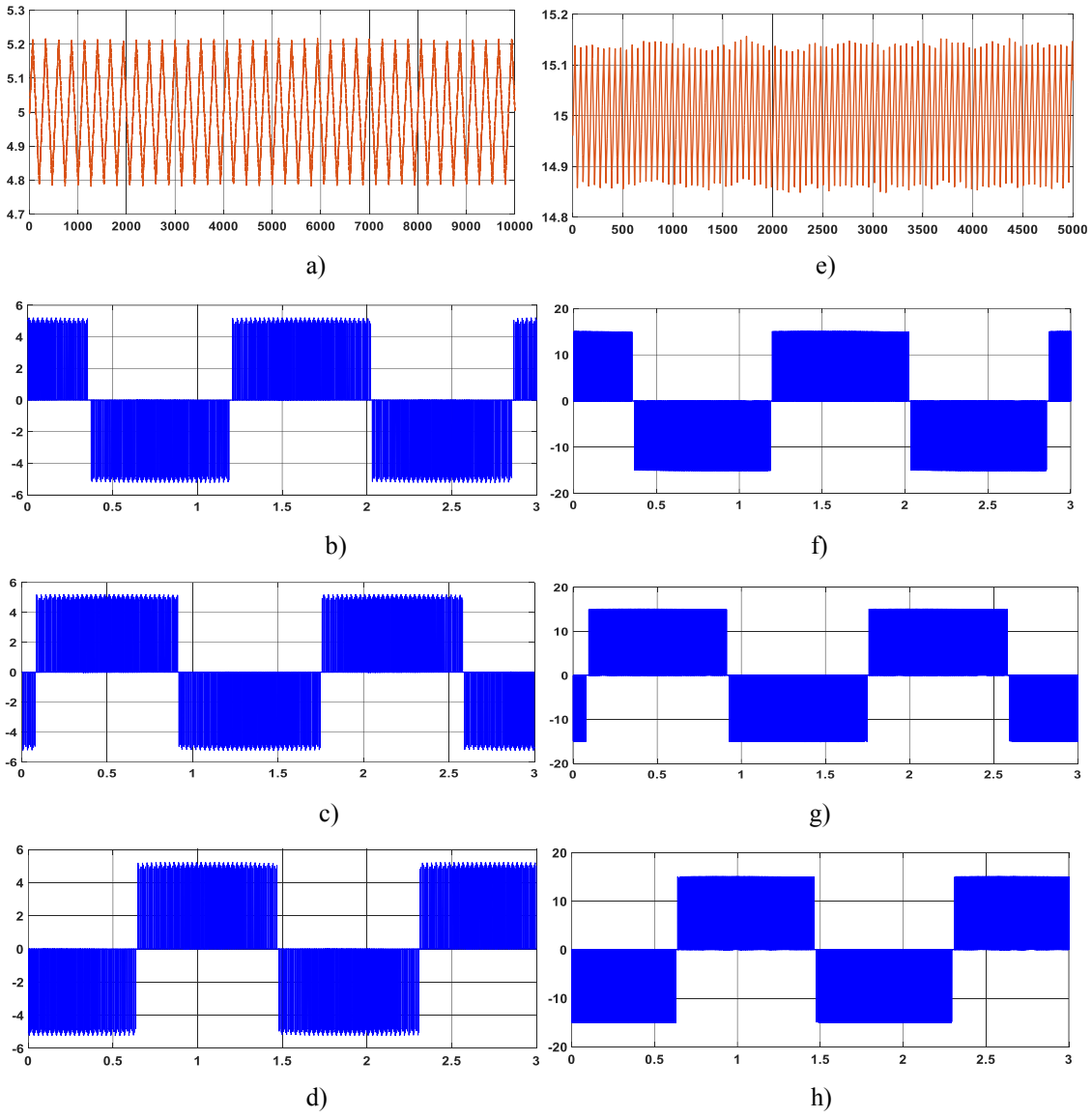

Fig 104. Simulink Result. a) Current input 5A, b),c),d) Output current PWM situation A. e) Current input 15A , f),g),h) Output current PWM situation B.

The currents and the three-phase voltage that are obtained for the situation at the output of the converter are shown in Fig. 105.

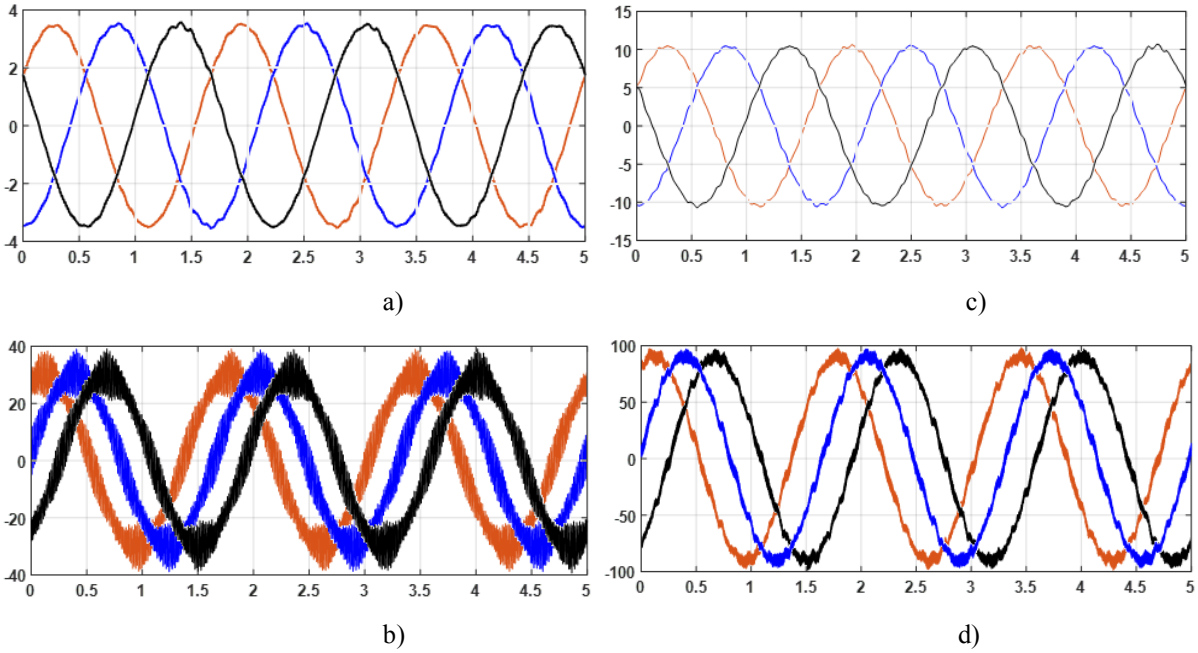

Fig 105. Currents and voltages in three phases. a) Currents output in situation A, b) Voltage output in situation A,c) Currents of output in situation B, d) Output voltages in situation B.

4.4 Results and validation of Method Proposed.

This section presents the implementation of the proposed method as well as the results obtained in simulation. The first part of the method consists in the regulation of the current through the V-I converter, this part was described analytically in the previous section. The main objective now is the integration and synchronization of the two converter topologies. This starts with the search for the switching frequency for each converter. A random frequency value (f_s) is assigned to the rules presented in equality (79) to start the analysis.

$$f_s = \begin{cases} f_{s(vi)} = f_{s(csi)} \\ f_{s(vi)} = 2f_{s(csi)} \\ 2f_{s(vi)} = f_{s(csi)} \end{cases} \tag{79}$$

Where $f_s(vi)$ is the frequency of switching of V-I converter and $f_s(csi)$ is the frequency of switching of CSI inverter. With this first analysis, we intend to know which of the two topologies should work at a higher frequency of switching and obtain a starting point to reach our goal, which is the reduction of THD and improve the efficiency of the system.

Considering these three conditions, the method follows the scheme shown in Fig. 106.

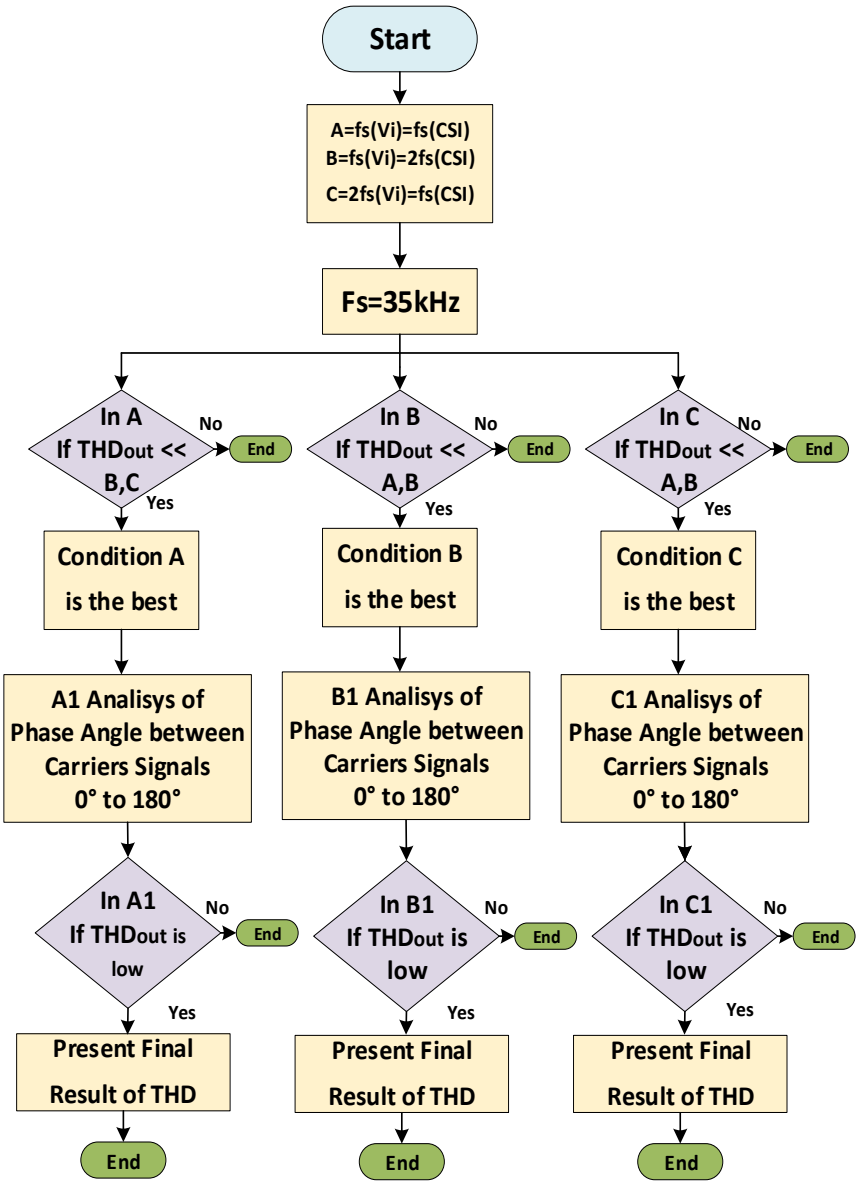

Fig. 106. Flow chart of method proposed for the three rulers or conditions.

Each rule is assigned a variable, in this case A, B, C, and then we select a frequency value, for our case 35 kHz. For each situation a harmonic distortion analysis (THD) is performed, the situation that has the lowest THD will be selected to continue with the next process. For each situation a harmonic distortion analysis (THD) is performed, the situation that has the lowest THD will be selected to continue with the next process.

The results of this part is presented in the Fig. 107, the value of current of input and controlled by the V-I converter is of 10 ampere.

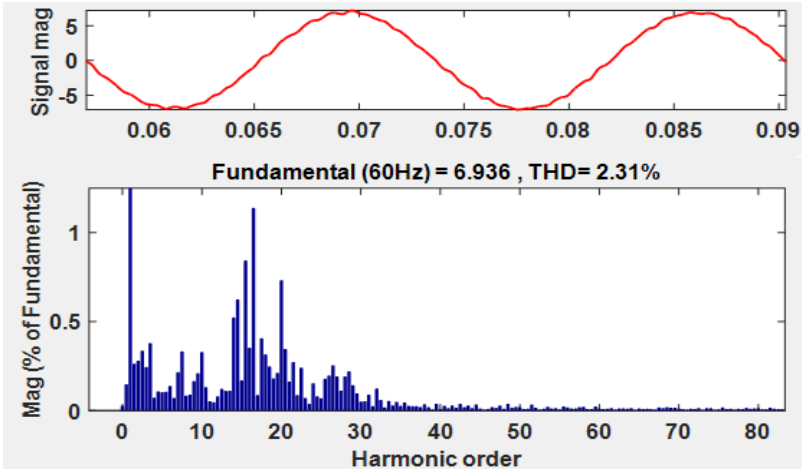

a)

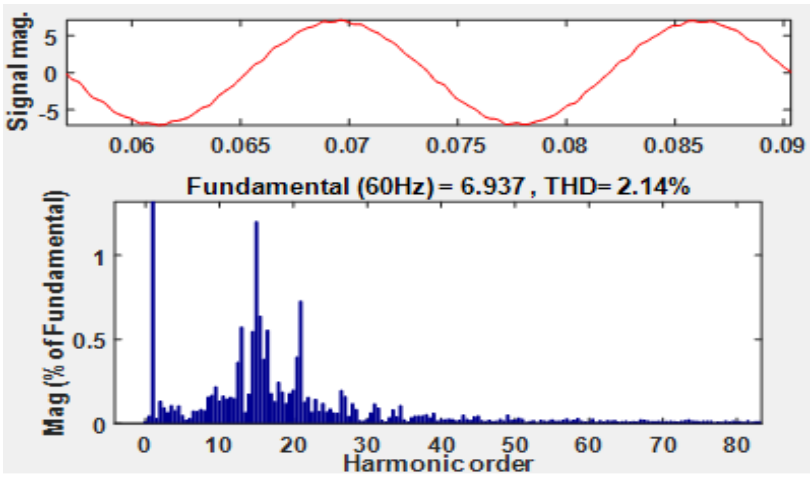

b)

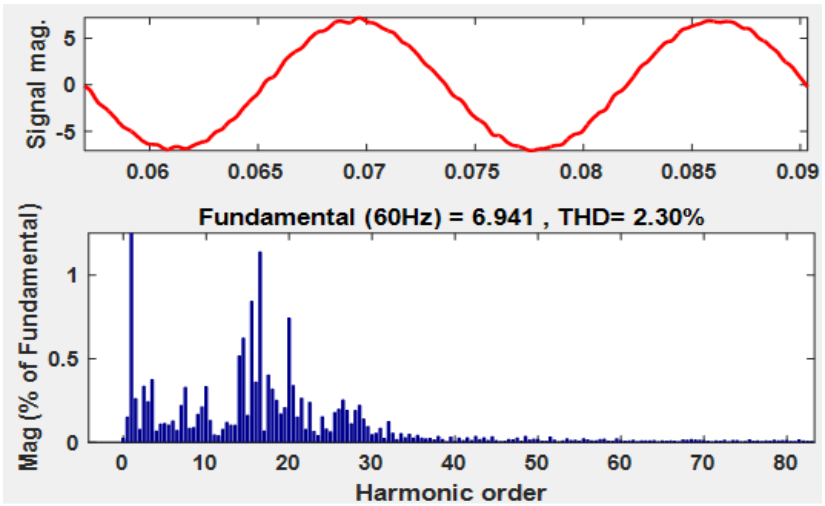

c)

Fig. 107. Results of THD a) THD results for variable A. b) THD results for variable B. c) THD result for variable C.

The results indicate that the variable B that contains the second rule obtains the best THD response (Fig108), the frequency of CSI is the double of V-I power converter. The selection of these 2: 1 frequencies could concentrate the harmonics of intermodulation in a specific range instead of scattering them throughout the spectrum. From this point on, this condition is used to perform the following steps.

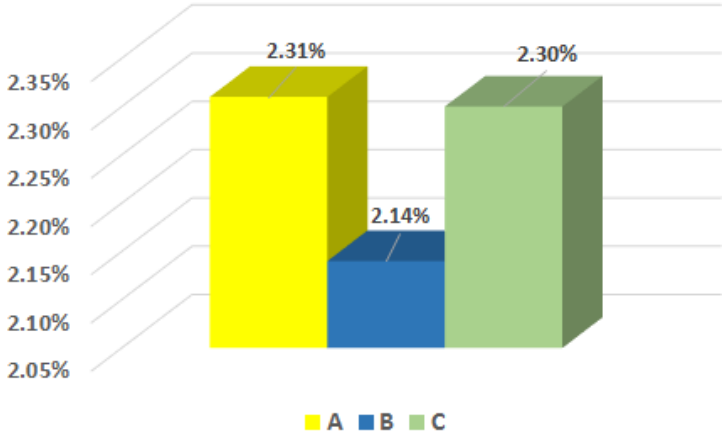

Fig. 108. THD comparisson of three variables.

An analysis is made before finalizing this part of the method. The analysis consists in verifying the current output of V-I checking the behavior of the converters and how they synchronize when they work in this condition fsvi=2fscsi. This allow demonstrate the switching pattern that follows to get to obtain a current output in the V-I with less harmonic content. The analysis is implemented for fsvi = 35 kHz and fscsi = 70 kHz is shown in the Fig. 109

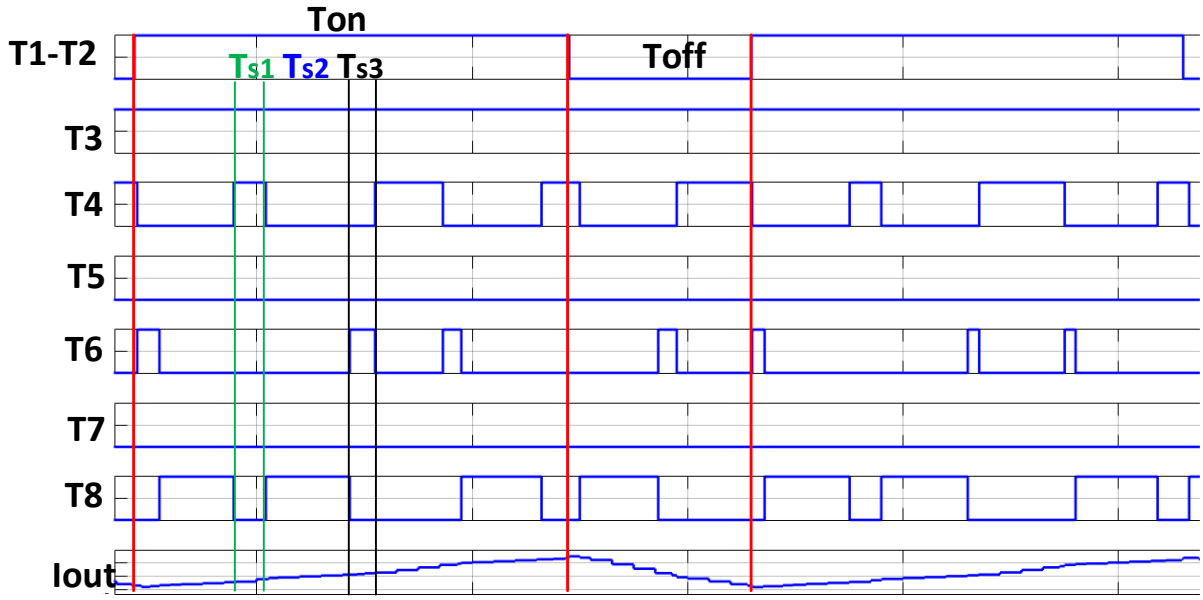

Fig. 109. Switching pattern signals for V-I - CSI to fsvi = 35 kHz and fscsi =70 kHz.

The V-I has two states on and off, each state has a time duration T_{off} and T_{on}. The current of the CSI is short-circuited when two transistors of one leg are switch in the same time (T_{s1}), in T_{s2} two transistors are closed one superior and another lower one of different branches (T_3 and T_8) and the current flows through the load connected to the CSI. This happens as long as transistors of V-I T_A-T_B are turned on (T_{on}). If they are open, the current descends and has a slope of fall for the duration of the T_{off}. Then in time, T_{s3} follows the conduction of the current but now it does it by the one of T_3 that is in the branch one upper part and T_6 that belong to the leg two lower parts through the load that has the CSI and the sequence is repeated. The result of THD in this case is shown in the Fig. 110.

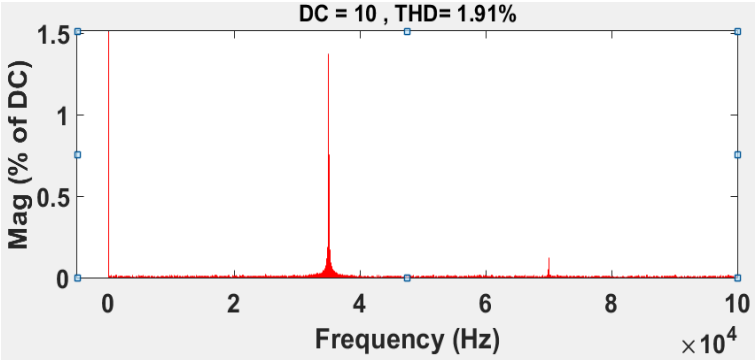

Fig. 110. THD in Dc current out in V-I - CSI to fsvi = 35 kHz and fscsi =70 kHz.

For the other situation when the frequency of V-I is the double of CSI, the current of CSI is short-circuited when two transistors of one leg are switch in the same time (T_{s1}), here the current have a slope positive. In the next time T_{s2} the current flows by the turn on of the two transistors of two legs differents (T_3-T_8) and close for the load connect to CSI. This happens as long as transistors of V-I T_A-T_B are turned on (T_{on}) (Fig. 111).

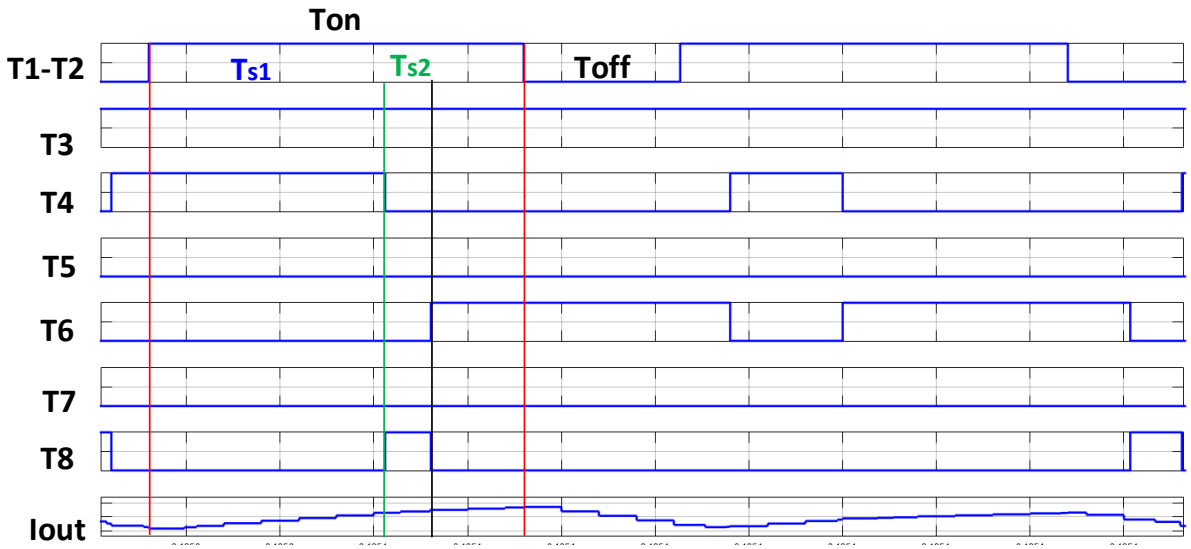

Fig. 111. Switching pattern signals in V-I -CSI to fsvi = 70 kHz and fScsi = 35 kHz.

The result of THD in this situation is shown in the Fig. 112.

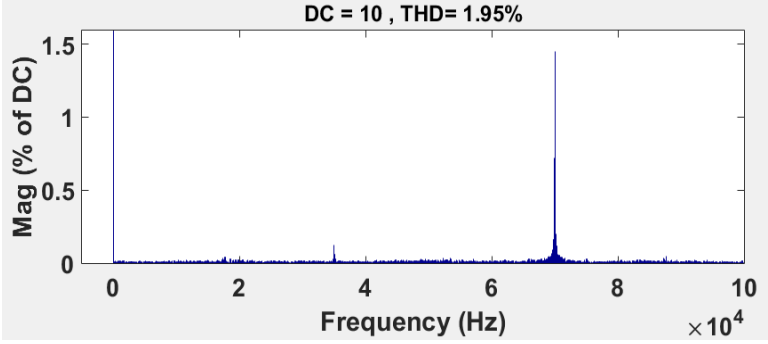

Fig. 112. THD in Dc current out in V-I - CSI to fsvi = 70 kHz and fscsi =35 kHz.

In this way, it is explained that the method in the first part seeks the optimum operating frequency for each converter in order to reduce the THD of the DC current of the VI output in order to reduce its effect on the current output in the CSI and to obtain a better total harmonic distortion response.

The next step of method is to perform a phase analysis between the angles of the carrier signals each converter has. The next step is to perform a phase analysis between the angles of the carrier signals each converter has. This analysis consists of taking the two carrier signals and generating different lag situations between the two signals. The CSI signal moves the V-I carrier signal is considered as the reference and the signal from the V-I will be the signal that is displaced. The range of tests carried out will be from 0° to 180° degrees, for each value a THD result will be obtained. To implement this step in the simulink model implemented, a transport delay is added to generalize the phase shift between the two carrier signals (Fig. 113).

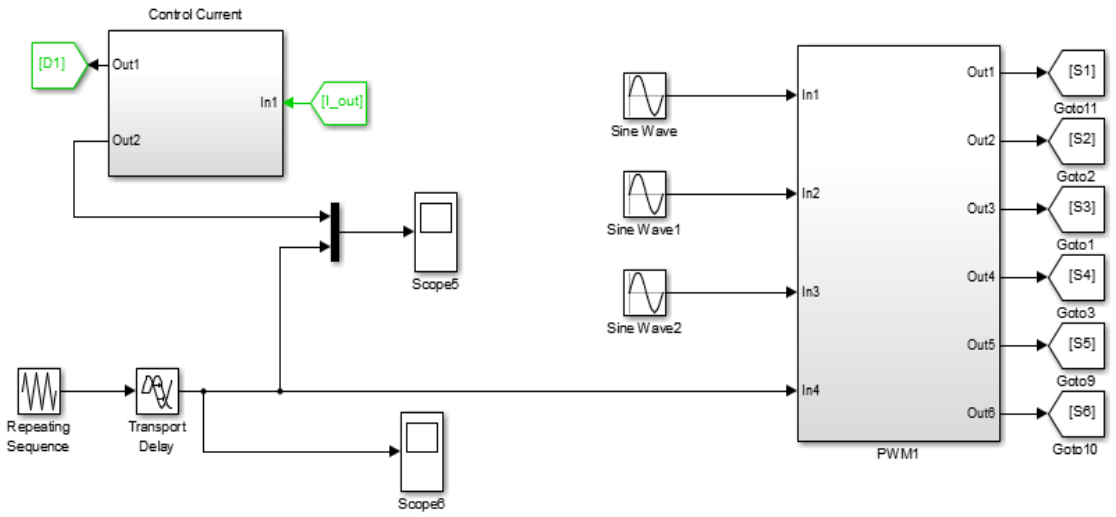

Fig. 113. Model in Simulink with phase shift between angles.

The figure 114 shown differents situations of lag and THD analysis for those situations.

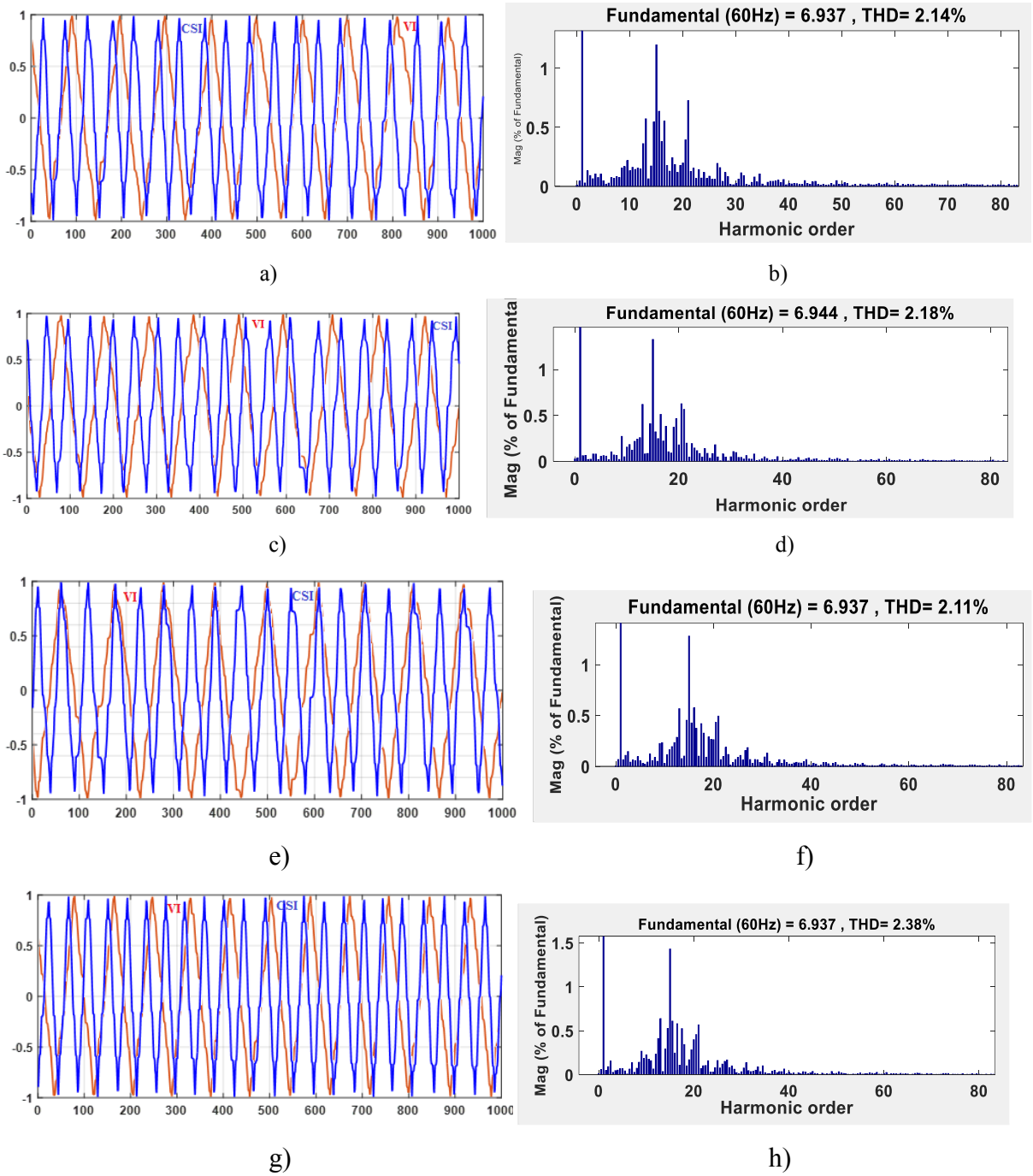

Fig. 114. Some results in simulation with phase shift. a) Situation to 0° between carriers signals. b) THD result for 0°. c) Situation to 30° between carriers signals. d) THD result for 30°.e) Situation to 60° between carriers signals. f) THD result for 60°.g)) Situation to 90° between carriers signals. h) THD result for 90°.

Performing the respective simulations for each lag situation, we obtain the results shown in Table 19.

Table 19
Result of change phase between signals carriers.

Angle	THD
0°	2.14%
10°	2.02%
20°	2.04%
30°	2.18%
40°	2.15%
50°	2.21%
60°	2.02%
70°	2.11%
80°	2.20%
90°	2.38%
100°	1.88%
110°	1.91%
120°	1.97%
130°	2.35%
140°	2.20%
150°	2.10%
160°	2.08%
170°	2.16%
180°	2.26%

Analyzing and compare the results obtained, it is observed that the harmonic distortion change for each situation. If the flow diagram of the method is followed, all these results are compared to reach a conclusion and determine the situation where the harmonic distortion of the currents is reduced. The angle where the THD is more reduced is in 100° and the results show that there is a THD change when the phase situations between the carrier signals modify and are generated in the simulation part (Fig.115); this allows us to continue with the final part of the proposed method that consists of the presentation of results.

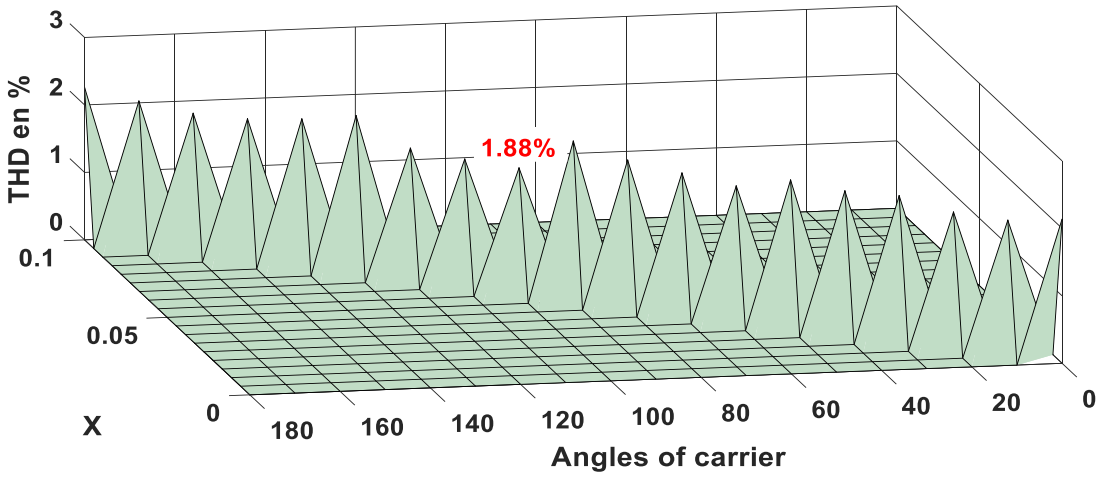

Fig. 115. Result of THD comparisson with lag of angle of signals carriers between 0° to 180°.

To understand the change of harmonic distortion in each phase change between carrier signals, the CSI and V-I activation signal map is analyzed, where a conduction and short-circuit sequence is established for each instant of turning on and off in the V-I converter. For the situation of 0° degrees of phase shift the signal activation map of CSI and V-I is shown in Figure 116.

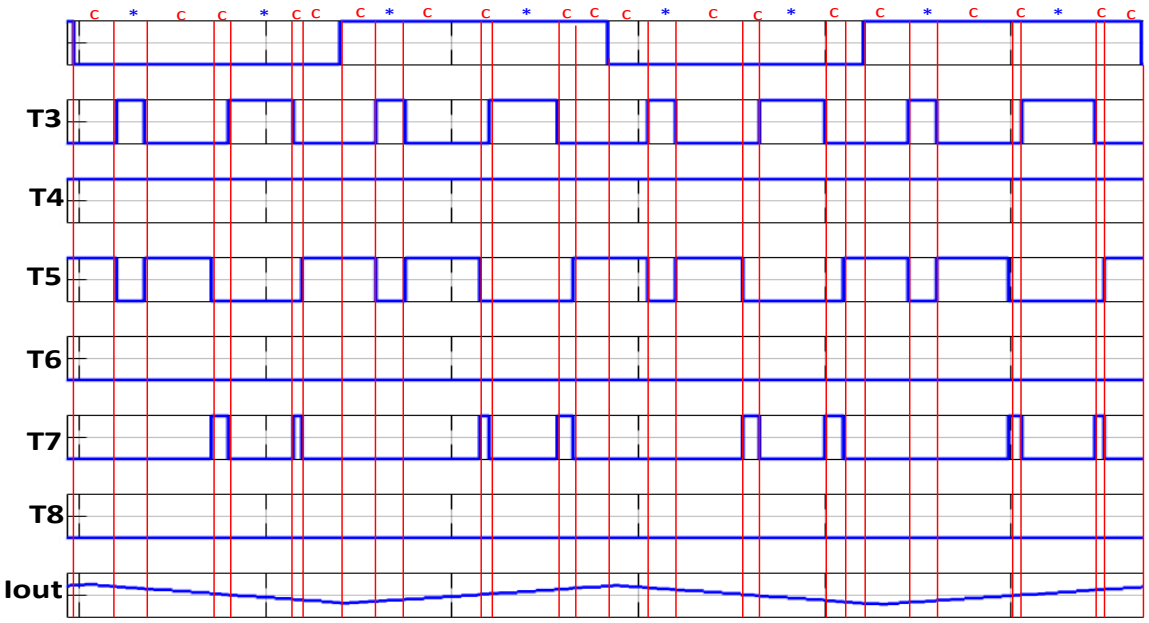

Fig. 116. Map signal in CSI and V-I in the 0° degrees of phase shift between the signals carrier.

Where C is the situation of conduction and * is the situation of short circuit. The sequence for this situation is C*CC*CC|C*CC*CC and it is repeated for all cycles. The map signal for the situations of 90° and 120° are shown in the Figure 117, in these situations you get the highest and lowest value THD.

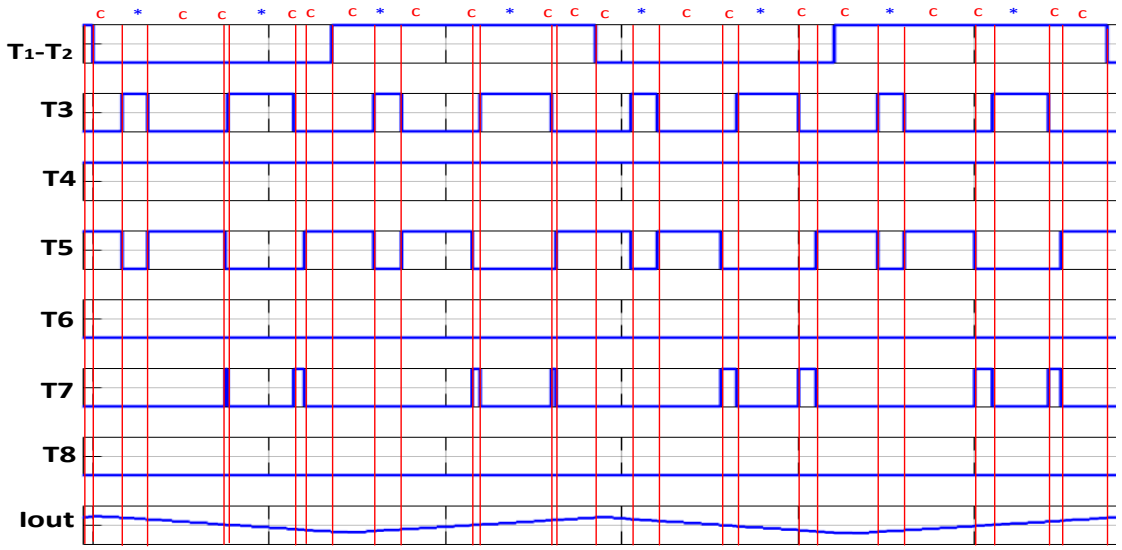

a)

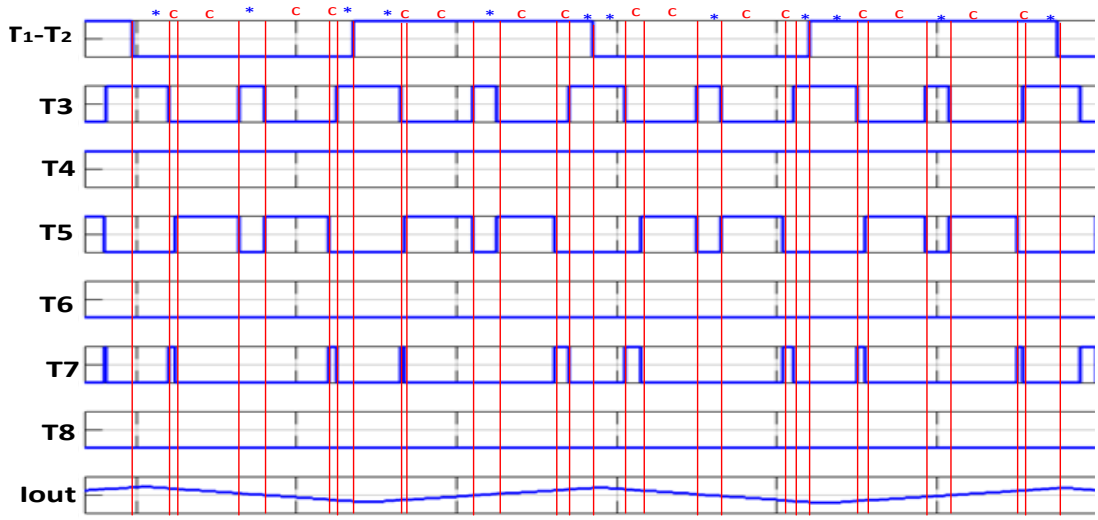

b)

Figure 117. Map signal in CSI and V-I a) Situation for 100° degrees of phase shift b) Situation for 120° degrees of phase shift.

In the first situation it is observed that there are two short-circuit states when the V-I converter is in the OFF state and two short-circuit states in the ON state. In the other situation it is observed that there are now three short-circuit states for each ON and OFF state of the V-I. From this analysis, it can be concluded that the more short-circuit states that occur in the CSI, the THD generates an increase in the currents and when there are fewer short-circuit states, a reduction in the THD is obtained. The Table 20 shown the result of THD for each situation of angle shift and sequence of conduction-short circuit obtained.

Table 20.
Result of THD with angle shift and sequence.

Angle of shift	Values of THD	Sequence ON | OFF
0°	2.10%	C*CC*CC|C*CC*CC
30°	2.22%	CC*CC*C|CC*CC*C
60°	2.39%	*CC*CC*|*CC*CC*
100°	1.88%	C*CC*CC|C*CC*CC
120°	2.25%	*CC*CC*|*CC*CC*
150°	2.13%	CC*CC*C|CC*CC*C
180°	2.15%	C*CC*CC|C*CC*CC

For the final part, the results obtained in the simulations with the analyzed values of frequency and phase in the development of the present method are shown in Fig.118.

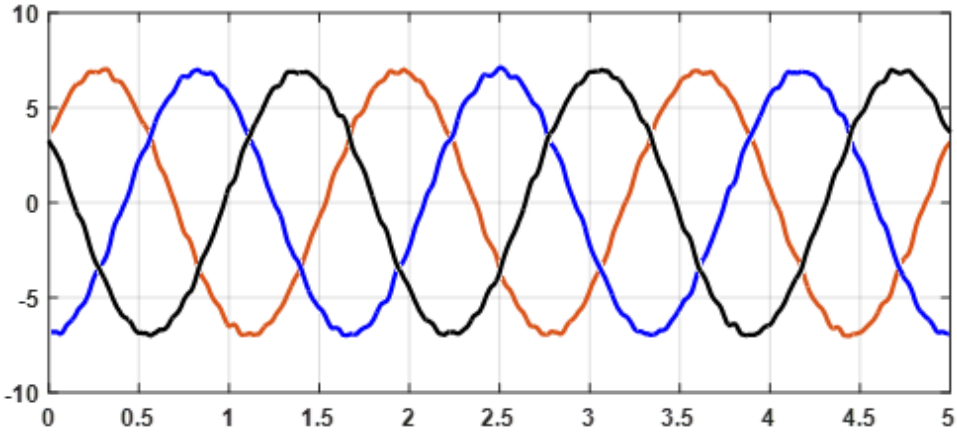

a)

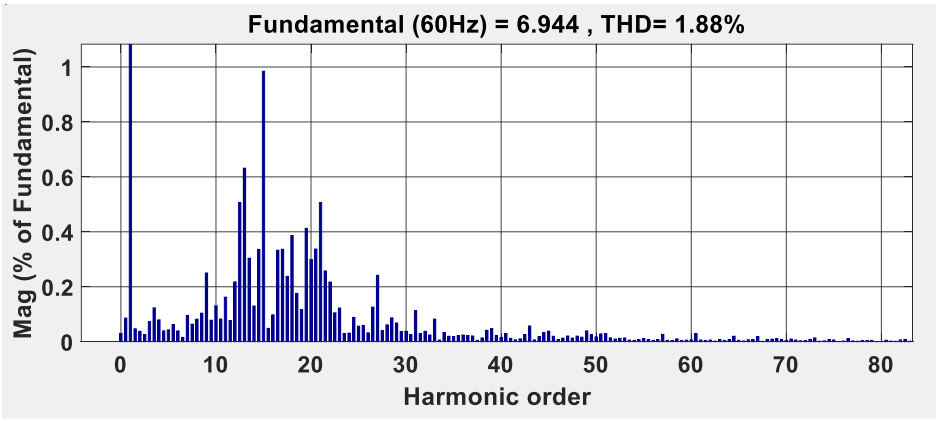

b)

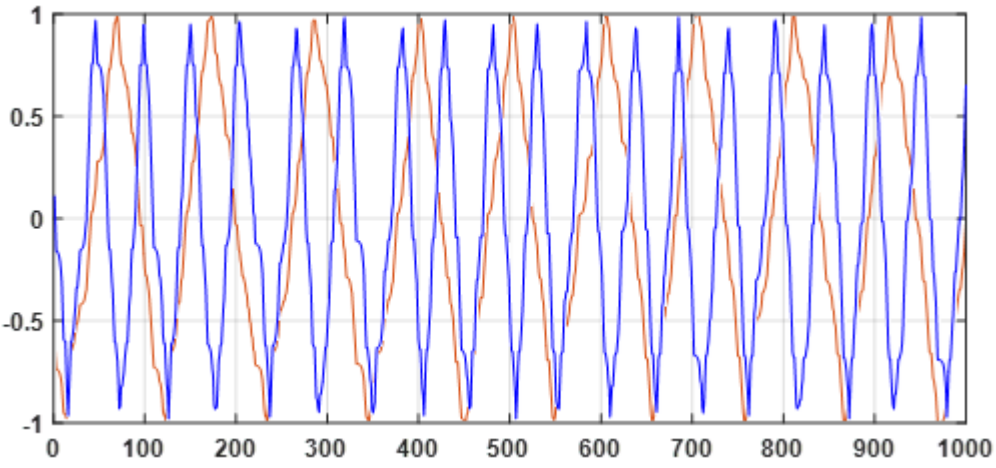

c)

Fig. 118. Results in simulation with values of f_{svi}=35 kHz, f_{scsi}=70 kHz and phase of 100°

At the conclusion of the validation of the simulation method and when interpreting the results, it is established that the application for the analyzed topologies reduces the harmonic distortion in the output currents of the converter, for this the phase shift between the carrier signals of the analyzed converters is important as well as the switching frequencies and their synchronization.

Besides its implementation allows to optimize and improve the operation of the CSI topology with a V-I converter as a current source, all these results analyzed contribute to the search of more efficient CSI topologies for future implementations in electric vehicles.

4.5 Conclusions.

This chapter presents the proposal and implementation of a method to reduce harmonic distortion in a CSI inverter topology with a V-I converter as current source. The results obtained and validated in simulation show that there is a reduction in the THD when the operating frequency of the CSI is double that of the V-I and the phases of the carrier signals move a certain angle.

The method first focuses on the selection of the operating frequencies of the converters where a condition is defined and then it is passed to the selection of the angle of lag between the carriers and with this obtains the results. In each step of the method, the respective analyzes and validations are developed.

In addition to the method the operation of the VI and the CSI inverter with SiC devices is analyzed, the use of this technology allowed to increase the switching frequency and improve the efficiency of the system discusses.

For the operation of the CSI, a PWM modulation technique is used that is known and presents by other investigations but adapts properly to the needs required in our study. The implementation of the PWM technique requires a digital analog circuit that is not complex and for its generation at a higher frequency it is necessary the help of a digital systems such as DSP or FPGA.

The final results show a tendency to reduce the THD with a frequency of 35 kHz in the V-I, a frequency of the CSI of 70 kHz and each carrier signal phase lag 100°, 1.88% harmonic distortion is obtained. These results show that in this type of topology the two topologies must work at different frequency ranges to obtain a better response in the output currents.

The methodology can be applied to other frequency conditions and loads, thus allowing reducing as much as possible the THD in a real applications by combining high frequency SiC devices with a proper switching frequency selection.

4.6 References

[1] S. von Malottki and K. Hameyer, "Extended base speed range by using a current-source-inverter-fed IPMSM for automotive application," 2014 16th European Conference on Power Electronics and Applications, Lappeenranta, 2014, pp. 1-8.

[2] G. J. Su and L. Tang, "Current source inverter based traction drive for EV battery charging applications," 2011 IEEE Vehicle Power and Propulsion Conference, Chicago, IL, 2011, pp. 1-6.
doi: 10.1109/VPPC.2011.

[3] Z. Wu and G. J. Su, "High-performance permanent magnet machine drive for electric vehicle applications using a current source inverter," 2008 34th Annual Conference of IEEE Industrial Electronics, Orlando, FL, 2008, pp. 2812-2817.

[4] K. B. Park, F. D. Kieferndorf, U. Drofenik, S. Pettersson and F. Canales, "Weight Minimization of LCL Filters for High-Power Converters: Impact of PWM Method on Power Loss and Power Density," in IEEE Transactions on Industry Applications, vol. 53, no. 3, pp. 2282-2296, May-June 2017.

[5] L. Tang and G. J. Su, "Boost mode test of a current-source-inverter-fed permanent magnet synchronous motor drive for automotive applications," 2010 IEEE 12th Workshop on Control and Modeling for Power Electronics (COMPEL), Boulder, CO, 2010, pp. 1-8.

[6] Hak-Jun Lee; Sungho Jung; Seung-Ki Sul, "A Current Controller Design for Current Source Inverter-Fed AC Machine Drive System," Power Electronics, IEEE Transactions on , vol.28, no.3, pp.1366,1381, March 2013.

[7] Su, G. and Tang, L., "A Current Source Inverter Based Motor Drive for EV/HEV Applications," SAE Technical Paper 2011-01-0346, 2011.

[8] R. Palaniappan and J. Vithayathil, "High-Frequency Current Source Inverter," in IEEE Transactions on Industry Applications, vol. IA-16, no. 3, pp. 431-438, May 1980.

[9] F. Shang, A. P. Arribas and M. Krishnamurthy, "A comprehensive evaluation of SiC devices in traction applications," 2014 IEEE Transportation Electrification Conference and Expo (ITEC), Dearborn, MI, 2014, pp. 1-5.

[10] Haizhong Ye, Y. Yang and A. Emadi, "Traction inverters in hybrid electric vehicles," 2012 IEEE Transportation Electrification Conference and Expo (ITEC), Dearborn, MI, 2012, pp. 1-6.

[11] D. Ronanki, K. Rajesh and P. Parthiban, "Simulation of SVPWM based FOC of CSI fed induction motor drive," 2012 Students Conference on Engineering and Systems, Allahabad, Uttar Pradesh, 2012, pp. 1-6.

[12] M. Salo and H. Tuusa, "Experimental results of the current-source PWM inverter fed induction motor drive with an open-loop stator current control," Applied Power Electronics Conference and Exposition, 2003. APEC '03. Eighteenth Annual IEEE, Miami Beach, FL, USA, 2003, pp. 839-845 vol.2.

[13] M. F. Tsai, T. C. Lee, C. S. Tseng, W. S. Syu, Y. Y. Chen and W. Y. Peng, "Vector control of current source inverter-fed axial-flux permanent magnet motors with space vector pulse width modulation," 2014 IEEE 23rd International Symposium on Industrial Electronics (ISIE), Istanbul, 2014, pp. 920-925.

[14] S. Nonaka and Y. Neba, "Current regulated PWM-CSI induction motor drive system without a speed sensor," Conference Record of the 1992 IEEE Industry Applications Society Annual Meeting, Houston, TX, USA, 1992, pp. 347-354 vol.1.

[15] M. Glab, Z. Krzeminski and M. Wlas, "PWM current source inverter with IGBT transistors and multiscalar model control system," 2005 European Conference on Power Electronics and Applications, Dresden, 2005, pp. 10 pp.-P.10.

[16] M. I. Masoud and A. S. Abdel-Khalik, "Vector controlled five-phase PWM-CSI induction motor drive," 4th International Conference on Power Engineering, Energy and Electrical Drives, Istanbul, 2013, pp. 258-264.

[17] M. A. Elgenedy, A. Abdel-Khalik, A. Elserougi, S. Ahmed and A. M. Massoud, "A new five-phase to three-phase back-to-back current source converter based wind energy conversion system," 2013 7th IEEE GCC Conference and Exhibition (GCC), Doha, 2013, pp. 193-198.

5.

Analysis of Power Losses and Efficiency.

This chapter present the analysis of power losses and efficiency and includes the mathematical explanation of the conduction and switching losses equations. The calculations of power losses are based on the two topologies of power converters V-I Dc-Dc and CSI inverter with silicon carbide devices, in the condition of lower THD analyzed in the previous chapter. In addition, an analysis of the losses in the motor is developed considering the optimization method previously analyzed. The analysis includes a study of the losses of power in the inductor, estimation of the size of the heatsink and analysis of the efficiency is implemented. Finally, the weighted average efficiency of the whole system (power converters + motor) in differents conditions of operations is presented.

CONTENTS:

5.1 Introduction

The power losses calculations of semiconductor SiC devices in power converters is important since it allows efficiency forecasting of the topologies of the converters and provides a estimation for the thermal management system selection. Once the SiC devices are selected, the losses of conduction and commutation in the inverters can be calculated as well as the thermal management, supported by the data provided by the data sheets of the devices and the operating conditions of the inverter.

In several studies, [1-3] different methods are used to calculate power losses in semiconductor devices. Generally, for the development of converters, three types of devices diodes, Mosfets or IGBTs are used. The most used method for the calculation of the losses consists of using the data provide by the datasheet that the manufacturers offer, such as on-state resistance and switching energy losses. These data are used in mathematical equations that allow calculating the losses of conduction and commutation.

This chapter presents the power losses of the topologies of converters with silicon carbide devices analyzed in the previous chapter.

5.2 Selection of Devices.

For the design of power converters is import the select of SiC devices and features of operation that depending on the current, voltage and power out of operating. For our design, the SiC SCT2450KE Mosfet and the SiC sckotty diode C2M0040120D are selected. The features of these devices are presented in the Table 22.

Table 21
Parameters of SiC devices selected

SiC Mosfet Device	Parameter	SiC Diode Sckotty	Parameter
SCT2450KE	Model	C3D08065I	Model
Voltaje drain source Vds	1200V	Voltage Rectifier V_{RRM}	650 V
Resistance drain source Rds	450 mΩ	Continuous forward Current	8A
Current Drain Id	10 A	Capacitive Charge Q_{cc}	21nC
Power dissipation Pd	85 W	Capsule	TO-220-2
Capsule	TO-247	Power dissipation	23.2W
T resistance, junction - case R_{thJC}	1.77 °C/W	Package Thermal Resistance	2.8 °C/W
Manufacture	ROHM	Manufacture	CREE
Applications	Solar inverters, - DC-DC converters, Motor Drivers	Applications	Boost diodes in PFC or DC/DC stages, DC/AC converters

After selecting the devices, it is important to describe the types of gate driver control. For this, it is necessary to know the different techniques that are currently used and that are described below.

5.2.1 Gate Driver Control.

For the design of the gate driver control, it is important to consider the type of technique to be used. The activation at high frequencies of these devices generate some advantages but also can cause some problems as parasitic current and voltage oscillations, electromagnetic interference (EMI) [4]-[5], to minimize all these effects have been implemented switching techniques of hard and soft- switching. To explain the operation of these two techniques, the analysis presented below is considered

The hard-switching of a SiC mosfet consists in two pulses with variable widths that are supplied to the gate driver of transistor SiC. For understand the application of this technique may generate the circuit of Fig.119, the first pulse has a larger width which determines the current rise in the inductor L, when the current reaches the desired level, the mosfet is turned off and the turn off transient waveforms can be observed. At this transient, the load current commutates to the Schottky diode from the mosfet channel. During the off state of the mosfet, the inductor current remains virtually constant. Then the smaller width pulse is applied to the gate driver and the turn on transient waveforms can be observed at the same current and voltage level of the turn off transient. When the smaller pulse finishes, the inductor current slowly decays in the closed loop it forms with the Schottky diode [5].

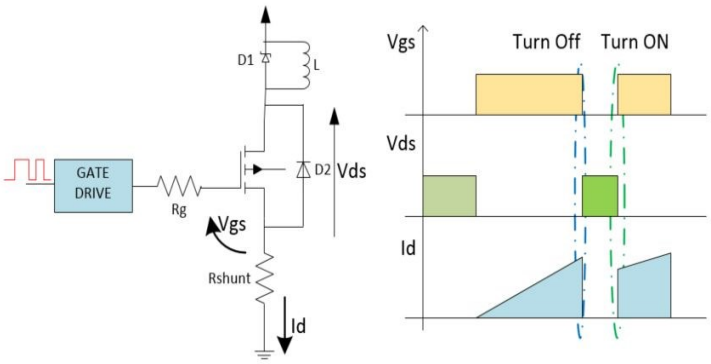

Fig.119. Hard- Switching technique in SiC Mosfet.

The soft-switching use a different circuit for analyze, the operation (Fig.120) a single gate pulse is given to the upper device, Q_1, so that the load current, I_L increases in the inductor, L, to the desired level, I_{dd}. Turning off Q_1 will turn on the body diode of Q_2 and I_L will start to decrease because of the reverse voltage across the inductor, L. After a dead time, a second gate

pulse, approximately double the width of the first pulse is applied to the lower device, Q_2. This forces the load current to change direction and reach I_{dd} [6].

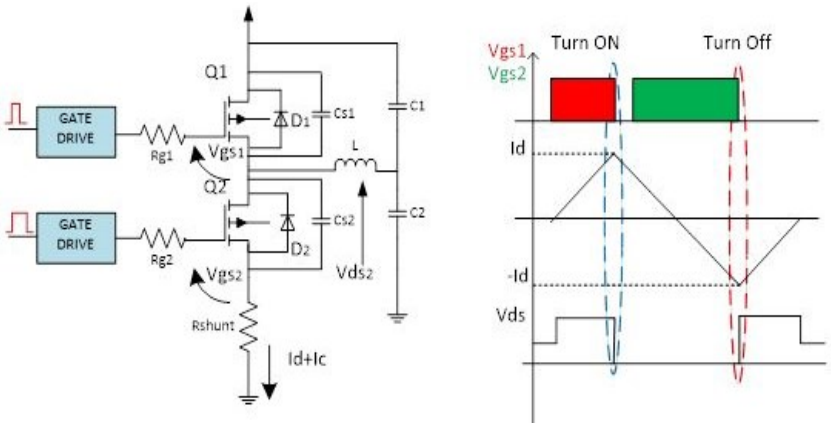

Fig.120. Soft- Switching technique in SiC Mosfet.

For the development of our application, a hard-switch technique is used. The next step is the description and mathematical analysis of the power losses in the silicon carbide devices used in our study.

5.3 Power Losses in V-I Dc-Dc Power Converter.

For the analysis of losses in the V-I Dc-Dc converter, two Mosfet SiC transistors and two sckotty diodes are considered. The losses by conduction and of commutation to the frequencies of operation of the topologies of converters analyzed previously are calculated.

5.3.1 Mosfet and Diode SiC Conduction Power Losses.

In the conduction or state On, a Mosfet SiC the switch works as a resistance that varies with the temperature of the union T_j and can be represented by the equivalent circuit Fig 121.

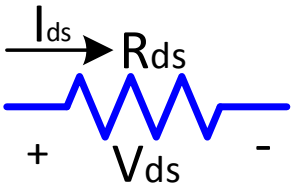

Fig.121. Equivalent circuit of state On OFF Mosfet SiC.

The power losses in the SiC mosfet is represented by the equation (80).

$$P_{cond\_MOSFET} = Rds_{(ON)} I_{rms}^{2} \tag{80}$$

Where R_{ds} is the drain-source resistor of SiC MOSFET, I_{rms} were the effective current flowing in the device [7]-[8].

The power losses in sckotty SiC diodes could be expressed for (81)

$$P_{cond\_Diode} = I_{rms}^2 R_D + I_{DC} V_D \tag{81}$$

Where I_{rms} is the effective current flowing in the device. I_{Dc} is the value of the current flowing through the diode and V_D is the tension of the diode, respectively [7]-[8]. The power losses by conduction in the Mosfet and diode SiC are presented in the Table 22.

Table 22
Conduction power losses in V-I power converter

Parameter	Power Losses
Pcond Mosfet SiC	44.98 W
Pcond Diodes SiC	43.16W
Total Pcond x 2 devices	88.14 W

5.3.2 Mosfet and Diode SiC Switching Power Losses.

The switching losses in the Mosfet SiC and SiC diode are expressed in (82) and (83).

$$P_{swM} = f_{sw}\left(E_{on} + E_{off}\right) \tag{82}$$

$$P_{swD} = f_{sw}\left(E_{swD}\right) \tag{83}$$

Where E_{ON} is turn-on switching energy, E_{OFF} is turn-off switching energy in the Mosfet SiC and E_{swD} is the energy of switching in the SiC Schottky diode [9].

For the calculation of turn-on switching energy and turn-off switching energy it is necessary to obtain the time intervals, t_{fi}, t_{ri}, t_{fu} and t_{ru}, these play an important role in MOSFET switching power loss calculation Fig 122.

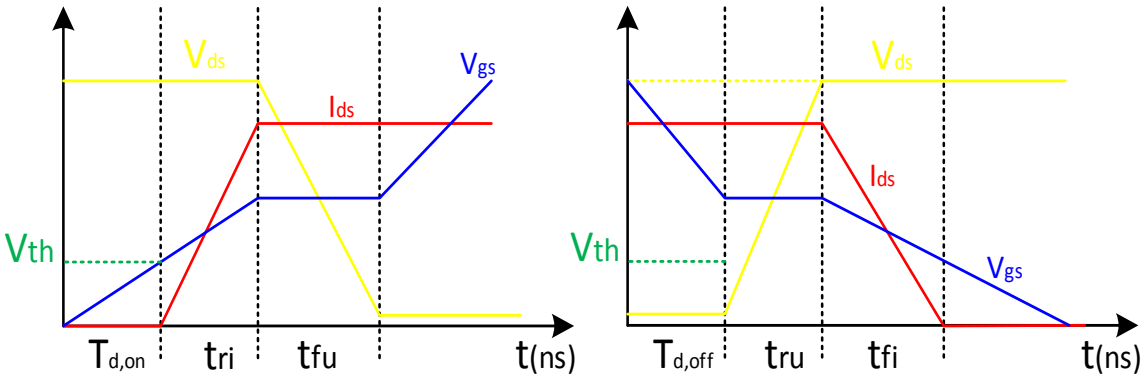

a) b)

Fig.122. Mosfet signals of voltage and current in switching mode, a) Turn on situation b) Turn off situation.

The E_{on}, E_{off} and E_{swD} in function of the time intervals are calculated by (84), (85) and (86).

$$E_{on} = \int_0^{tri+tfu} V_{ds}(t) I_D(t) dt = V_{dc} I_{on\_rms} \left(\frac{tri + tfu}{2} \right) + Q_{rr} V_{dc} \tag{84}$$

$$E_{off} = \int_0^{tru+tfi} V_{ds}(t) I_D(t) dt = V_{dc} I_{off\_rms} \left(\frac{tru + tfi}{2} \right) \tag{85}$$

$$E_{swD} = \int_0^{tri+tfu} V_d(t) I_f(t) dt = \frac{1}{4} Q_{rr} V_{dc} \tag{86}$$

Where V_{DS} is the voltage drain source, I_D continuous drain current V_{dc} is the voltage Dc link; The t_{ri}, t_{fu},t_{ru},t_{fi} are time intervals and Q_{rr} is the interval of time for the diodes [8]. All these parameters are in the datasheet of the devices. In this way, we can calculate the switching power losses for this type of devices. The parameters for calculations are presented in the Table 23.

Table 23
Values of time intervals and parameters of functions

Parameter	Values
t_{ri}	9ns
t_{fu}	6ns
t_{ru}	14ns
t_{fi}	15ns
Qrr	283nC
V_{dc}	100V
I_{dc}	10A
f_{sw}	35 kHz

The power losses by switching in the Mosfet and diode SiC are presented in the Table 24.

Table 24
Switching power losses in V-I power converter

Parameter	Power Losses
P_{sw} Mosfet SiC	22.87 W
P_{sw} Diodes SiC	0.0296 W
Total Psw in V-I converter x 2 device	45.799 W

The rated power of V-I converter with SiC devices is of 1.5 kW.

5.3.3 Inductor Core Losses.

The losses in the inductors are from the following sources, hysteresis loss, copper or winding loss and Eddy current loss.

The hysteresis loss is due to the materials intrinsic properties due to the energy used to align and re-align the magnetic domains. The general form of the losses for hysteresis (P_m) is calculated by the expression (87)

$$P_m = k.f^a B_{\max}^d \tag{87}$$

Where a, d and k are constants depending of the type of material, for this case is ferrite. This form is known as Steinmetz equation. Steinmetz parameters given in most datasheets for sinusoidal excitation.

Eddy current loss from the circulating currents within the magnetic materials due to the differential in flux voltage inside the cores itself [10]. These losses is high dependent upon the thickness of the walls of the cores. The Eddy current loss per unit of volume can be calculated by the expression (88).

$$P_{ec} = \frac{\eta^2 f^2 B_{\max}^2}{6\rho} \tag{88}$$

Where η is the Steinmetz hysteresis constant and ρ is the density of the material. The copper losses are an undesirable transfer of energy, as are core losses, which result from induced currents in adjacent components. The copper losses in the inductor are calculated by the expression (89)

$$P_{copper} = {i_{dc}}^2 R_{coil} \tag{89}$$

The total power losses in the inductor are obtained by the expression (90) and are shown in the Table 25.

$$P_{inductor} = P_m + P_{sc} + P_{copper} \tag{90}$$

Table 25
Inductor core losses

Parameter	Value
Hysteresis losses	0.0517 W/cm3
Eddy current losses	0.2738 W/cm3
Copper losses	29.93 W/cm3
Total of losses in the inductor	30.255 W/cm3

The total losses in the V-I power converter including the SiC devices and the passive elements is detailed in the expression (91). The total power loss obtained is 164,194W.

$$P_{TotalV-i} = P_{Tcond} + P_{Tsw} + P_{Tinductor} \tag{91}$$

5.4 Power losses in CSI.

In the case of the CSI converter, the important rule for the calculation of losses is that there is at least one device turned on in the converter [8]. The expressions that are implemented to calculate the losses for switching and conduction are as in the previous section. Now it is considered in the topology a Sckotty SiC diode connected in series with each SiC MOSFET, two for each branch that ultimately increases the losses.

The results of power losses in CSI converter by switching and conduction to 70 kHz and 100° of phase shift in PWM carriers are presented in Table 26. The rated power of CSI converter is of 1.5 kW.

Table 26
Conduction and switching power losses in CSI power converter with SiC devices

Parameter	Power Losses
P_{cond} Mosfet SiC	134.94 W
Pcond Diodes SiC	129.48 W
P_{sw} Mosfet SiC	26.88 W
P_{sw} Diodes SiC	1.45 W
Total of power losses in CSI	292.75 W

The results of these losses expressed in percentages for each one of the topologies of converters previously analyzed are presented in Fig 123.

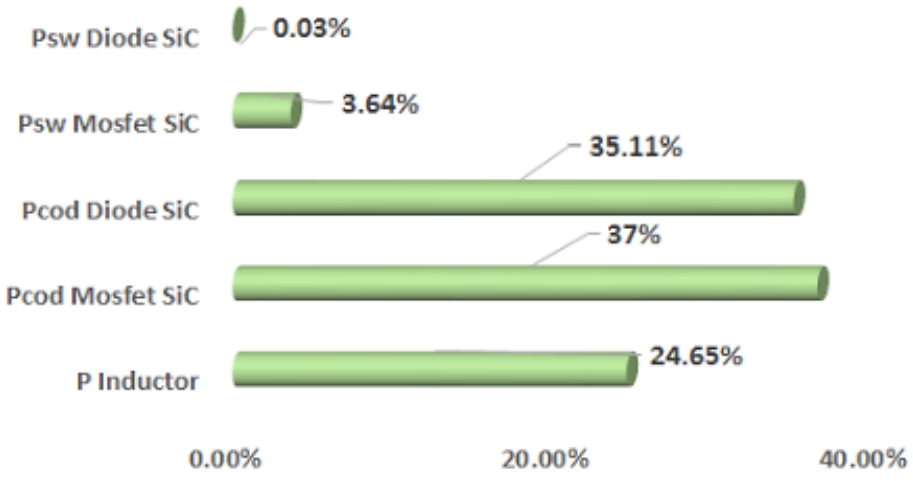

a)

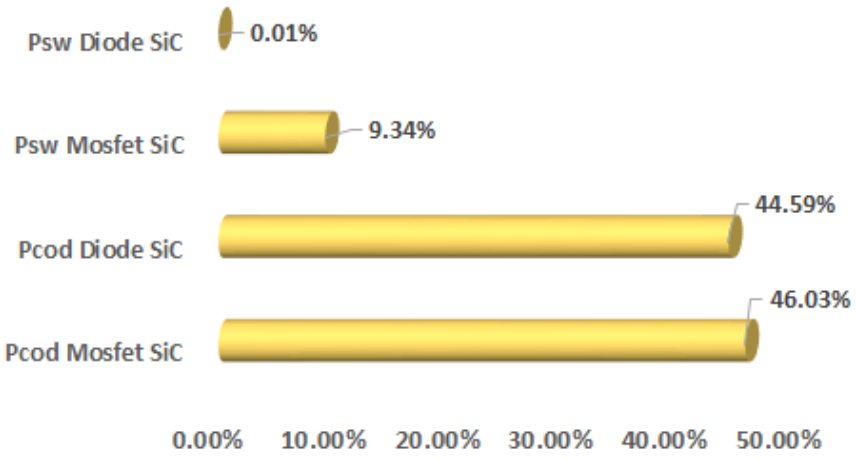

b)

Fig.123. Power losses expressed in percentages, a) V-I topology b) CSI topology.

5.5 Power losses in Electric Motor.

This section presents the analisys of power losses in the electric motor considering four situations of operation previously analyzed, 0 degrees, 60 degrees, 90 degrees (angle with lower THD), 120 degrees of phase shift in PWM carriers for V-I and CSI converters. This analysis aims to perform a comparative study and show that the reduction of harmonics allows improving the efficiency of the electric motor.

In the PMSM are two main electrical losses, the core losses in the iron core and the copper losses in the winding. The fundamental iron loss consists of hysteresis loss and eddy current loss and copper losses, which are caused by the stator coil resistance R_s [11]-[12]. The copper losses are the losses due to the heat (Joule effect) that produces the current when it is circulated by a conductor and can be expressed by (92). In the analysis, it is considered the data of a PMSM engine implemented in another previous study [13-14].

$$P_{CU} = mR_s I^2 + \sum_{h=3}^{\infty} I^2{}_n R_{n,ac} \tag{92}$$

Where m is the number of phases, Rs is the resistance and I is the DC current, In is the rms of the nth current harmonic. Rn,ac is the value of the ohmic for the nth harmonic that is determinate by the expression (93).

$$R_{n,ac} = R_{dc}\left(K_{n.se} + K_{n,pe}\right) \tag{93}$$

Where K_{nse} is the resistance gain cause for the effect skin and the $K_{n,pe}$ is the resistance gain caused for the proximity effect. The iron losses is calculated in bases to expression (94).

$$P_{iron} = kP_{FEo}\left(\frac{f}{f_o}\right)^{\frac{2}{3}}\left(M_d\left(\frac{B_d}{B_o}\right)^2 + M_{ce}\left(\frac{B_{ce}}{B_o}\right)^2\right) \quad (94)$$

Where K is the coefficient of additional losses in iron, PFE0, for magnetic sheet M250-50A, f_o is the frequency, B_o is the maximum induction value, B_d maximum induction in the teeth, B_{ce} is the maximum induction in the stator crown, M_d is mass of the teeth and M_{ce} is the mass of stator crown. The result of power losses in the PMSM for the four situations are show in the Fig. 124.

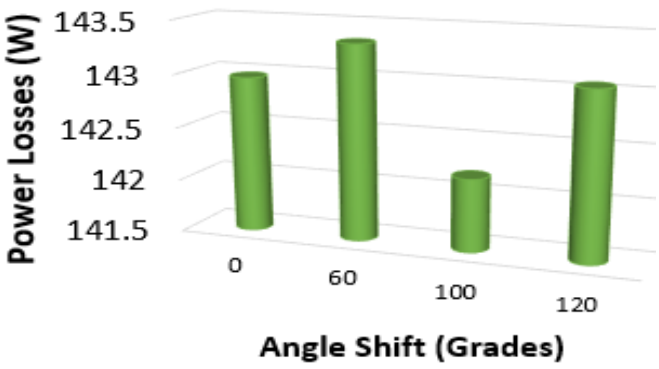

Fig.124. Power Losses in PMSM with shift-angle in 0°, 60°, 100° and 120° in the power converters.

5.6 Analysis of Efficiency.

This section presented an analysis of efficiency for each topology of power converter previously analyzed. The goal is validate the method proposed and obtained a improve in the efficiency for each topology and electric motor. Then a whole system efficiency study is established (power converters + motor), this to establish a more advanced vision on the advantage of using silicon carbide devices in the analyzed topologies and electric traction systems. Finally, a comparison between converters analyzed with all-SiC technology and converters with hybrid technology is realized to verify the impact and benefices of the SiC devices in the power converters efficiency.

The Efficiency for each topology is calculated with the expression (94).

$$\eta = \frac{P_{out}}{P_{out} + \Sigma P_{Losses}} \quad (94)$$

The efficiency results for the V-I SiC topology in differents power of output is presented in the Fig. 125.

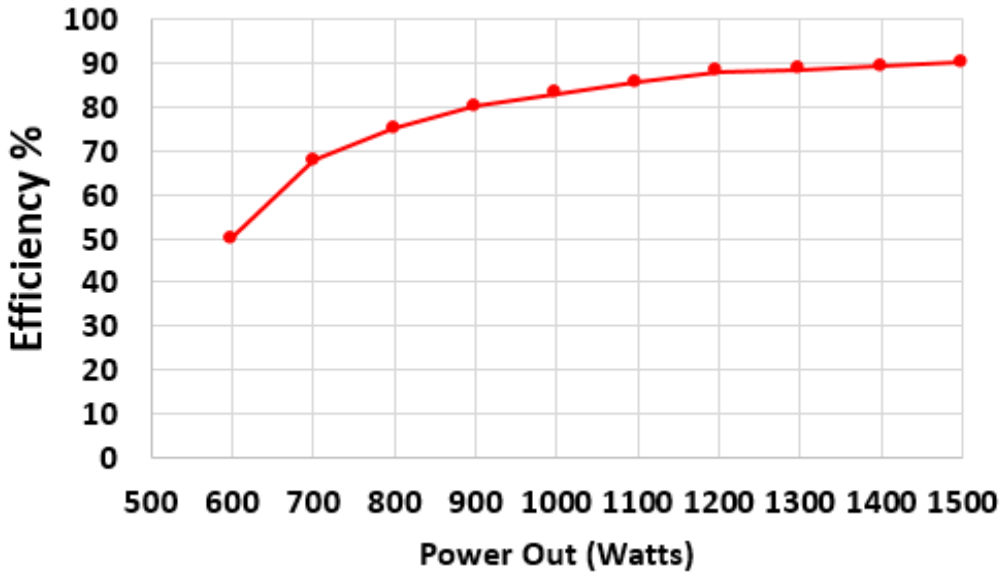

Fig.125. Results of efficiency in V-I power converter with SiC devices.

The efficiency results for the CSI SiC topology in differents power of output is presented in the Fig. 126.

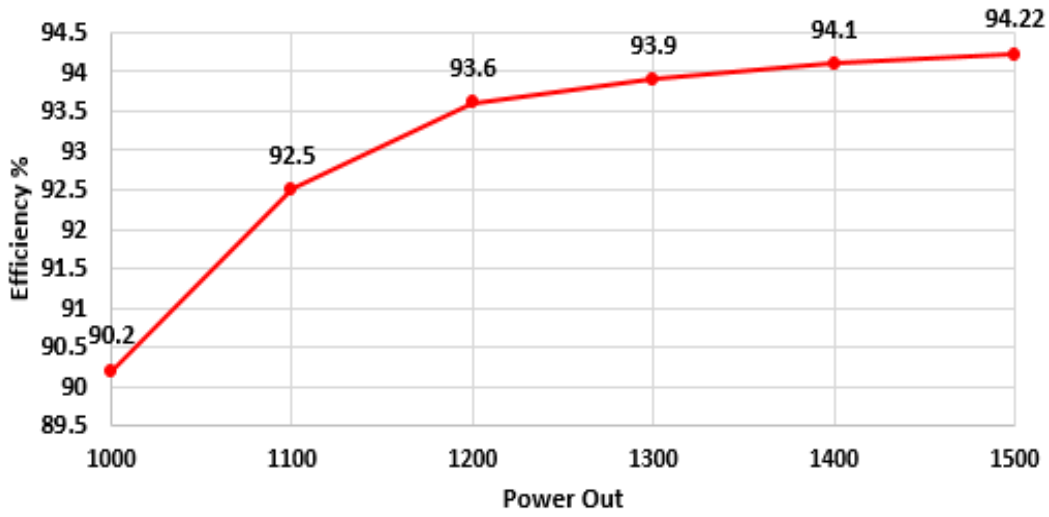

Fig.126. Results of efficiency in CSI power converter with SiC devices.

The representation of the efficiency of the motor for the situations of shift-phase angles (0°, 60°, 100° and 120°) are shown in Fig. 127 are compared for different power outputs.

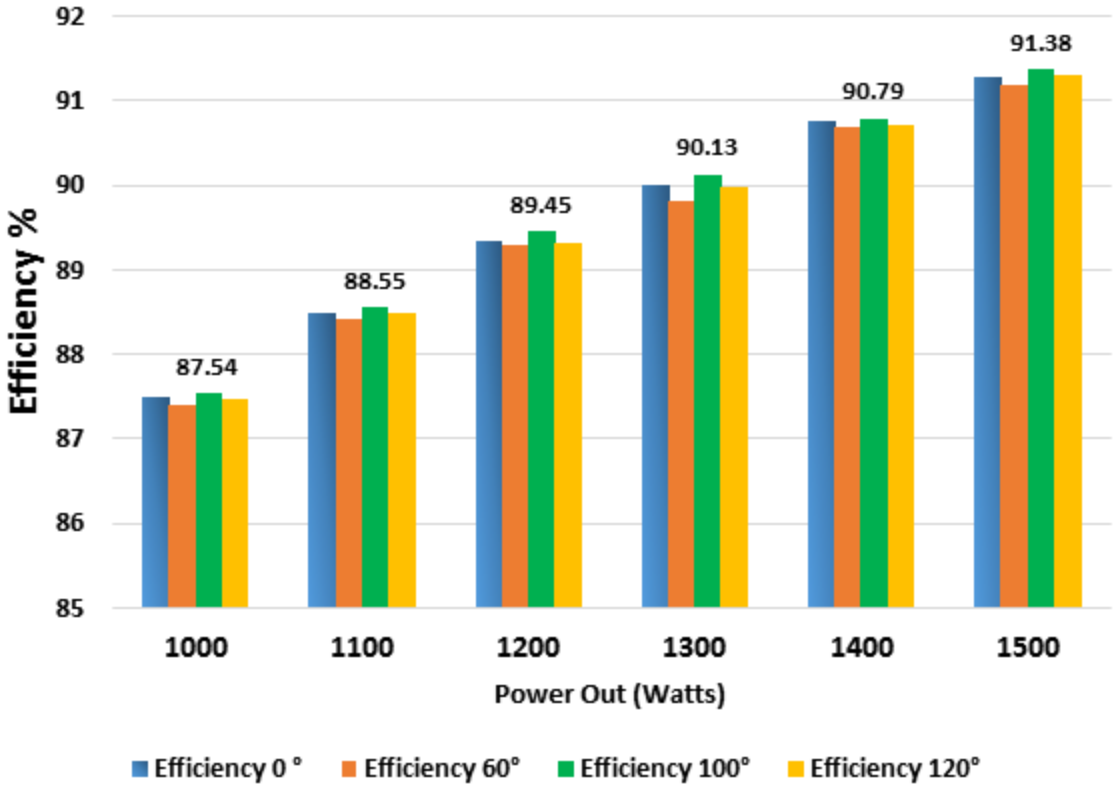

Fig.127. Efficiency in electric motor for shift angle in 0°, 60°, 90° and 120° in the power converters.

The weighted average efficiency of the whole system (power converters + motor) in the situations of 0° and 100° is shown in Table 27 and Fig. 128.

Table 27
Average efficiency of the whole system

System	Efficiency in 0°	Efficiency in 90°	Power Out
V-I	88.25%	90.1%	1.5 kW
CSI	93.8%	94.22%	1.5 kW
Motor	91.2%	91.38%	1.5 kW
Average	91.08%	92%	1.5 kW

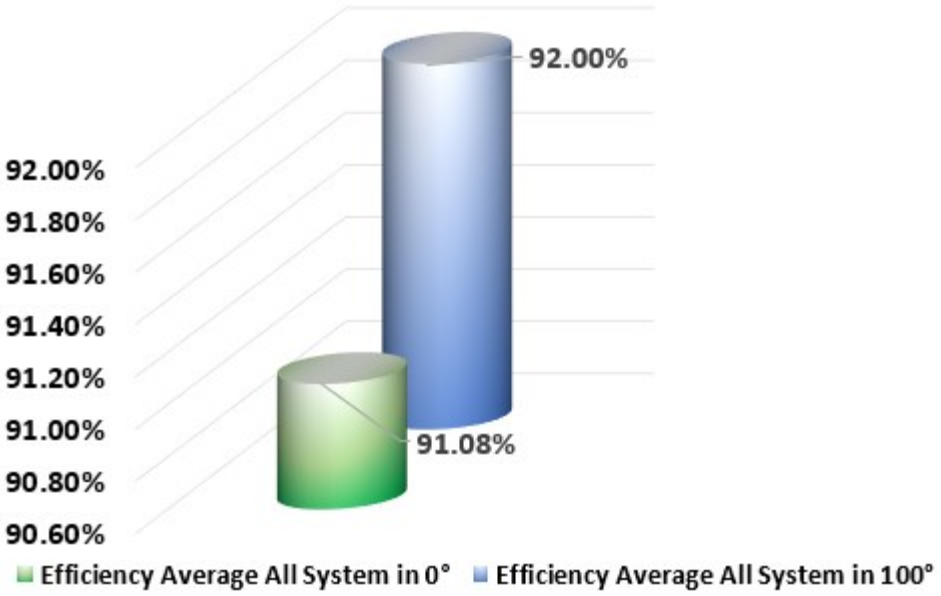

Fig.128. Efficiency average in all system for 0° and 100°.

The study allows demonstrating that using the proposed method an improvement in the efficiency of the systems analyzed is obtained. Application of the proposed modulation patters produces a gain in efficiency that is not highly significant (0.91%), but it is good enough to reduce the thermal stress of the power converters, the thermal behavior of the whole system, as well as the improvement of the wave shape of motor currents.

5.7 Heatsink Estimation.

The use of a cooling system or heat sink is important for the operation of converter topologies. Using a simple thermal model for SiC devices, containing a junction and a case before the heatsink and assuming all devices are placed on the same plate, a maximum thermal resistance for the heatsink can be estimated following the method described in [15]. The maximum allowable thermal resistance for the heatsink is calculated for the expression (24).

$$R_{thhs} = \frac{T_h - T_a}{\sum_{i=1}^{n} P_{d,i}} \tag{24}$$

Where the R_{thhs} is the heatsink temperature, T_a is the temperature ambient and the P_d is the power dissipated by the component. Applying this method gives an estimate of the heatsink of 0.68 °C/W for the V-I converter and 0.22 °C/W for the CSI inverter with an operating temperature of 142°C and 25°C of the temperature ambient.

5.6 Conclusions.

This chapter describes the calculation of the power losses in the topologies of V-I and CSI converters with SiC devices, using the THD reduction method with the shift-angle phase for the synchronization of the two topologies.

The results obtained show that the use of the proposed method allows to improve the efficiency in the whole electric traction system (power converters + electric motor) and reduces the harmonic distortion in the output currents when working with the appropriate phase angle.

The reduction of THD in the currents allows reducing the losses in the electric motor and thereby improving the operation within an electric traction system.

The use of the CSI topology with SiC devices and with higher switching frequency allows improving the design of the size of the passive elements in this case the input coil; by this way more compact systems with higher power density can be obtained.

In addition, an improvement in the efficiency is observed by varying the phase angle between PWM carriers of both power converters switching modulators, V-I and CSI. According to the comparative analysis, the results shown that the efficiency increases from 91.08% to 92% by changing the phase angle from 0º degrees to 90º degrees of shift angle.

The cooling system of the power converters is crucial for its optimal performance and operation. For a proper cooling, heatsink estimation is very important for the dissipation of temperature, because prevents excessive heating of the SiC devices and improves the heat dissipation of the system. The methodology here presented for the calculations of power losses helps for the better design of the cooling system.

5.7 References.

[1] X. She, A. Q. Huang, Ó. Lucía and B. Ozpineci, "Review of Silicon Carbide Power Devices and Their Applications," in IEEE Transactions on Industrial Electronics, vol. 64, no. 10, pp. 8193-8205, Oct. 2017.

[2] A. Merkert, J. Müller and A. Mertens, "Component design and implementation of a 60 kW full SiC traction inverter with boost converter," 2016 IEEE Energy Conversion Congress and Exposition (ECCE), Milwaukee, WI, 2016, pp. 1-8.

[3] Y. Attia, A. Abdelrahman, M. Hamouda and M. Youssef, "SiC devices performance overview in EV DC/DC converter: A case study in a Nissan Leaf," 2016 IEEE Transportation Electrification Conference and Expo, Asia-Pacific (ITEC Asia-Pacific), Busan, 2016, pp. 214-219.

[4] J. Fabre, P. Ladoux, and M. Piton, "Characterization and Implementation of Dual-SiC MOSFET Modules for future use in Traction Converters," IEEE Transactions on Power Electronics,vol. 30, no. 8, pp. 4079-4090, 2015.

[5] M. R. Ahmed, R. Todd and A. J. Forsyth, "Analysis of SiC MOSFETs under hard and soft-switching," 2015 IEEE Energy Conversion Congress and Exposition (ECCE), Montreal, QC, 2015, pp.2231-2238. doi: 10.1109/ECCE.2015.7309974

[6] W. Jun, Z. Tiefu, L. Jun et al., "Characterization, Modeling, and Application of 10-kV SiC MOSFET," IEEE Transactions on Electron Devices, vol. 55, no. 8, pp. 1798-1806, 2008.

[7] F. Shang, A. P. Arribas and M. Krishnamurthy, "A comprehensive evaluation of SiC devices in traction applications," 2014 IEEE Transportation Electrification Conference and Expo (ITEC), Dearborn, MI, 2014, pp. 1-5.

[8] M. H. Bierhoff and F. W. Fuchs, "Semiconductor losses in voltage source and current source IGBT converters based on analytical derivation," 2004 IEEE 35th Annual Power Electronics Specialists Conference (IEEE Cat. No.04CH37551), 2004, pp. 2836-2842 Vol.4.

[9] M. Mohammadi, J. S. Moghani and J. Milimonfared, "A Novel Dual Switching Frequency Modulation for Z-Source and Quasi-Z-Source Inverters," in IEEE Transactions on Industrial Electronics, vol. 65, no. 6, pp. 5167-5176, June 2018.

[10] Co Huynh Liping Zheng Dipjyoti Acharya Losses in High Speed Permanent Magnet Machines Used in Microturbine Applications Journal of Engineering for Gas Turbines and Power 2009.

[11] Q. Guo, C. Zhang, L. Li, J. Zhang, J. Liu and T. Wang, "Efficiency Optimization Control of Permanent-Magnet Synchronous Machines for Electric Vehicle Traction Systems," 2016 IEEE Vehicle Power and Propulsion Conference (VPPC), Hangzhou, 2016, pp. 1-5.

[12] W. Hassan and Bingsen Wang, "Efficiency optimization of PMSM based drive system," Proceedings of the 7th International Power Electronics and Motion Control Conference, Harbin, 2012, pp. 1027-1033.

[13] Harry Nick Aguilar Gamarra Diseño de un motor síncrono con imanes de ferritas 2014.

[14] Co Huynh Liping Zheng Dipjyoti Acharya Losses in High Speed Permanent Magnet Machines Used in Microturbine Applications Journal of Engineering for Gas Turbines and Power 2009.

[15] A. Antonopoulos, H. Bangtsson, M. Alakula and S. Manias, "Introducing a silicon carbide inverter for hybrid electric vehicles," 2008 IEEE Power Electronics Specialists Conference, Rhodes, 2008, pp. 1321-1325.

6.

General Conclusions

The main contributions of this thesis research, as well as the general conclusion, are presented in this chapter.

CONTENTS:

6.1 General Conclusions.

The topologies of converters with silicon carbide devices for application in traction systems for electric vehicles are becoming interesting for researchers and manufacturers. The improvement in efficiency and size are important factors that contribute to the search for more compact and more power-density traction systems to meet the needs of electric vehicle brands.

The **main goal** of this thesis has been to improve the efficiency of a topology with a current source inverter CSI and an elevator DC-DC type VI with the use of silicon carbide devices y the implementation of a method to couple the two topologies according to the frequency and shift-phase angle between carrier signals that generate the modulations to reduce the harmonic content in the output currents of the inverter.

The **first contribution** of this study is to propose a simple method for the coupling of two converter topologies with SiC devices and with different operating frequencies. The proposed method consists in first analyzing different frequency conditions for each converter. With this a harmonic distortion response (THD) is obtained for each condition. The frequency ratio with the lowest THD is the one selected for the second part, which consists in shifting the angle between the carrier signals between a ranges of 0° to 180° in order to see if there is a THD reduction with the previously selected frequency ratio.

The proposed method includes the implementation of a PI controller for the input of current to the CSI. The topologies of converters are simulated with the proposed method and it is observed that in the condition of frequency 2: 1 and with a phase angle of 100° the THD is reduced. As a result of the implementation of the method, the losses are reduced by analyzing in conjunction with the electric motor, which improves the efficiency of the entire system.

The **second contribution** of the document is to carry out an analysis of the topologies and their behavior during the coupling with the frequency values used 2: 1 where it is verified according to the map of activation signals of the converters that the fewer states of short circuits present a lower THD reduction is obtained. With this analysis it is established that the most optimal selection of frequencies to obtain a better efficiency in converter topologies is that the V-I works with a frequency lower than the CSI in this case with a ratio of 1: 2

The **third contribution** of this study is to evaluate the efficiency of the topologies of the converters, the analysis includes the losses of power of commutation and conduction of the semiconductor devices, passive and of the electric motor, where it is shown that the biggest losses are concentrated in the CSI and the electric motor. The efficiency in the electric motor considering different conditions of shift -phase of the carrier signals and power output indicates that the most optimal for its operation is the one that has been selected within the proposed method (100° grades). After an efficiency analysis of the whole system is performed (electric motor + converters) where it is observed that the efficiency is of 92% using the conditions of the proposed method compared with the 91% of efficiency obtained when method is not used.

The final conclusion of this study can be written as:

The use of SiC devices in topologies of CSI converters with DC-DC type VI and the implementation of a coupling method considering the values of switching frequency of the devices and lag angles of the carrier signals of the modulations used for each converter, they allow to improve the efficiency of the converters and the electric motor, obtaining as a result a more efficient and compact traction system.

7.

Thesis results dissemination

The direct contributions resulting from this Thesis work, in international journals as wells as in specialized conferences, are collected in this Chapter.

CONTENTS:

7.1 Publications: Thesis contributions

Journals

E. Fernandez, L. Romeral Martinez and V. Sala, "Power converters and its application in electric traction systems. Analysis Present and Future Technologies," in IEEE Latin America Transactions, vol. 14, no. 2, pp. 631-638, Feb. 2016.

E. Fernandez, L. Romeral and V. Sala, "Impedance networks and its Application in Power for Electric Traction Systems," in IEEE Latin America Transactions, vol. 14, no. 3, pp. 1146-1155, March 2016.

E. Fernandez, A. Paredes, V. Sala and L. Romeral, "Control and Modulation Techniques Applied to converters with impedances networks for traction systems," in *IEEE Latin America Transactions*, vol. 15, no. 1, pp. 21-30, Jan. 2017.

Fernández, E.; Paredes, A.; Sala, V.; Romeral, L. A Simple Method for Reducing THD and Improving the Efficiency in CSI Topology Based on SiC Power Devices. Energies 2018, 11, 2798

Book chapter

E. Fernández, Luis Romeral Dispositivos de Carburo de Silicio en Sistemas de Tracción Eléctrica Libro Desarrollo Tecnológico en Ingeniería Automotriz Universidad Politécnica Salesiana Ecuador 2017

Conferences

E Fernández.; Paredes, A.; Romeral, L.; Sala, V., “Analysis of power converters with devices of SiC for applications in electric traction systems International Power Electronics and Motion Control Conference IEEE EPE-PEMC.2016.

E. Fernández, A. Paredes, M. Coello, L. Romeral and V. Sala, "Analysis of power losses in Z-SiC current source inverter, using technique of modulation PWM and high frequency," 2016 IEEE ANDESCON

E Fernández, Paredes, A.; Sala, V.; Romeral, L. “Implementation of high frequency SVM in a digital system for CS-SiC inverter”. ICREPQ International Conference on Renewable Energies and Power Quality 2017.

E Fernández, Paredes, A.; Sala, V.; Romeral, L. “Control method of impedance network in SiC power converters for HEV/EV”. ICREPQ International Conference on Renewable Energies and Power Quality 2017.

E Fernández, Paredes, A.; Sala, V.; Romeral, L “Comparative analysis of impedance source-SiC converters for traction systems”. IEEE Conference on Power Engineering, Energy and Electrical Drives Powereng 2017.

A. Paredes, H. Ghorbani, V. Sala, **E. Fernandez** and L. Romeral. “A new active gate driver for improving the switching performance of SiC MOSFET”. 2017 IEEE Applied Power Electronics Conference and Exposition (APEC).

E. Fernández, V. Sala, A. Paredes and L. Romeral, "Method to reduce THD and improve efficiency in SiC power converter," 2018 IEEE International Conference on Industrial Technology (ICIT), Lyon, 2018.

Paredes, V. Sala, **E. Fernandez** and L. Romeral, “Performance analysis of switching devices for wireless EV charging systems” 2018 IEEE International Conference on Industrial Technology (ICIT), Lyon, 2018.

Paredes, **E. Fernandez**, V. Sala, H. Ghorbani and L. Romeral “Switching trajectory improvement of SiC MOSFET devices using a feedback gate driver” 2018 IEEE International Conference on Industrial Technology (ICIT), Lyon, 2018.